POLYANILINE GOLD NANOCOMPOSITES

A Thesis
Presented to
The Academic Faculty

by

J. Anthony Smith

In Partial Fulfillment
Of the Requirements for the Degree
Doctor of Philosophy in Chemistry

Georgia Institute of Technology
June 2004

POLYANILINE GOLD NANOCOMPOSITES

Approved by:

Dr. Jiri Janata, Advisor
School of Chemistry

Dr. Mira Josowicz
School of Chemistry

Dr. Lawrence Bottomley
School of Chemistry

Dr. Mohan Srinivasarao
Textile and Fiber Engineering

Dr. Robert Dickson
School of Chemistry

November 20, 2004

To my Mother and my two Fathers

ACKNOWLEDGEMENTS

I feel it the greatest honor to express my sincerest thanks to my advisor, Professor Jiří Janata, and Dr. Mira Josowicz for their unwavering support and guidance throughout my graduate studies. I would also like to thank Professor Lawrence A. Bottomley, Professor Robert M. Dickson and Professor Mohan Srinivasarao for serving on my thesis advisory committee.

I am grateful to Dr. David Hatchett at the University of Nevada Las Vegas for his continued collaboration and friendship during the course of our investigations.

I would like to thank my unfailingly pleasant and interesting group members for their friendship and assistance. I would also like to thank Yolande Berta for her assistance with the TEM measurements and Professor Z. L. Wang for his help with TEM interpretation and for maintaining the excellent Georgia Tech Electron Microscopy Center.

I would like to thank my parents who embody all that is best in humanity by their selflessness, dedication and integrity.

This work was funded by NSF grant number 9816017.

TABLE OF CONTENTS

LIST OF FIGURES

LIST OF SYMBOLS AND ABBREVIATIONS

C: Capacitance

CV: Cyclic voltammetry/voltammogram

E: Potential

E_F: Fermi level

FTIR: Fourier transform infrared

HRTEM: High Resolution Transmission Electron Microscopy

I, *i*: Current

OCP: Open Cell Potential

Q: Charge

PANI: Polyaniline

SAD: Selected Area Diffraction

SEM: Scanning Electron Microscopy

TEM: Transmission Electron Microscope

UV-Vis: Ultraviolet-Visible-Near Infrared

XPS: X-ray Photoelectron Spectroscopy

Φ: Work Function

μ_e: Electrochemical Potential

Ψ: Electrostatic Potential

SUMMARY

This thesis describes the properties and synthesis by three methods of polyaniline-fiber / gold-particle composites. The composites were initially developed as sensing materials for chemical sensors but their creation and characterization became the substantive motivation. The methods are: Chemical - One step formation via simultaneous aniline oxidation / $AuCl_4^-$ reduction resulting in powder materials of polyaniline coated gold particles; Electrochemical / Chemical - Two-step composite growth by electrochemical polyaniline thin film growth followed by immersion into $AuBr_4^-$ solution and spontaneous reduction to gold particles; Electrochemical - Freestanding polyaniline thin film / gold nanoparticle growth by electrochemical polyaniline thin film growth on a sacrificial gold layer. This is followed by controlled electrochemical particle growth in chloride solutions. The incorporated particles show size-dependent photoelectron binding energy shifts and also reveal an offset whose origin is attributed to the development of a polyaniline / gold contact potential. Composite applications include use as chemically sensitive layers, corrosion inhibition materials, and use as probes to evaluate particle substrate interactions.

CHAPTER I

POLYANILINE/GOLD COMPOSITES

1.1 Introduction

Polyaniline is one of a class of organic polymers that are intrinsically conducting. Other common intrinsically conducting polymers are polythiophene, polypyrrole, and polyacetylene. The roots of this work are in polyacetylene and Shirikawa, Heeger, and MacDiarmid received the Nobel Prize in Chemistry for their research in this area in 2000. Each of these materials achieves conductivity via delocalization of its π orbital electrons. These are different from the σ orbital electrons which form the structure in large part. Among these, polyaniline stands out as it is air stable. It is also processable and tunable due to its ability to be acid doped. Its nitrogen heteroatoms can be protonated and deprotonated in order to improve conductivity or solubility. It can be chemically or electrochemically oxidized from the monomer aniline into powder, thin films, or fibers.

One of the unusual characteristics of polyaniline is that it may be treated as an alternating block copolymer of benzenoid and quinoid units. This assumes a head to tail (that is 1,4 bonding or para bonding)

and an even oxidation state wherein there are 50% benzenoid and 50% quinoid units. This is nearly true when the polyaniline is in its emeraldine salt form. Between each benzenoid and quinoid there is a different nitrogen group. They are referred to as imino and amino groups. These heteroatom moieties are often used as sites for selective acid doping. And their ability to be protonated or deprotonated allows the PANI to be dissolved in strong acids or bases. They also show a strong affinity for the tetrahaloaurates, $AuCl_4^-$ and $AuBr_4^-$. That is to say that the K_{eq} between an imino nitrogen group and a $AuCl_4^-$ ion is ~ 10^{10}. This strong association forms the basis for a wholly different doping scheme based on contact potential theory.

Polyaniline is an interesting material from the standpoint of the chemist but lacks commercial applicability in its native, undoped state. It's been proposed to work for many applications including electrochromics, sensing, etc. It's relatively air stable, processable, can be doped chemically, photochemically[1-3]. It can be mass produced via chemical oxidation with average molecular weights from 10-200k a.m.u.(measured via GPC usually). It may also be grown electrochemically (3k-10k a.m.u) which produces more regular material but also adds some complexity to the processing.

The synthesis and characterization of PANI using a variety of synthetic methods and analysis techniques is well documented[4-7]. More

recently PANI/metal composite properties have been investigated. For example, the electrocatalytic properties and sensing applications of PANI/Pt[8-17] and PANI/Pd[18-22] have been examined. In many cases the incorporation of metal clusters in the polymer matrix also provides discrete reaction sites that can be probed electrochemically.[8-19] However, the use of metal clusters in polymer matrices to explore metal-ligand interactions in solution has been largely overlooked in the literature. It is important to produce the PANI/Au while maintaining the doping and oxidation state of the polymer, in order to preserve high conductance, a requisite for many applications.

The study of composite materials of conducting polymers and metal nanoparticles has been mostly limited to the mixing of these materials after previous separate growth or of sorption of metal anions by the previously formed polymer. This study examines the interaction of aniline and polyaniline with tetrachloroaurate as both an oxidant and a post polymerization dopant. Previous studies examining the interaction between tetrachloroaurate ($AuCl_4^-$) and conductive polymers such as polyaniline and polypyrrole have focused on the sorption properties of the materials. The processes rely on the pre-formed polymer's ability to spontaneously reduce $AuCl_4^-$.[18,20,21] Accumulation of gold in the sorption process has been reported to be as high as five times the original polymer weight.[19] However, lack of chemical control of the

gold-polymer sorption process at the imino nitrogen remains a key limitation of such processes. If the goal is to produce uniform metallic clusters encapsulated in the polymer matrix[22], then sorption processes are not adequate. Specifically, the dispersion of the metal in the polymer is limited because the anion typically reduces at the point of contact rather than dispersing into the polymer matrix. The polymer can be finely ground to ensure a larger, unobstructed surface area for the metal anion to contact but this does not ensure uniform metal dispersion. Lack of metal dispersion is not a great concern when the goal is gold recovery from solution. To obtain a homogeneous mixture of intrinsically conducting polymer with evenly dispersed gold clusters, more novel techniques must be employed.

Electrochemical methods offer precise control of the polymer oxidation state, thus influencing the degree of interaction between the polymer and the metal anion. For example, Pt[5], Au[23], Ag[24] and Pd[25] have all been reduced into polyaniline using electrochemical methods. Diffusion of the metallic ions occurs as the oxidation state of the polymer is changed restoring charge neutrality in the system. These metallic ions are then reduced into the polymer matrix as the polymer is reduced using the applied potential. This technique has been utilized to control the uptake and reduction of $AuCl_4^-$ ions, forming gold clusters with variable dimensions within the polymer matrix. However, the

quantity of material produced from electrochemical methods is limited by the electrode size and the polymer/metal interface must withstand the processing steps required for use on external devices. In addition, the formation of oxidized units in the polymer occurs as the metal anion is reduced and the polymer oxidized. The end result is a higher number of oxidized units in the polymer and reduced conductivity of the material.

In the course of the electrochemical composite formation the role of the $AuCl_4^-$ anion as an oxidizing agent was examined. In addition, this study suggested that $AuCl_4^-$ is an effective oxidizing agent for aniline. The chemical synthesis of polyaniline using $AuCl_4^-$ provides both the aniline radical cations necessary for polymer formation and metallic gold colloids in the system for designed chemical reactivity. This synthetic process should also eliminate the over-oxidation of the polymer with the formation of the polymer building block tied to the reduction of $AuCl_4^-$ by aniline rather than the pre-formed polymer.

1.2 References

1. Potje-Kamloth, K.; Polk, B. J.; Josowicz, M.; Janata, J. *Chemistry of Materials* **2002**, *14*, 2782-2787.
2. Potje-Kamloth, K.; Polk, B. J.; Josowicz, M.; Janata, J. *Advanced Materials (Weinheim, Germany)* **2001**, *13*, 1797-1800.
3. Polk, B. J.; Potje-Kamloth, K.; Josowicz, M.; Janata, J. *Journal of Physical Chemistry B* **2002**, *106*, 11457-11462.

4. Huang, W.-S.; Humphrey, B. D.; MacDiarmid, A. G. *J. Faraday Discuss. Chem. Soc.* **1986**, *82*, 2385.

5. Heeger, A. J. *Synth. Met.* **1993**, *55-57*, 3471.

6. MacDiarmid, A. G. *Synth. Met.* **1997**, *84*, 27.

7. MacDiarmid, A. G.; Epstein, A. *J. Synth Met.* **1995**, *69*, 85.

8. Kost, K. M.; Bartak, D. E.; Kazee, B.; Kuwana, T. *Anal. Chem.* **1988**, *60*, 2379.

9. Kitani, A.; Akashi, T.; Sugimoto, K.; Ito, S. *Synth. Met.* **2001**, *121*, 1301.

10. Coutanceau, C.; Croissant, M. J.; Napporn, T.; Lamy, C. *Electrochim. Acta* **2001**, *46*, 579.

11. Lai, E. K. W.; Beatttie, P. D.; Holdcroft, S. *Synth. Met.* **1997**, *84*, 87.

12. Kao, W.-H.; Kuwana, T. *J. Am. Chem. Soc.* **1984**, *106*, 473.

13. Ficicioglu, F.; Kadirgan, F. *J. Electroanal. Chem.* **1997**, *430*, 179.

15. Wang, Y.; Huang, J.; Zhang, C.; Wei, J.; Zhou, X. *Electroanalysis* **1998**, *10*, 776.

16. Conn, C.; Sestak, S.; Baker, A. T.; Unsworth, J. *Electroanalysis* **1998**, *10*, 1137.

17. Zhang, Z.-R.; Bao, W.-F.; Liu, C.-C. *Talanta*, **1994**, *41*, 875.

18. Maksimov, Y. M.; Kolyadko, E. A.; Shishlova, A. V.; Podlovchnko, B. I. *Russ. J. Electrochem.* **2001**, *37*, 777.

19. Hasik, M.; Drelinkiewicz, A.; Choczynski, M.; Quillard, S.; Pron, A. *Synth. Met.* **1997**, *84*, 93.

20. Drelinkiewicz, A.; Hasik, M.; Kloc, M. *Catalysis Lett.* **2000**, *64*, 41.

21. Josowicz, M.; Li, H.-S.; Domansky, K.; Baer, D. R. *Electroanalysis* **1999**, *11*, 10.

22. Kang, E. T.; Ting, Y. P.; Neoh, K. G.; Tan, K. L. *Synth. Met.* **1995**, *69*, 477.

23. Radford, P. T.; Creager, S. E., *Anal. Chim. Acta,* **2001**, *449(1-2)*, 199.

24. Kang, E.T.; Ting, Y. P.; Neoh, K. G.; Tan, K. L. *Polymer*, **1993**, *34*, 4994.

25. Ting, Y. P.; Neoh, K. G.; Kang, E. T.; Tan, K. L. *J. Chem Technol. Biotechnol*. **1994**, *59*, 31.

26. Hatchett, D. W.; Josowicz, M.; Janata, J. *Chem. Mater*. **1999**, *11*, 2989.

27. Tian, Z. Q.; Lian, Y. Z.; Wang, J. Q.; Wang, S. J.; Li, W. H. *J. Electoanal. Chem.*, **1991**, *308*, 357.

28. Li, H.-S.; Josowicz, M.; Baer, D. R.; Engelhard, M. H.; Janata, J. *J. Electrochem. Soc.* **1995**, *142*, 798.

29. Angelopoulos, M.; Asturias, G. E.; Ermer, S. P.; Ray, A.; Scherr, E. M.; Macdiarmid, A. G.; Akhtar, M.; Kiss, Z.; Epstein, A. J. *Mol. Cryst. Liq. Cryst*. **1988**, *160*, 151.

CHAPTER II

CHEMICAL SYNTHESIS OF POLYANILINE/GOLD NANOCOMPOSITES USING TETRACHLOROAURATE

2.1 Introduction

In the course of the electrochemical composite formation the role of the $AuCl_4^-$ anion as an oxidizing agent was examined. In this study, p-aminophenol was titrated with $AuCl_4^-$ and the reaction product and unreacted starting product were monitored using their characteristic UV/Vis bands. A clear transition between the p-aminophenol and p-iminoquinone was observed based on the spontaneous reduction of the tetrachloroaurate in solution as demonstrated by an isosbestic point in the titration. This study confirmed that the amino groups play a key role in both the electron transfer process and the reduction of tetrachloroaurate to Au(0). In addition, this study suggested that $AuCl_4^-$ is an effective oxidizing agent for aniline. The chemical synthesis of polyaniline using $AuCl_4^-$ provides both the aniline radical cations necessary for polymer formation and metallic gold colloids in the system for designed chemical reactivity. This synthetic process should also

eliminate the over-oxidation of the polymer with the formation of the polymer building block tied to the reduction of $AuCl_4^-$ by aniline rather than the pre-formed polymer.

Although the chemical synthesis of polyaniline using oxidizing agents such as ammonium peroxydisulfate[1-3] is well characterized, the synthesis and mechanism of polyaniline using $AuCl_4^-$ is inherently more complex. For example, issues such as the final oxidation state of the metal and polymer, degree of proton doping, degree of incorporation of the metal into the polymer matrix, and chemical composition of the polymer must be addressed. This describes a new synthetic route for the direct synthesis of PANI/Au composite using $AuCl_4^-$ as the oxidizing agent in solutions containing the acid, HBF_4. The synthetic process is detailed and the chemical characteristics of system are evaluated and compared to PANI doped with only HBF_4. *In-situ* UV/Vis studies are used to monitor products and reactants simultaneously and a synthesis mechanism is proposed. In addition, optical imaging and TEM diffraction are used to probe the metal distribution, size, and crystallinity in the PANI matrix. FTIR and XPS studies are used to examine the chemical properties of the polymer with and without metal clusters. Finally the sheet conductance of PANI/HBF_4 and PANI/Au are investigated using a four point probe. The synthesis of PANI/Au composite using $AuCl_4^-$ suggests that other polyaniline/metal

composites can be produced to exploit the symbiotic relationship between the polymer and encapsulated metal.

2.2 Experimental Section

2.2.1 Chemicals and Solutions

Tetrafluoroboric acid, HBF_4 (Aldrich, 44 wt.%, 20,793-4), potassium tetrachloroaurate, $KAuCl_4$ (Aldrich, 98%, 33,454-5), ammonium peroxydisulfate, $(NH_4)_2S_2O_8$, (Mallinckrodt, 7277-54-0) and aniline, $C_6H_5NH_2$ (Aldrich, 99.9%, 13,293-4) were used as received. All solutions were prepared using 18.3 MΩ•cm water obtained from a Barnstead E-pure water filtration system.

2.2.2 PANI/Au Composite Material Synthesis

Bulk PANI/Au composite used for FTIR and XPS measurements was produced by mixing 20 ml of $KAuCl_4$ 2.5 x 10^{-2} M with 20 ml of 0.25 M aniline both dissolved in 1 M HBF_4, representing a mole ratio of ~1:10 ($KAuCl_4$ to aniline). The material was allowed to settle for 24 hours and then collected using vacuum filtration, washed copiously with water, and dried under ambient conditions. The filter paper had pore diameters on the order of 3 μm. For comparison, the gold particle size was on the order of 0.8 – 1 μm (verified by SEM and optical microscopy). Therefore, any free gold not encapsulated by the polymer could be washed through the filter paper during the rinsing cycles. Samples were

also dried in a vacuum oven at ~ 70°C prior to performing the FTIR experiments to remove residual water. The synthetic process was repeated and resulted in an average product weight of 0.0780 g ± 1.25%. It is important to note that the weight of the product showed no acid concentration dependence. HBF_4 was chosen as the dopant acid because it does not degrade the polymer in the same manner observed for acids such as H_2SO_4 and HCl.[2] Pure PANI samples without gold were synthesized via previously published methods using ammonium peroxydisulfate as an oxidant in 1 M HBF_4.[2]

2.2.3 UV-Vis Spectroscopy

All spectra were obtained using a StellarNet EPP2000 fiber optic spectrophotometer equipped with a D_2 lamp and tungsten filament source that were coupled into a single fiber. The transmitted light was collected after it passed through the cuvette by a second fiber and relayed to the detector. The integration time for the detector was typically 200 ms. The data acquisition times were varied to minimize the volume of data collected and stored. All UV/VIS measurements were performed in a single, teflon capped, quartz cuvette with a 1 cm path length. The *in-situ* characterization of reactants and products was performed using an episodic data capture routine. The data was collected at regular intervals using an integration time of 28 ms per

scan. The episode capture time was initially 0.5 seconds to ensure that changes in solution conditions were monitored with sufficient spectroscopic detail.

The *in-situ* UV/VIS samples were prepared and monitored using 0.20 ml 2.50 x 10^{-2} M $KAuCl_4$ and 3.00 ml of 0.02 M aniline in 0.10 M HBF_4, respectively. A large excess of aniline was used to facilitate the complete reaction of the $KAuCl_4$. However, the overall concentration of each species in the cuvette was lowered to ensure optical transparency and the ability to obtain measurable signal throughout the reaction. The solution conditions employed were used to keep the magnitude of the signal below two absorbance units at all times.

2.2.4 FTIR Spectroscopy

All FTIR measurements were performed using a BIO-RAD FTS-7000 spectrometer using a photoacoustic detector. Each sample was scanned 64 times with a resolution setting of 4 cm^{-1} and averaged to produce each spectrum. All samples were vacuum dried overnight prior to measurement.

2.2.5 Optical Imaging

Optical images of the composites were obtained using an Olympus BX41 optical microscope. The optical dimensions of the microscope image were determined using a 0.1 mm per division standard. For

example the 100x objective provides a viewing area of 9625 μm^2 based on the x and y axis dimensions (x = 110 μm, y = 87.5 μm). The images were obtained using an Olympus DP-11 2.5 mega-pixel color CCD digital camera in the transmission light mode.

2.2.6 Transmission Electron Microscopy

TEM samples were placed on a copper grid in a dry state and then mounted in a holder. The images were made in the selected area using normal diffraction mode with a Hitachi HF2000 field emission gun transmission electron microscope poised at 200 kV.

2.2.7 X-ray Photoelectron Spectroscopy

XPS data were collected using a Surface Science SSX-100 system with an Al Kα X-ray excitation source (1486.67 eV). The system was equipped with a hemispherical electron analyzer with a position sensitive anode. The polyaniline/gold powder samples were mounted on a double-sided carbon tape placed on a piece of aluminum foil. For this study the carbon 1s peaks were assigned a binding energy of 284.6 eV and used as the energy reference. A chamber pressure of 5×10^{-9} Torr or lower was maintained for each sample measurements.

2.2.8 Conductance Measurements

A 1.25 cm radius pellet was pressed from each material using three metric tons of pressure. The contacts were made using a Cascade Microtech C4S-64/50 probe head with Tungsten Carbide electrodes. The four point probe sheet resistance of each pellet was then measured at locations across the surface of the pellet using an HP 34401A digital multimeter connected through a Cascade Microtech CPS-05 probe station. Constant pressure for each measurement was maintained for the probed head contacting the substrate. A total of at least five measurements at different locations are presented with representative standard deviations and relative standard deviations.

2.3 Results and Discussion

2.3.1 PANI/Au Synthesis

The spectra of the reactants, reaction products, and the reaction filtrate are presented in figure 2.1. The reactants, aniline and $AuCl_4^-$ are presented in figure 2.1a and 2.1b, respectively. Both reactants have UV/Vis absorbance bands between 200 – 290 nm, which makes distinguishing the changes in the concentration of these species difficult. The aniline and $AuCl_4^-$ band are centered at 260 nm and 311.7 nm, respectively. The absorbance band for $AuCl_4^-$ can be examined prior to and after completion of the reaction to determine if

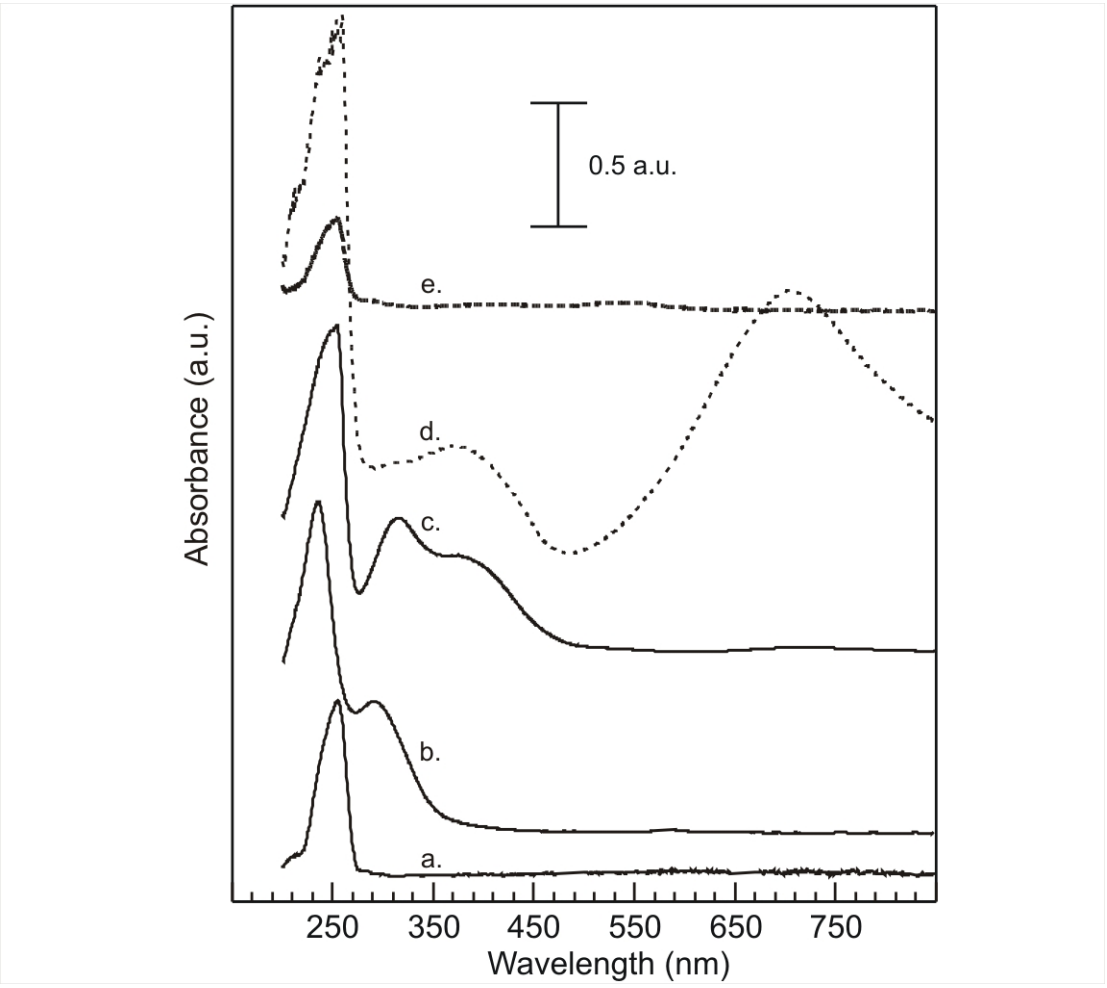

Figure 2.1 Bottom to top, UV/Vis spectra of, (a) 0.02 M aniline in 0.10 M HBF_4, (b) 2 mM $KAuCl_4$ in 0.1 M HBF_4, (c) chemically synthesized PANI/Au colloid in aqueous solution obtained by mixing 0.2 ml of 2.5 x 10^{-2} M $KAuCl_4$ and 3 ml of 0.02 M aniline in 0.1 M HBF_4 at time 10 s, (d) same conditions as c., data acquired at time 70 s, (e) solution after PANI precipitation and filtration.

the consumption of the gold anion is complete. It is difficult to use this band *in-situ* to examine the consumption of $AuCl_4^-$ during the reaction because the PANI can have polaron bands that overlap with the reactants. For example, PANI (emeraldine salt) has a π-π* transition between 320 - 360 nm and a polaron-π transition band at approximately 440 nm that can shift depending on solution conditions.[4-6] In fact, spectral shifts for the polaron transition are common and indicate oxidative or morphological changes in the polymer.[7-10]

The time dependant changes of the reaction mixture containing aniline and $AuCl_4^-$ in 0.10 M HBF_4 solution are presented in figure 2.1c (t = 10 s) and 1d (t = 70 s), respectively. Two bands associated with the product are observed at 381.3 nm and 727.5 nm. The assignment of the band located at 381.3 nm is difficult because it lies between the π-π* transition of the benzene ring for the polymer and the band associated with the polaron-π transition. The band at 727.5 nm has been assigned previously to the localized polaron-π* transition of the polymer.[6-10] This band is also known to shift in wavelength as a function of structural and oxidative changes.[3-5] The bands at 381.3 nm and 727.5 nm were used to monitor the formation of PANI (*in-situ*) during the polymerization process.

The degree of $AuCl_4^-$ reduction, formation of polymer, residual oligomeric material in the system was determined using the filtrate from

the reaction shown in figure 2.1e. The benefit of examining the filtrate is that the overlapping bands associated with the polymer are eliminated leaving any unreacted aniline and $AuCl_4^-$ behind. Excess aniline is clearly observed in the filtrate spectrum. In addition a small shoulder exists consistent with a small amount of unreacted $AuCl_4$. The amount of gold species remaining is considered to be negligible in order to estimate the weight percent of gold in the PANI. With this assumption we find the weight percent of the gold is on the order of 60% Au in PANI. This value will be compared to an estimate of the percent gold from elemental analysis data. The weight percent Au in the PANI can be varied by changing the reaction conditions. The degree of Au in PANI can be adjusted using the excess aniline and a traditional oxidant to increase the amount of polymer relative to gold if desired.

2.3.2 In-Situ UV/Vis Spectroscopy of Composite Synthesis

The *in-situ* studies were performed using a mixture of 0.20 ml of 2.50×10^{-2} M $KAuCl_4$ and 3.00 ml of 0.02 M aniline in 0.10 M HBF_4. A large excess of aniline was used in comparison to $AuCl_4^-$ to facilitate the complete reduction of $AuCl_4^-$ in the solution. The mixed absorption bands of both aniline and $AuCl_4^-$ are observed between 200 and 290 nm in figure 2.2a. We expect the bands associated with these species to diminish over time leaving the signature of unreacted aniline if all of the

gold species is consumed in the reaction. However, we find that the band for aniline actually increases over the first 70 seconds. Over the same period of time the characteristic π-π* and polaron-π bands associated with the polymer emerge as PANI is formed in the solution. Based on these initial results it is not apparent that the consumption of $AuCl_4^-$ and aniline and the formation of the polymer in solution are linked. However, the isolated absorbance for $AuCl_4^-$ (λ = 311.7 nm) over the first 20 seconds displays an initial drop consistent with the consumption of this species from solution (figure 2.2b). The increase in intensity of the aniline band is based on the formation of colloidal gold in solution shown in the reaction below.

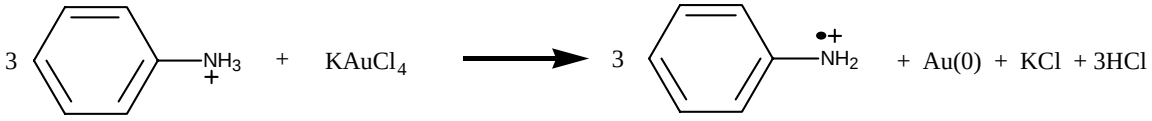

The gold particles remain suspended in solution causing an increase in the amount of light scattering. This increase causes a shift in the baseline of each spectrum to higher intensity. This trend is observed in figure 2.2a which shows that the spectra shift to higher absorbance as the concentration of the colloidal gold increases during the reaction. The trend is also repeated for the aniline/$AuCl_4^-$ combination absorbance bands and the bands associated with the formation PANI. Therefore, true quantitative analysis of the species

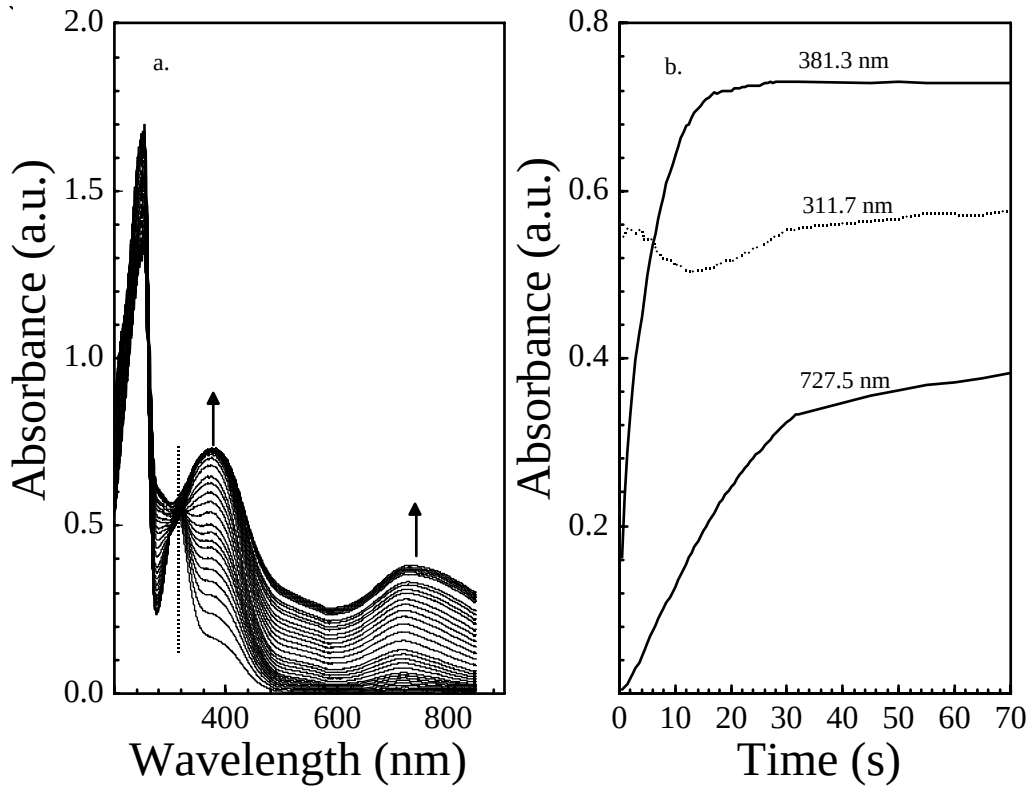

Figure 2.2 (a) In-situ UV/Vis spectra of a mixture of 0.20 ml of 2.50 x 10-2 M KAuCl4 and 3 ml of 0.02 M aniline both in 0.1 M HBF4. The data shown includes spectra obtained from 0.5 – 5.0 seconds (0.5 second interval), 6 – 10 seconds (1 second interval), 12 – 32 seconds (2 second interval), and 45 – 70 seconds (15 second interval). Arrows indicated direction of band growth as a function of time. The dashed line passes through the center of the AuCl4- band at 311.7 nm. (b) Plot of UV/Vis absorbance intensity versus time for the absorbance bands for AuCl4- (311.7 nm) and product bands (381.3 nm and 727.5 nm).

concentrations is not possible at true quantitative analysis of the species concentrations is not possible at this point in the reaction due to the large degree of light scattering by the colloidal gold in solution. However, reactions trends are clearly visible and can be monitored during the reaction.

The bands located at 381.3 and 727.5 nm are key to understanding the synthetic process. There are two clear differences between the band at 381.3 and 727.5. First, our spectroscopic data shows that the band at 727.5 nm appears after a very short lag time in comparison to the band located at 381.3 nm (~2 seconds). The rate of formation in solution is also quite different. The rate of formation for the species giving rise to the band at 381.3 nm rises rapidly, reaching a maximum at ~10 s. In contrast, after the lag time, the band at 727.5 nm increases at a much slower rate eventually showing a significant change in rate of formation at ~30 s. However, this band continues to rise gradually over the next 40 s in contrast to the band at 381.3.[10-11] This indicates that the kinetics for the formation of the two species is significantly different and likely due to two different chemical species. Wei and co-workers[9-10] have observed this same trend while monitoring the species present in the reaction mixture during the electrochemical formation of polyaniline. Based on their linear sweep voltammetry results the authors confirm the initial product formed in the synthesis of

polyaniline is the dimer species (p-aminodiphenylamine). In fact, the oxidation of the aniline monomer to form dimer intermediates was proposed as the rate-limiting step in the reaction.

The spectro-electrochemical analysis of PANI synthesis by Genies and co-workers[11] showed that the absorbance band for the polymer located below 400 nm is *primarily* due to the formation of soluble polymer intermediates with a small contribution from the large polymer units. We believe that the leveling of this peak with the continued growth of the absorbance band at 727.5 nm is based on the consumption of short chain intermediate structures to form the long chain units in solution. In addition, the differences in rate of formation and the lag time between the bands at 381.3 nm and 727.5 nm suggest that the increase in absorbance occurs at the cost of both the short chain oligomeric material (381.3 nm) in the solution and the continued reduction of $AuCl_4^-$. The band at 727.5 nm is consistent with the formation of the long chain polymeric unit which has been observed previously.[3-5,11-13] Although the UV/Vis spectroscopic data collected over the first 70 seconds is fairly complex, it indicates a colloidal mixture of PANI, short chain intermediates, gold, and the remaining aniline monomer is present in the reaction mixture.

Significant changes in the absorbance bands are observed in figure 2.3a and 3b after the first 70 seconds. The rate of formation of

the short chain intermediates (381.3 nm) slows, while the band at 727.5 nm continues to increase in intensity. This increase can either be attributed to light scattering of gold colloids as their concentration increases in solution, or to the consumption of the short chain intermediates and the formation of longer chains. It can be surmised from the previous discussion that the reduction of $AuCl_4^-$ will result in the formation of short chain dimers, trimers and tetramers with a corresponding increase in the absorbance at 381.3 nm. In contrast, the decrease in intensity of the band at 381.3 nm relative to the increase at 727.5 nm is consistent with increasing chain growth of the polymer at the expense of the smaller chain units in solution. The data indicates that oligomer consumption is critical in the formation of long polymer chains. We expect chain growth to occur at the expense of oligomer units until intermediate species are consumed.

Termination of the synthetic process can be attributed to two related processes. First the continued reduction of $AuCl_4^-$ and formation of intermediates ceases when the gold species is consumed. In addition, the reaction of these intermediate units to form long PANI chains slows and ceases as the intermediates are consumed. It is not clear from the spectroscopic data when $AuCl_4^-$ is completely consumed due to the overlap between the absorbance bands of the intermediates and the gold

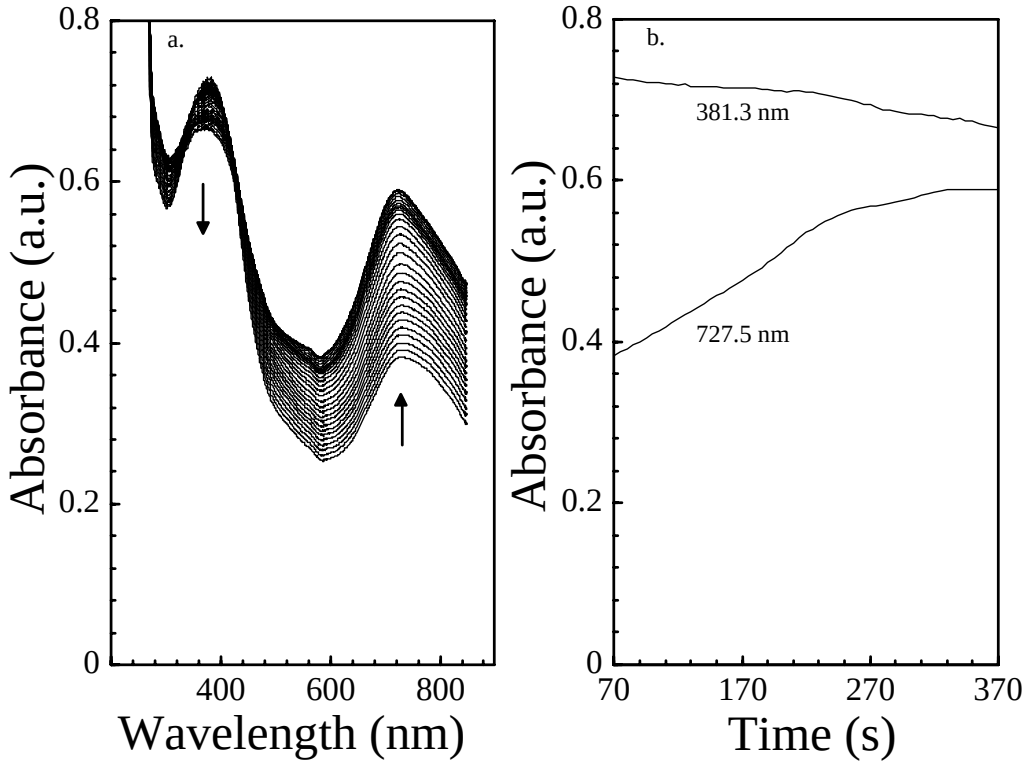

Figure 2.3 (a) The continued reaction of the mixture from figure 2.2 at times, 70-370 seconds (10 second interval). Arrows indicated direction of band growth as a function of time. (b) Plot of time dependent UV/Vis absorbance intensity for the product absorbance bands (381.3 nm and 727.5 nm).

anion. However, consumption of short chain intermediates is not complete prior to 220 s (see figure 2.3b). The band at 381.3 nm for the intermediate gradually decreases while the band at 727.5 nm continues to increase at a slower rate of increase than prior to 220 s. This trend implies that the consumption of $AuCl_4^-$ is complete. Once the reduction of the $AuCl_4^-$ ceases, the reaction of intermediate structures to form long chain structures becomes dominant and the solubility of PANI becomes an issue.

Precipitation of the PANI from solution occurs when the solubility limit of PANI is finally exceeded. In the case of the chemical synthesis the precipitation of PANI is solely related to the lack of solubility of PANI in aqueous solvent. In this system the interaction of the polymer with the gold particles in solution is also an issue. The spontaneous nucleation of PANI onto platinum and gold electrodes is well known and an integral part of the formation of PANI membranes at electrochemical interfaces.[14-16] The UV/Vis spectra displayed in figure 2.4a clearly show the precipitation of PANI from solution. In this figure, selected spectra are shown for the reaction, which was monitored every 60 seconds from 420 seconds to 7680 seconds. The data clearly shows the decrease in both polymeric bands located at 381.3 and 727.5 nm (figure 2.4b). A rapid decrease in the intensity of the signal is observed between 2280

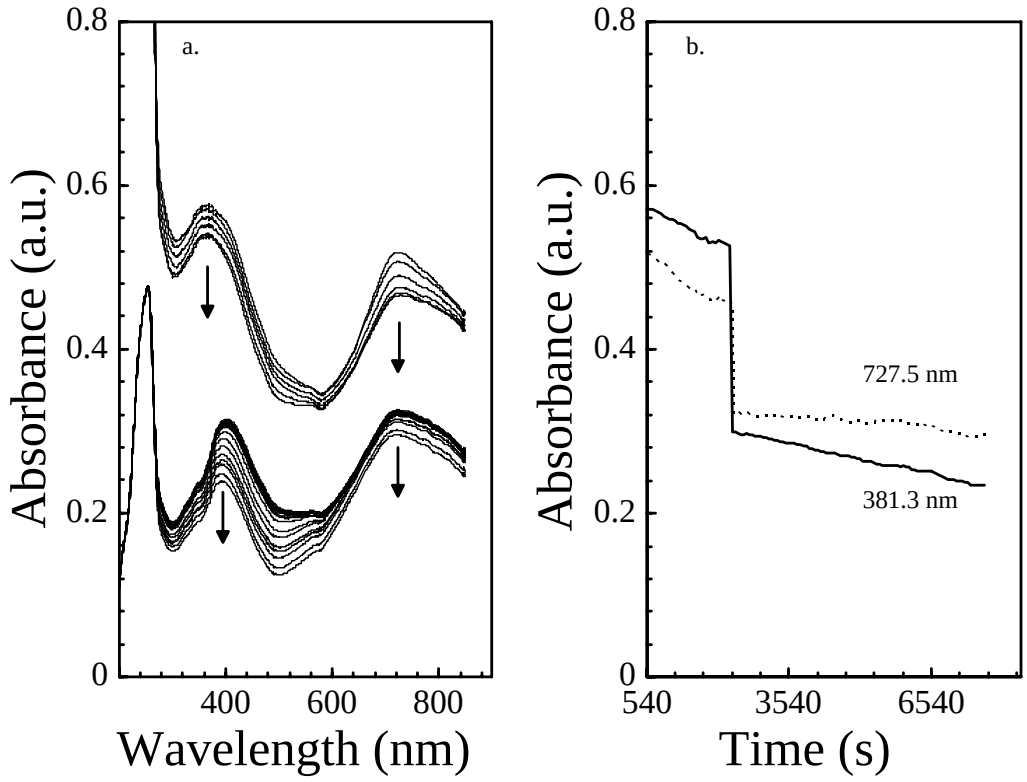

Figure 2.4 (a) The continued reaction of the mixture from figure 2.2 at times, 540 – 2340 seconds (300 second interval), 2340 - 2940 seconds (60 second interval), and 3240 – 7380 seconds (600 second interval). Arrows indicated direction of band growth as a function of time. (b) Plot of time dependent UV/Vis absorbance intensity for the product absorbance bands (381.3 nm and 727.5 nm).

and 2340 seconds due to the composite precipitation, which is marked by the appearance of a diminished aniline and background signal.

The diminished background signal is primarily the result of a decrease in light scattering associated with the loss of gold colloids in solution. This behavior suggests that the polymer and gold are not independent species in the solution. The formation of a polymer/metal composite occurs simultaneously. It is interesting to note that not all of the polymeric material has precipitated at the end of this experiment (time = 7680 seconds). However, if the solution is allowed to sit for a few additional hours the signal approaches the baseline leaving the signature band of unreacted aniline in the solution (figure 2.1e).

2.3.3 Mechanism for the Formation of PANI/Au Composites

The interaction of conducting polymers with $AuCl_4^-$ has been examined previously by a number of groups. In each case the polymer was produced separately and then reacted with the gold anion. For example, the chemical synthesis of a polypyrrole/Au has been reported previously. In the reported reaction the formation of colloidal polypyrrole was accomplished using ferric chloride as the oxidant prior to the introduction and reduction of the $AuCl_4^-$.[17] Our system is unique because the PANI/Au is formed without the aid of any chemical species other than the $AuCl_4^-$ anion and aniline.

The chemical synthesis of the PANI using $AuCl_4^-$ is similar to the chemical synthesis of PANI using a more common oxidizing agent such as peroxydisulfate. Our spectroscopic data indicates that $AuCl_4^-$ produces intermediate species in solution that are used as building blocks in the polymerization reaction. We also observe clear differences in the rates of formation between intermediate species and the long chain polymer. Our spectroscopic data suggests that consumption of the intermediate species is critical in the formation of PANI. Although we believe that the mechanism of PANI formation is very similar to that described by Genies, our system is clearly different. Specifically, *in-situ* nucleation and growth of the polymer onto colloidal metallic surfaces represents a significant deviation from previous mechanisms for the formation of PANI and PANI/metal composites.

2.3.4 Imaging and Diffraction of PANI/Au Composites

Although the loss of $AuCl_4^-$ and the increased baseline in figure 2.2a is consistent with the reduction of the anion to the metallic species, questions regarding the final oxidation state of the metal species and the relationship between the gold and the polymer remain unanswered. It is well known that the nucleation of aniline radicals and their continued formation once polymeric units have formed results in the growth of uniform and cohesive films at noble metal surfaces such as Pt and Au.

However, the nucleation of PANI onto gold particles in solution in the absence of potential control has not been studied in detail.

Examination of the reaction product using an optical microscope in the transmission mode reveals that the PANI formed in the solution nucleates onto the gold particles. Gold particles appear as uniformly dispersed dark spots in the polymer matrix with an average diameter of ~ 1 μm (figure 2.5a). It is impossible to sample and resolve the entire three-dimensional structure using optical objectives in transmitted mode, and some optically dense regions are clearly observed in the image, (figure 2.5b). In addition, the image shows regions where no PANI/Au is observed (figure 2.5c).

The crystal structure of the gold particles encapsulated by PANI was also examined using TEM diffraction. The use of TEM diffraction in figure 2.6 provides information regarding both the polymer and the metallic particles. From the diffraction pattern two clear conclusions can be drawn. First, the polymer is amorphous producing the characteristic rings in the diffraction pattern. More importantly, the gold particles in the PANI are not amorphous. The metallic diffraction pattern is in the form of spots superimposed on the rings. This is consistent with diffraction by many different crystallographic orientations. From the data it is clear that the composite consists of amorphous PANI with encapsulated poly-crystalline gold particles.

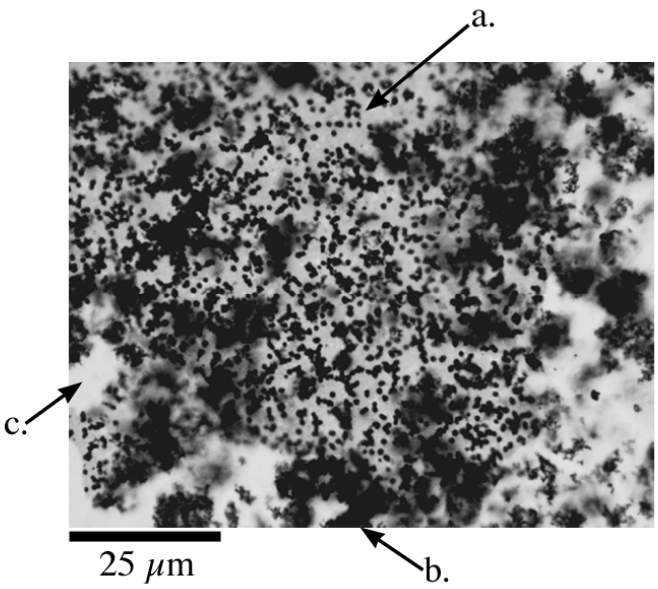

2.5. Optical image (100x) of Au/PANI composite in the reaction solution using transmitted light. (a) Optically dense region of the PANI/Au composite. (b) Gold particles (black dots) encapsulated by polymer (light gray). (c) Void space (absence of Au(0) or PANI).

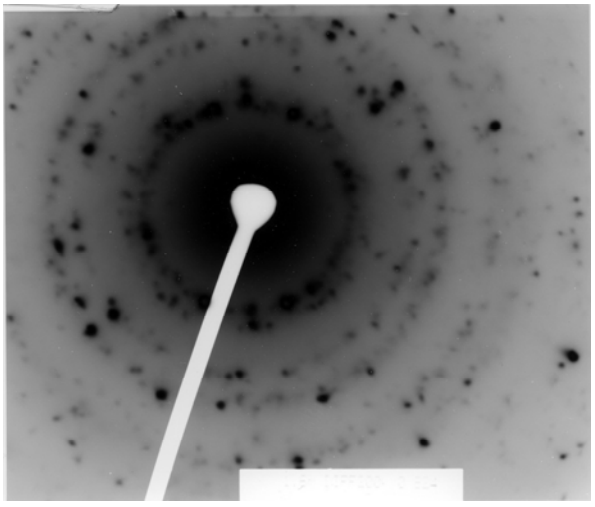

2.6. Transmission TEM diffraction image obtained from PANI/Au composite.

2.3.5 FTIR Spectroscopy of PANI/Au Composites

FTIR analysis of the finger print region between 700 - 1600 cm-1 is particularly useful for examining the resonance modes of the benzenoid and quinoid units, and individual bonds (i.e., out of plane C-H and C-N) of PANI.[16] The FTIR spectra of pure PANI/HBF_4 and PANI/Au are presented in figure 2.7. The characteristic ring bands for aromatic C-C stretching are located at 1597 and 1512 cm^{-1} versus 1593 and 1510 cm^{-1} for the pure polymer and the composite, respectively. In addition, the IR bands for the out-of-plane C-H are in good agreement with values of 832 cm^{-1} and 829 cm^{-1} for PANI/HBF_4 and PANI/Au. The shifts are well within the 4 cm^{-1} resolution used for data acquisition.

The characteristic bands associated with the benzenoid phenyl ring (~1500 cm^{-1}) and quinoid phenyl ring (~1590 cm^{-1}) of the polymer are labeled on the figure. These bands can be used to estimate the oxidation state of the polymer, where the percent oxidized units, x, versus reduced units, 1-x, are obtained by integrating the IR bands as shown in the schematic below.[16] For emeraldine salt the integrated peaks have shown that the benzenoid and quinoid units are approximately equal (i.e., $R \approx 1$). Integration of the peaks for PANI/HBF_4 and PANI/Au give values of R = 0.96 and 0.89, respectively. These values correspond to a 49/51 and 47/53 ratio of benzenoid/

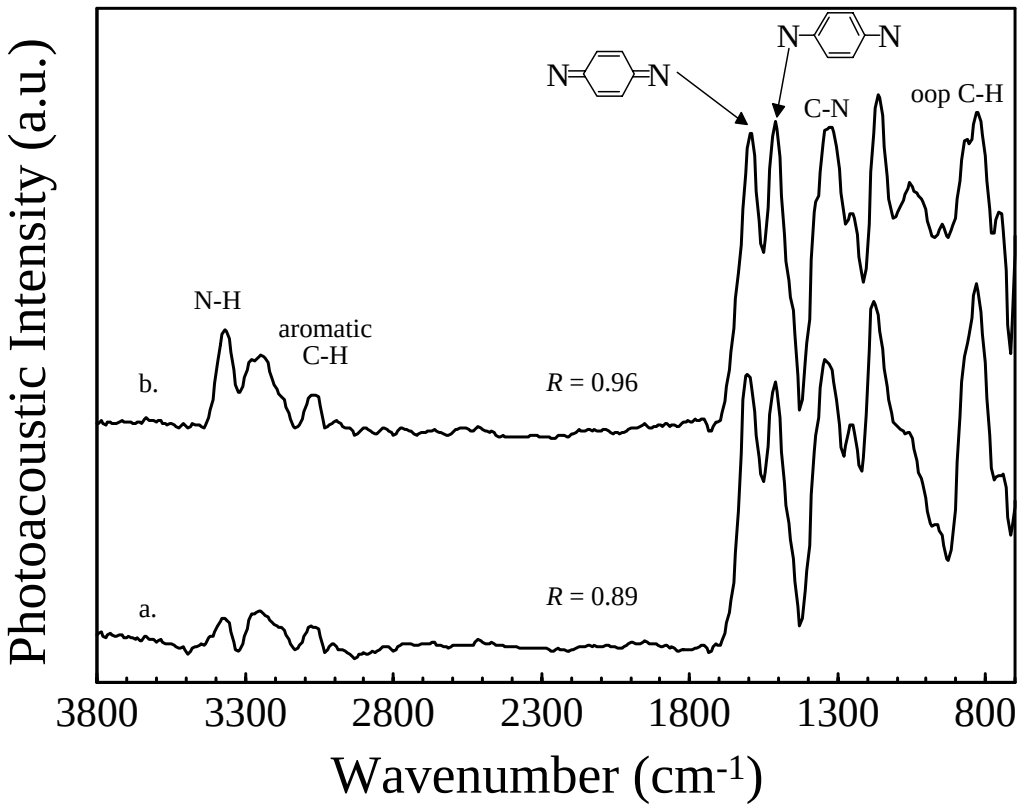

Figure 2.7. Photoacoustic FTIR spectra of, (a) Pure PANI•HBF_4 (without Au particles) and (b) PANI•Au composite produced during chemical synthesis using $AuCl_4^-$ as the oxidant. FTIR band assignments and the ratio R, of the reduced and oxidized units, are labeled for clarity.

quinoid units in the polymer. The data suggests that each material contains nearly identical percentages of oxidized and reduced units.

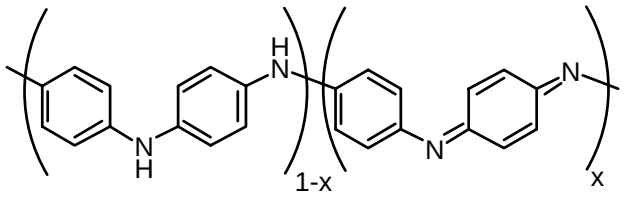

$$\text{where,}\quad R = \frac{1-x}{x} = \frac{Area_{reduced}}{Area_{oxidized}} = \frac{Area_{\nu_{(1590cm^{-1})}}}{Area_{\nu_{(1500cm^{-1})}}}$$

The effect of Au on the oxidized and reduced units within the polymer is fairly small. However, a significant shift for the semiquinoid C-N stretch is observed when comparing the two materials. The band is located at 1335 cm^{-1} for PANI/HBF_4 shifting to lower energy (1323 cm^{-1}) for PANI/Au. The 12 cm^{-1} shift to lower energy is significant because it is directly related to differences in chemistry and electron density at the nitrogen group. This difference indicates that the C-N bonds (or amino, imino bonds) within the polymer are influenced by the gold particles. The energy shift indicates that the Au directly influences the electron density of the C-N bond. The shift is consistent with the donation of electron density from the metal to the imino nitrogen units in the polymer increasing the number of free charge carriers in the system. The interaction of the Au with nitrogen groups is also consistent with the nucleation of PANI onto the gold clusters, discussed previously. It is, however, interesting to note that no large change in the energy for

the N-H band is observed (3373 cm^{-1} and 3369 cm^{-1}). It is likely that the electron density of the C-N bond is more strongly perturbed by the presence of the gold particles in the PANI matrix.

2.3.6 X-Ray Photoelectron Spectroscopy

The photoelectron spectra of PANI/HBF_4 and PANI/ Au, are shown in figure 2.8a and 2.8b, respectively. Although TEM was used to verify the crystalline nature of Au embedded in PANI, it is indicative of other gold species that may be present. XPS provides information concerning the speciation of the metal in the polymer. In addition, it provides information concerning the doping species present in the polymer. The presence of metallic gold in the PANI/Au spectrum is marked by the appearance of a double peak for Au(0) located at 84.4 ($^4f_{7/2}$) and 88.1 eV ($^4f_{5/2}$). These values are consistent with the previously determined energies for metallic gold in PANI. Any $AuCl_4^-$ present in the polymer would give rise to XPS peaks for Au(III) in the form of a doublet at 87 ($^4f_{7/2}$) and 92 eV($^4f_{5/2}$).[21] The absence of any peak at 92 eV indicates that no Au(III) species exist in the polymer. The data also clearly shows that PANI/HBF_4 sample does not have any XPS peaks associated with Au species.

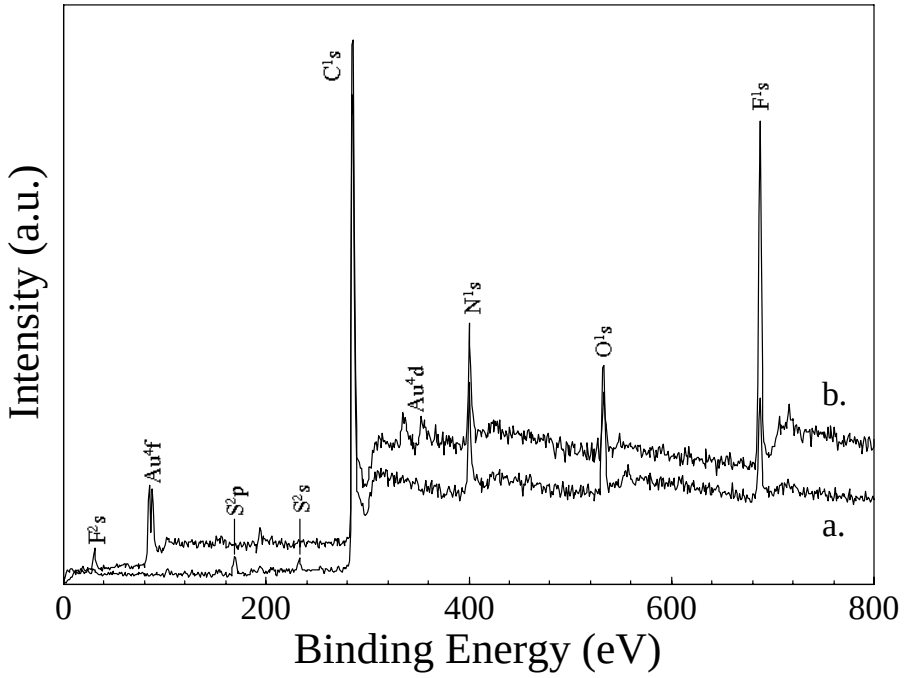

Figure 2.8. XPS surveys of, (a) PANI•HBF_4. and (b) PANI•Au composite. The XPS peaks are labeled for clarity.

Identification of Fluoride and Sulfur in the XPS spectra provides qualitative information concerning the anion doping. The data is also used to estimate the anion doping by F. The identification of F is the straight forward with a strong band at 687eV for both materials. For the elemental analysis data we found that the PANI/HBF_4 had a smaller percentage of F in comparison to PANI/Au. Comparison of the ratio of F to N peaks allows the relative percent of dopant versus N in the unit formula to be compared to the XPS data. Each species must be first scaled by the element's XPS sensitivity factor (F = 1 and N = 0.42), and the stoichiometry of the doping species (four F per dopant anion) must be considered. Using a single gaussian to integrate the Nitrogen and Fluorine XPS data confirms the degree of doping by BF_4^- with values of 0.09 and 0.22 for PANI/HBF_4 and PANI/Au, respectively. The values are consistent with the diminished signal observed in the XPS analysis for PANI/HBF_4. These numbers are comparable to the values of 0.10 and 0.15 obtained from elemental analysis. Finally, low energy sulfur peaks centered at 164 eV (S^2p) and 230 eV (S^2s) can be identified in figure 2.8a, which are consistent with doping by SO_4^{2-} in the PANI/HBF_4.

2.3.7 Electronic Resistance/Conductance

The synthesis of PANI/Au was carried out in the presence of 1 M HBF_4 to ensure the polymer would be proton doped. It has been

reported that the conductivity of PANI increases six-fold as a function of pH decrease from 6 to 0. The range of conductance values for PANI doped with HCl has been reported to be between 2 – 10 S/cm in the literature for multiple synthetic processes. Optimization of synthetic conditions has shown that the highest conductivity is obtained in when the polymer contains a dopant/N ratio of 0.5 and an equal number of oxidized and reduced units in the polymer. The conductance value for PANI/HBF_4^- (9.0 ± 10% S/cm) is in agreement with this observation. Our results also indicate that the combined doping ratio is on the order of 0.3 for PANI/Au for the dopant/N ratio. In addition, the FTIR analysis of the material confirmed that the polymer consisted of equal number of oxidized and reduced units. The four point probe sheet conductance for a pressed pellet of PANI/Au using the four point probe is 3.2 ± 12% S/cm. The results indicate that insertion of Au metal in the polymer and the small decrease in proton/anion doping associated with the process does not result in a large decrease in the conductivity for the material. More importantly it suggests that the single-step synthesis of highly conductive PANI/metal composites is possible using the metal anion as the monomer oxidant.

2.4 Conclusions

This study has shown that $AuCl_4^-$ is a suitable oxidizing agent for the direct chemical polymerization of aniline. The formation of the PANI/Au composite proceeds spontaneously until all of the $AuCl_4^-$ and radical aniline species in solution are consumed. Precipitation of the composite occurs as the polymer chain length increases and the solubility limit of the colloidal suspension is exceeded. Optical images clearly show polymer encapsulated gold particles that are uniformly distributed throughout the material. In addition, optical and TEM images indicate the particle diameter is relatively constant (~1 μm). The uniformity in gold particle distribution and dimension in the images suggest that solution parameters such as concentration of oxidizing/reducing species as well as the mole ratio of each component can be used to control particle size. This synthesis provides a new method for producing gram quantities of polymer/metal composite materials with uniform high metal dispersion (up to ~60 w/w%) and high chemical reproducibility. Moreover, the results suggest that the gold encapsulated by the PANI does not adversely affect the electronic properties of the polymer. This is in direct contrast to the uptake and reduction of metallic anions using electrochemical methods. The composite conductance is comparable to the chemically produced

PANI/HBF_4 in spite of the decreased proton and anion doping for the composite.

2.5 Acknowledgements

I would like to acknowledge John Kinyanjui, Dr. David Hatchett and Dr. Mira Josowicz with whom this text was produced and the research performed. Also thanks to Dennis Lindle and Dr. Allen Johnson for their help in obtaining the XPS results.

2.6 Summary

The one-pot synthesis of polyaniline fiber/gold particle composite was accomplished by replacing the third party aniline oxidant by $KAuCl_4$. This was accomplished by mixing aniline and $KAuCl_4$ both in 2 M HBF_4. The synthesis proceeded by tetrachloroaurate oxidizing aniline monomers to dimers, tetramers and other oligomers. As a consequence, colloidal gold collected in solution. As the colloids grew large enough, the aniline oligomers precipitated onto the colloid surface and the composite material precipitated from solution. This had lower conductivity than aniline prepared by $Na_2S_20_8$ reduction and treatment with 2 M HBF_4.

2.7 References

1. Quillard, S.; Louarn, G.; Lefrant, S.; Macdiarmid, A. G. *Phys. Rev. B* **1994**, *50*, 12496.

2. Syed, A. A.; Dinesan, M. K. *Talanta*, **1991**, *38*, 815.

3. Higuchi, M.; Imoda, Daisuke, Hiroa, T. *Macromolecules* **1996**, *29*, 8277.

4. Venugopal, G.; Quan, X.; Johnson, G. E.; Houlihan, F. M.; Chin, E.; Nalamasu, O. *Chem. Mater.* **1995**, *7*, 271.

5. Neoh, K. G.; Young, T. T.; Looi, N. T.; Kang, E. T.; Tan, K. L. *Chem. Mater.* **1997**, *9*, 2906.

6. Han, C-C.; Hong, S-P. *Macromolecules* **2001**, *34*, 4937.

7. Wang, P.; Tan, K. L.; Zhang, F.; Kang, E. T.; Neoh, K. G. *Chem. Mater.* **2001**, *13*, 581.

8. Albuquerque, J. E.; Mattoso, L. H. C.; Balogh, D. T.; Faria, R. M.; Masters, J. G.; MacDiarmid, A. G. *Synth. Met.*, **2000**, *113*, 19.

9. Wei, Y.; Hsueh, K. F.; Jang, G-W. *Macromolecules* **1994**, *27*, 518.

10. Wei, Y.; Tang, X.; Sun, Y. J. *Poly. Sci.: Part A: Poly. Chem.*, **1989**, *27*, 2385.

11. Genies, E. M.; Boyle, A.; Lapkowski, M.; Tsintavis, C. *Synth. Met.*, **1990**, *36*, 139.

12. Diaz, A. F.; Logan, J. A. *J. Electroanal. Chem.*, **1980**, *111*, 111.

13. Genies, E. M.; Tsintavis, C. *J. Electroanal. Chem.*, **1985**, *195*, 109.

14. Genies, E. M.; Syed, A. A.; Tsintavis, C. *Mol. Cryst. Liq. Cryst.* **1985**, *121*, 181.

15. Henry, M. C.; Hsueh, C.-C.; Timko, B. P.; Fruend, M. S. *J. Electochem. Soc.*, **2001**, *148*, D155.

16. Hatchett, D. W.; Josowicz, M.; Janata, J. *J. Phys. Chem. B* **1999**, *103*, 10992.

17. Travers, J.P.; Chroboczek, F.; Devereux, F.; Genoud, F.; Nechtschein, M.; Syed, A.A.; Genies, E.M.; Tsintavis, C. *Mol. Cryst., Liq. Cryst.*, **1985**, *121*, 195.

CHAPTER III

ELECTROCHEMICAL/CHEMICAL POLYANILINE/GOLD COMPOSITE SYNTHESIS VIA SPONTANEOUS TETRABROMOAURATE REDUCTION

3.1 Introduction

There is much interest in electronically conducting polymers with nanoclusters for various applications such as nanoelectronics[1], gas sensors[2, 3], biosensors[4], capacitors[5] and catalysts.[6, 7] Their properties are dependent on cluster size and distribution as well as the identity of the polymer. In this research, polyaniline (PANI) has been chosen as the support matrix, since it can be doped by protons and by electrons.[8] Further, the porosity and surface area of the conducting polymer greatly depends on the type and size of the counter-ion[9] as well as film thickness.[10]

The functionalization of PANI with metal clusters originates at the solution/polymer interface leading to the modification of interfacial electronic structure. The redox potential of PANI and of the oxidizing agent ($AuBr_4^-$) determines the outcome of the heterogeneous reaction. The oxidation of PANI supplies the necessary electrons for the reduction

reaction of $AuBr_4^-$. Therefore the redox potential of PANI must be negative of the standard potential of gold complex.

$$PANI \Rightarrow PANI^{n+} + ne^- \qquad E_{PANI} < 0.80V$$

$$AuBr_4^- + 3e^- \Rightarrow Au + 4Br^- \qquad E_o < 0.62V$$

It is important to note that PANI cannot be treated as an inert electrode in this case. It is, in fact, a reducing agent in the above system. The protonated imine repeating units of PANI have a high affinity for AuX_4^- complexes.[11, 12] This means that $AuBr_4^-$ will preferentially localize at these sites within PANI matrix. Since imine unit availability will change the nucleation rate of the gold particles is expected to change as well. That charge-transfer complex interaction results in a decrease in the imine repeating units and in an increase of positively charged nitrogen.[13]

In our previous work, the deposition of palladium clusters into electrochemically synthesized PANI film by relaxation from the oxidized state or reduced state in sulfuric acid in the presence of $PdSO_4$ salt, respectively, showed that the system formed by metal deposition into/onto conjugated polymers is rather complex.[14] The deconvoluted N1s XPS spectra of the oxidized PANI system after metal nucleation showed that during the nucleation process the amount of protonated imine and amine moieties decreases whereas the quantity of

unprotonated amine species remains the same. This leads to a significant increase in the ratio of unprotonated to protonated amine groups.[15, 16] The PANI which acts as an 'anode' in this reaction is then reprotonated by the acid medium.[15] The preservation of the polymer 'anode' thus allows the continued reduction of the $AuBr_4^-$ anion until the reaction is stopped by polarization effects on the electrode.

For a deeper and more general understanding of these systems, in this study we investigated how the growth of gold clusters in PANI film affects the work function (WF) of the resulting nanocomposite system.

3.2 Experimental

3.2.1 Chemicals

Tetrafluoroboric acid (HBF_4; Aldrich, 48 wt % solution in water, 20,793-4), potassium tetrabromoaurate ($KAuBr_4$; Aldrich, 99.9%, 39,845-4), aniline (Aldrich, 99.5+%, 24,228-4) and acetic acid (CH_3COOH, Fisher, 99.8%, 64-19-7) were all used as received.

3.2.2 Polyaniline Film Synthesis

The electrochemical polymerization of PANI was carried out in 0.1 M aniline/2 M HBF_4 aqueous solution within the potential range of -0.1 to +0.85 V in reference to Ag/AgCl in 1 M KCl//1 M KNO_3 electrode using a Solartron SI1287 electrochemical interface. Films were prepared using two different methods. In the first method films were produced

using 150 cycles with a 50 mV/s scan rate. These were recorded at room temperature using a three electrode cell arrangement with a platinum coil as the counter electrode and a stainless steel plug coated with platinum (5000 Å) as the working electrode (area 1.13 cm^2). In the second method the growth endpoint was determined by matching all films to the same current density value at the 0.12 V (vs. reference) peak during the positive potential sweep. These films were grown on 0.25 mm thick platinum discs (area 0.32 cm^2) glued to stainless steel plugs as before but with donut shaped epoxy of the same thickness surrounding the disc out to the edge of the plug. After growth the films were vigorously rinsed in methanol for one minute then placed in a vacuum desiccator for at least one hour to dry. The films were then returned to the electrochemical cell and cycled in either HBF_4 or CH_3COOH acid and labeled PANI•HBF_4 or PANI•CH_3COOH respectively. The counter ion exchange was carried out within the same potential window used for the potentiodynamic growth and the film was removed at open cell potential. The films were always dried for 1.0 hour in the vacuum desiccator. This treatment minimized the relaxation effects in the films.[14]

3.2.3 PANI/Au nanocomposite preparation

The nucleation of gold clusters in PANI•HBF_4 and PANI•CH_3COOH films was initiated 1 hour after acid doping by immersing the PANI

coated part of the substrate plugs into 750 μL of solution containing 0.5 mM $KAuBr_4$ in 2 M HBF_4 for a set time. Afterwards the substrates were washed briefly with methanol and dried under vacuum for at least 1 hour.

3.2.4 Spectroscopic measurements

All measurements were performed on a Shimadzu UV-Vis 3101PC spectrophotometer using a quartz cuvette with 1 mm path length. In order to determine the quantity of Au reduced into the PANI film, the absorbance change of a standard aliquot of $KAuBr_4$ solution in 2 M HBF_4 at λ_{max} (384 nm) was measured after the sample immersion. A set of calibration solutions was prepared that bracketed the range of experimental absorbances and from these the extinction coefficient, ε, was found to be 7.57 x 10^3 L mol^{-1} cm^{-1}. Because $AuBr_4^-$ is light sensitive the solutions were measured immediately after film immersion and the corresponding absorption recorded. Since all solutions began with the same initial $KAuBr_4$ concentration, and thus the same absorbance, the value of the mass of gold uptake into the film was obtained from the difference. From the change in the concentration of $AuBr_4^-$ the number of moles of gold which nucleated into the PANI films was calculated.

3.2.5 Work Function

The WF of each PANI film before and after gold cluster nucleation was obtained from the contact potential difference (CPD) measured in automatic balancing mode vs. a vibrating gold grid reference electrode (diameter 2.5 mm) which was facing the center of the sample. The instrumentation was a Besocke Delta-Phi-Electronik Type S Kelvin probe whose voltage output was connected to an Agilent Technologies 34401A digital multimeter interfaced to a computer via an IEEE 488.2 GPIB bus. Software written by the authors using National Instruments Labview v 5.1® was used to record CPD vs. time at 5 second intervals. Because WF measurements are affected by changes in the ambient atmosphere (temperature, humidity) the process of measuring was performed as rapidly as possibly after drying. The measurement process allows the sample probe to stabilize until the WF value was stable for a period of at least five minutes. Typically, the relative standard deviation of the signal-to-noise ratio of these data sets was less than 1% over the last 100 data points.

3.2.6 Size, shape and density of the gold clusters

After the WF measurements were performed the PANI-Au composite films were imaged by a CCD equipped Hitachi S-800 scanning electron microscope (SEM) at 15kV. The SEM micrographs were

analyzed with ImageJ v1.26 analysis software. The analysis of the images led to a series of histograms of particle size distributions for each sample. This analysis method represents an easy and automated way to analyze and interpret large numbers of particles and images. An extended analysis procedure has been developed. It can be found at: http://bizoki.chemistry.gatech.edu/anthony/image-analysis.ppt.

3.3 Results

3.3.1 General features of the PANI/Au nanocomposite

Figure 3.1 shows SEM micrographs of two electrochemically grown PANI films after their immersion in 0.5 mM $KAuBr_4$ in 2 M HBF_4 for six minutes. Gold clusters are the bright spots on the darker PANI strands. The films were polymerized under the same conditions and to the same thickness (see Experimental section). Consequently the morphology of both films should be identical. Looking more closely, it can be observed that sample (b) is more porous than sample (a). The nucleation of gold clusters in sample (a) was initiated after the PANI•HBF_4 film was cycled from -0.1 to 0.85 V (vs. the reference electrode) in 2 M CH_3COOH acid or for sample (b) in 2 M HBF_4. Usually 20 cycles were employed to exchange the anions.

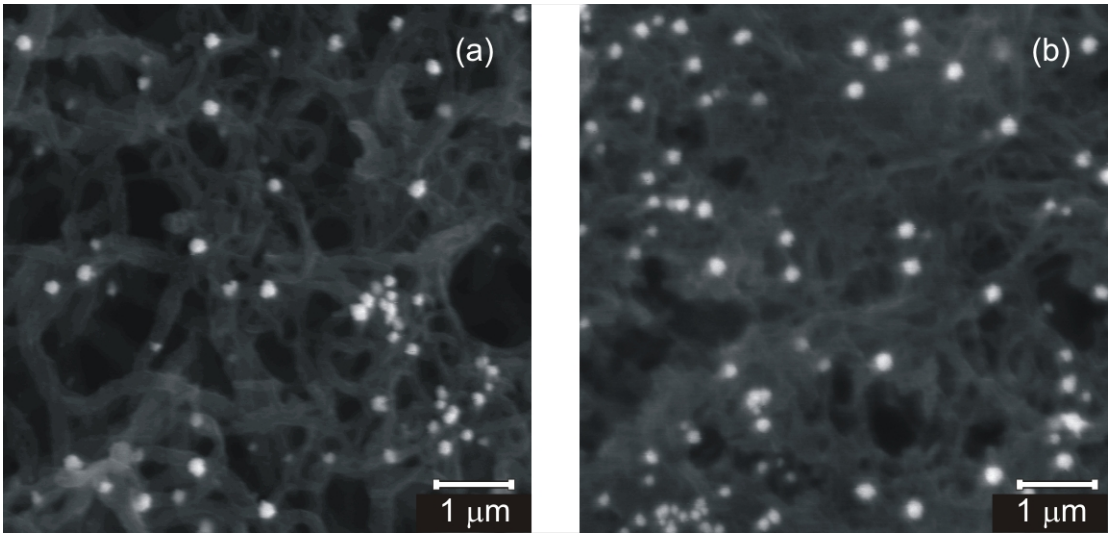

Figure 3.1 SEM micrographs of (a) PANI•HBF_4 and (b) PANI•CH_3COOH films after 6 minutes of gold nucleation from 750 μL of solution containing 0.5 m<u>M</u> $KAuBr_4$ and 2 <u>M</u> HBF_4 solution.

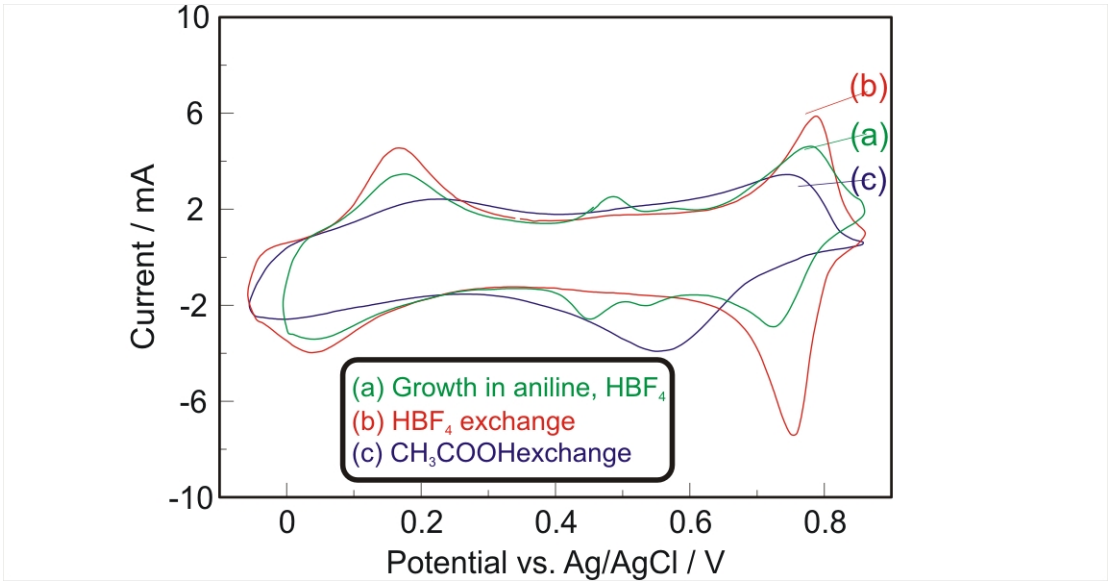

Figure 3.2 Typical final voltammograms recorded during (a) PANI growth from 0.1 <u>M</u> aniline and 2 <u>M</u> HBF_4 and cycling in (b) 2 <u>M</u> HBF_4 or (c) 2 <u>M</u> CH_3COOH. All cyclic voltammograms were recorded at 50 mV/s.

Figure 3.2 shows the CVs recorded during the final polymerization of the PANI•HBF_4 film and during the anion exchange process. It is necessary to mention here that spontaneous acetic acid exchange does not take place just by immersing the PANI•CH_3COOH film into HBF_4.[17] The voltammetric behavior of the PANI indicates that both, protons and anions of the secondary dopant acids influence the redox properties of the polymer. The ability of the anion and proton of an acid to interact with the PANI correlates with the relative strength of the acid and of the amine and imine groups within the polymer.[17] The pK_a values for the two acidic nitrogen groups within PANI have been determined to be 3.5 and 5.5 for ($-NH_2^+-$) and ($-NH^+=$), respectively.[18, 19] Therefore HBF_4, protonates both ($-NH_2^+-$) and ($-NH^+=$) groups whereas CH_3COOH protonates only the imine group. In order to satisfy the weak acid equilibrium, the acetic acid becomes trapped in the PANI film and yields the dependence of the peak potential on the concentration of the undissociated acid in the polymer.[17]

To asses the time-varied performance of the tetrabromoaurate solution as oxidizing agent for PANI•HBF_4 and PANI•CH_3COOH films, respectively, changes in a normalized ratio of the molar concentrations of $[AuBr_4^-]$ / $[AuBr_4^-]_o$ in solution (where $[AuBr_4^-]_o$ represents the initial concentration of $AuBr_4^-$) have been evaluated in figure 3.3. The system obeys Beers law within the experimental range (see inset). Figure 3.3

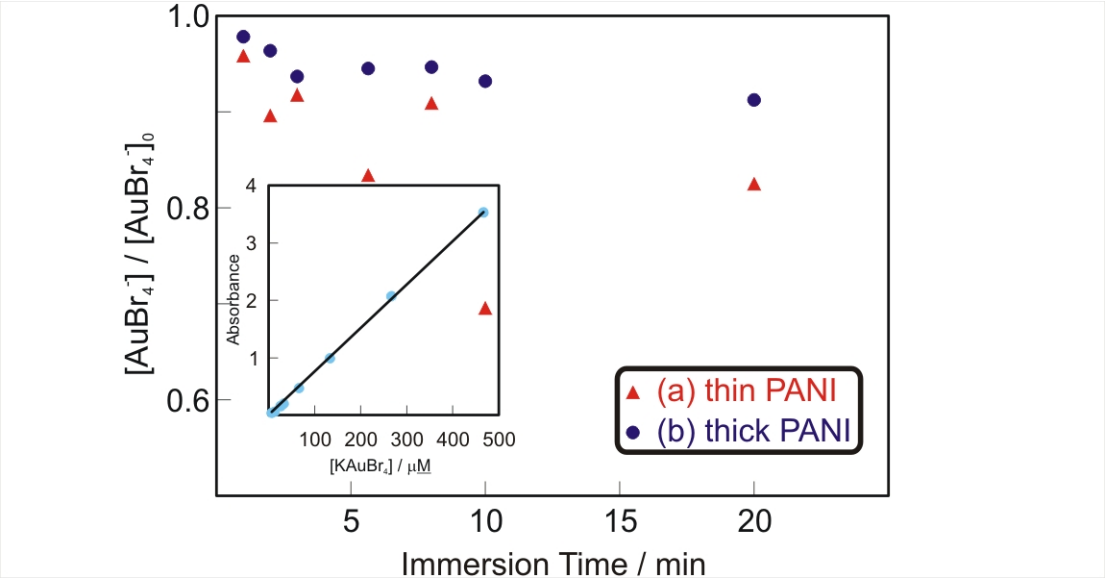

Figure 3.3 The uptake ratio of gold, $[AuBr_4^-]/ [AuBr_4^-]_o$ for (a) PANI•HBF_4 and (b) PANI•CH_3COOH acid films from 750 μL of solution containing 0.5 m<u>M</u> $KAuBr_4$ and 2 <u>M</u> HBF_4 solution as a function of immersion time. The inset is the calibration curve for the $AuBr_4^-$ species at 254 nm in the range of 5 to 500 μ<u>M</u> ($\varepsilon = 7.57 \times 10^3$ L mol^{-1} cm^{-1}).

shows that the nature of the $AuBr_4^-$ uptake by PANI•HBF_4 differs significantly from the uptake by PANI•CH_3COOH. The nucleation process is governed by electron transfer and the level of protonation of the amine and imine groups. Therefore the differences are presumably attributed to the strength of the acids accommodated within the films. This corresponds to the different morphologies illustrated in figure 3.1. The CVs of the films in 2 M HBF_4 before and after gold nucleation do not show any difference. This indicates that although the imine groups act as nucleation sites, when Au(s) is formed it no longer blocks the imine site.

Additionally, the number of proton exchange sites is not significantly affected by the gold incorporation. This is also supported by the apparent aggregation and migration of gold atoms leading to the formation of micron size clusters clearly visible in the figures 3.4 and 3.5. The electron affinity, surface properties, morphology and stabilization of the $AuBr_4^-$-imine interactions result in growth of gold clusters of different sizes. The scatter in figure 3.3 curve (a) is also attributable to the differences in the acids. This will be discussed later.

3.3.2 Size distribution of gold clusters in PANI films

Figure 3.4 shows a series of histograms of Au nucleation in films of PANI•HBF_4 and PANI•CH_3COOH obtained for different immersion

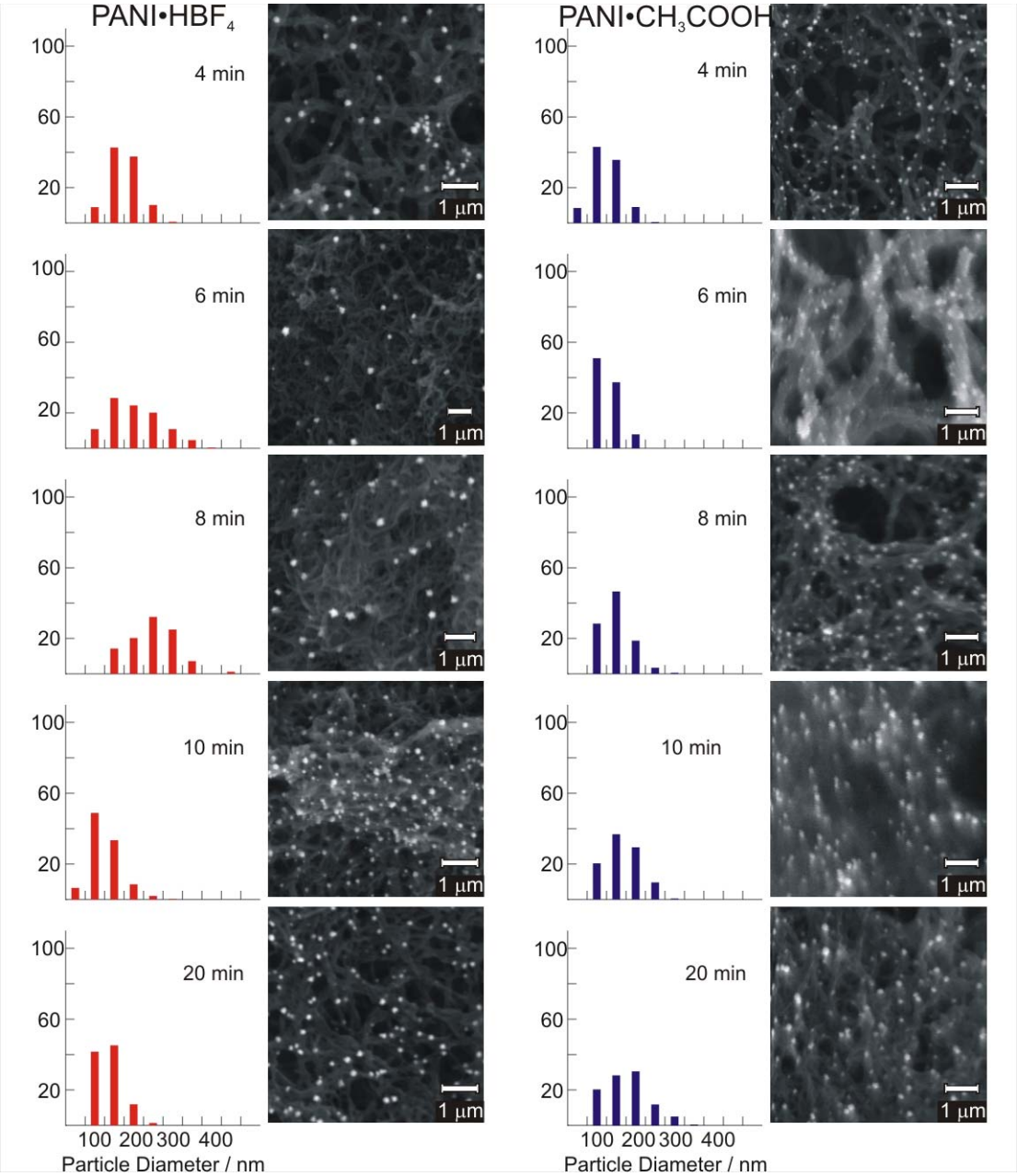

Figure 3.4 Normalized size distribution of Au metal particles in PANI•HBF_4 and PANI•CH_3COOH as a function of immersion time of 4, 6, 8, 10, and 20 minutes respectively. Representative SEM images are shown for each film in the series. The gold nucleation conditions are the same as in figure 3.1.

times. For each composite film a representative SEM image is also shown. In order to determine the size and distribution characteristics of the gold clusters in the composite PANI films several images (at least 4 to 6) were taken from several positions. The clusters were digitally analyzed and binned into different sizes. These bins were then converted to their fractional percentage of the total number of particles plotted versus the particle size.

As can be seen the from the SEM images particle diameters range from 25 nm to 400 nm, with most particles of diameter about 150 nm. The PANI•CH_3COOH films exhibit a clear trend in the growth of the particles from smaller to larger as a function of time. In the 4 minute sample, the particle diameter range is from 50 nm to 200 nm with the majority of particles peaking between 100 and 150 nm. In the 6-20 minute samples the 50 nm particles are displaced by larger particles. The 100 and 150 nm particle percentage steadily changes accompanied by distribution broadening leading to the shift in the peak maximum from 100 nm in the 4 minute sample to 200 nm in the 20 minute sample. In the 20 minute immersion sample the particle range is 100 to 300 nm. For the PANI•HBF_4 series the particles size distribution does not follow any recognizable pattern.

The adjacent SEM micrographs illustrate the morphology of the metal particles. As the nucleation process progresses more particles of

the larger size are seen presumably due to aggregation of new gold clusters between existing gold particles. This can be explained by considering the decreased number of available protonated imine sites. It may also be that the $AuBr_4^-$ prefers to nucleate on preexisting gold particles.

Morphology of gold deposits on PANI.— Figure 3.5 shows the gold particles, their sizes and shapes in four stages of growth. At 1 minute (figure 3.5a) ~50 nm particles are scattered along the surface of a PANI bundles in such a way that they appear to be partially embedded. While not spherical they have regular shape, and are well separated. At 6 minutes (figure 3.5b) the ~150 nm particles become spherical but no longer appear to be embedded in the PANI bundles. They are widely separated but some have begun to agglomerate, forming clusters groups. At 30 minute (figure 3.5c) the 400 nm particles have taken on irregular shape and have begun to cluster. They appear to simply rest on the surface of the bundles. The detail of the “rosette” shape is shown in Fig 3.5d. It is evident that the nucleation and growth of the Au particles in PANI matrix is much more complex process than was initially anticipated.

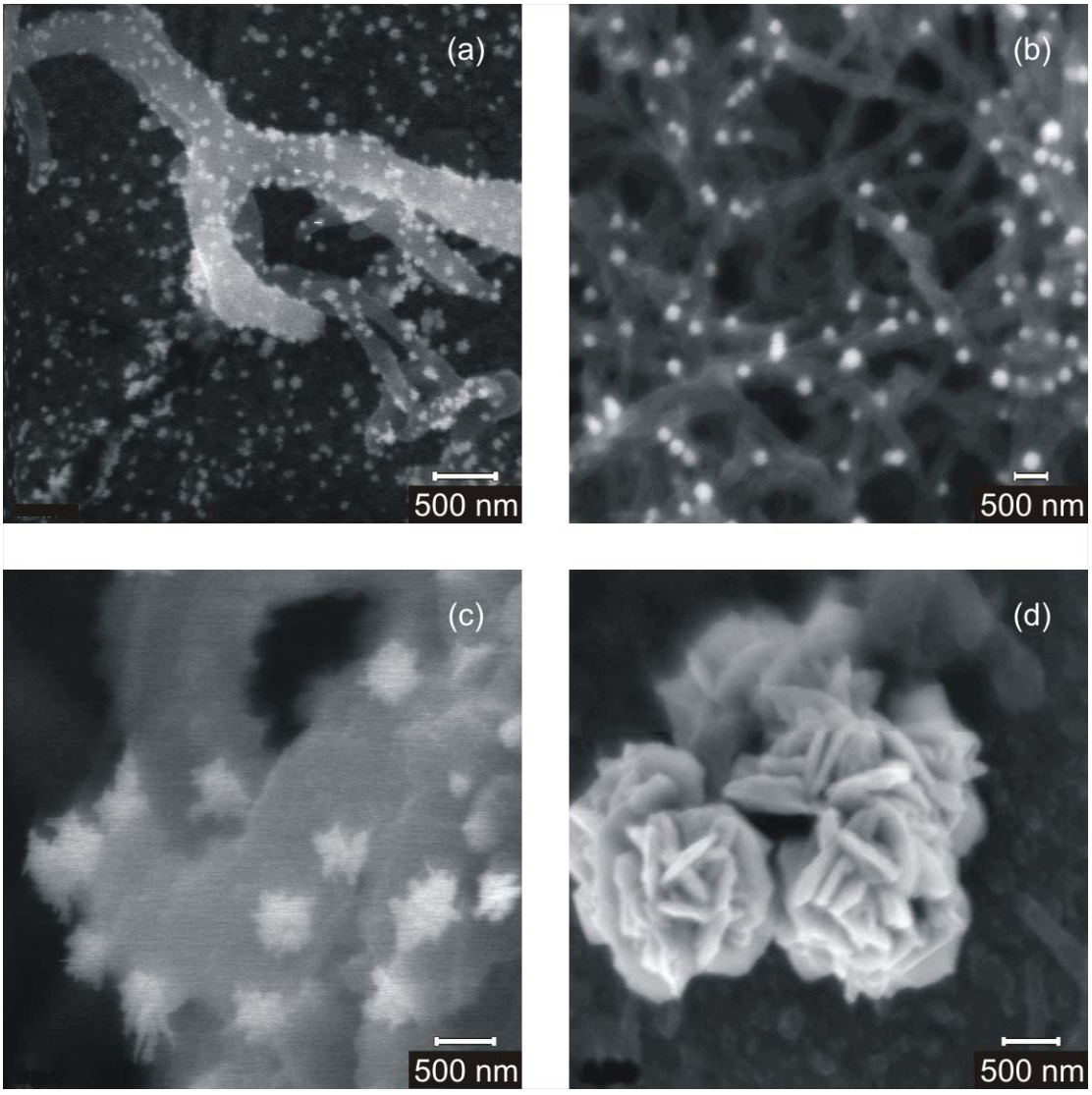

Figure 3.5 Observation of the Au particle nucleation and growth obtained by SEM for PANI•HBF_4 films. The immersion times for the images were (a) 1 min, (b) 6 min, (c) 30 minute and (d) overnight. The gold nucleation conditions are the same as in figure 3.1.

3.3.3 Electron affinity of the PANI gold composites

Figure 3.6 shows the correlation between the work function (WF) of the composite film (measured by Kelvin Probe) and the amount of gold incorporated. For all films the changes in the gold mass were determined from changes in solution concentration of the $KAuBr_4$ as mentioned above (see figure 3.2). The low correlation coefficient (R^2 = 0.24) between WF and gold mass uptake in the PANI•HBF_4 films (curve a) can be explained by lack of reproducibility in WF of the initial material, even before its exposure to $AuBr_4^-$. As observed previously by us[17], this is caused by an unknown and irreproducible amount of the residual strong acid remaining in the film. The amount of residual acid depends on the difficult to control washing procedure. Any ambient humidity change then, can give rise to a large change in the acid doping (and therefore the WF) of the film.

The situation is entirely different in the case of weak acids such as acetic because they act as a buffer.[18] For instance, more correlated data (R^2= 0.75 and 0.91) were obtained for two different PANI•CH_3COOH films (curves b and c). Curve (b) represents a PANI film grown to a fixed number of cycles (150) which resulted in films of different thicknesses while curve (c) represents a film grown to a nominal constant current density (for details see experimental section). All films grown under these conditions had nearly identical final CVs (not shown). The

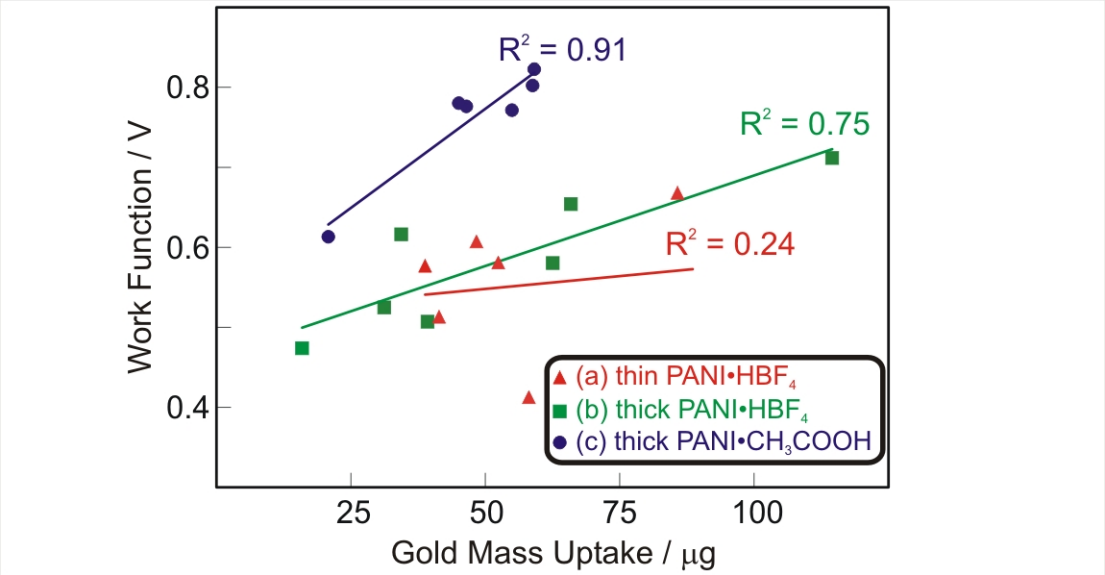

Figure 3.6 Relates the work function to gold mass uptake for PANI•HBF_4 curve (a) and PANI•CH_3COOH curves (b) and (c). Curve (b) represents a PANI film grown to a 150 cycles while curve (c) represents a film grown to a nominal constant current density at the 0.12V (vs. reference) peak during the positive potential sweep as shown in figure 3.2a. The gold nucleation conditions are the same as in figure 3.1.

correlation coefficient for curve (b) was determined to be R^2= 0.75 and for curve (c) R^2 = 0.91. This demonstrates that changes in film thickness strongly influence the nucleation rate. The variation in the state of the surfaces makes the sample-to-sample correlation of WF measurements with Kelvin Probe notoriously difficult. For this reason we consider the correlation achieved in the series of PANI/Au materials presented in figure 3.6 curve (c) as satisfactory.

3.4 Conclusions

The growth of polymer-metal nanoclusters is a general redox process that occurs between conducting polymers and metal halide complexes. In unpublished work this lab has produced PANI•Au from $AuBr_4^-$ and $AuCl_4^-$. Additionally, PANI•Pt, PANI•Ir, PANI•Ni, PANI•Pd, PANI•Fe and PANI•Cu composites have been produced. To obtain the best results a system might be found wherein the reduction process does not occur spontaneously and for which a cyclic or pulse voltammetry train could be employed to supply electrons to the metal anion at the proper potential.[20]

PANI•Au composite films can be prepared with a range of work functions. The morphology of these films is a dense network of PANI fibrils or bundles with small Au spherulites attached along their surface. The cluster surfaces are largely open to solution and may be further

functionalized by attaching thiol[21] or amine[22] terminated compounds onto the Au surface. The purpose of modification is to create specific binding sites for sensing purposes.

The nucleation and growth of the gold particles is a complex interplay between the initial film properties and the nucleation and diffusion of the gold anion in solution. On the films side, the morphology of the film changes as a function of thickness. Each film progresses through a compact flat layer (< 300 nm), through fibril nucleation, then to continued growth primarily though fibril extension. Additionally, the initial oxidation state and the identity of the incorporated acid will affect which nucleation sites are available and how readily electrons may be transferred to reduce the $AuBr_4^-$. On the solution side, the cluster growth is largely nucleation and diffusion controlled. Incoming gold anions will reduce preferentially at previously formed clusters at the expense of new cluster formation at PANI chains. Both processes occur simultaneously thus the broadening of the distribution curves at the same time as the average size shifts to higher values (figure3.4b).

To acquire the best results, it is necessary to exchange the initial strong acid from which the films were grown for a weak acid with appropriated pK_a and buffering capacity. By growing films to the same value of charge the process effectively controls the number of electrochemically active sites available for either ion exchange (during

the course of the potential sweep in cyclic voltammetry) or $AuBr_4^-$ complexation and eventual reduction to Au^o along on the PANI chains.

In regard to the measurement of WF changes in the PANI upon addition of Au particles, the shape of the particles must be considered. For a system in which the particles are spherical a model can be proposed in which the gold spheres abstract electron density from the PANI and distribute the charge evenly about their surface. This changes the composite work function because the electrons are more closely bound to the gold clusters, changing the Fermi level of the system. However, with complex shapes such as those in figure 3.5d it is difficult to propose a model which accounts for the changing surface energy of the particles and therefore the relative electron affinity of the gold versus the PANI and thus the overall work function. Nevertheless, the goal of producing thin, electrically and chemically stable polymer-metal composites with a range of work functions has been accomplished.

3.5 Acknowledgements

The authors would like to thank the Electron Microscopy Center of The Georgia Institute of Technology directed by Z.L. Wang. This work was supported by the National Science Foundation, Grant No. CHE-9816017.

3.6 Summary

This chapter discusses electrochemical/chemical synthesis of PANI/Au composite thin films as well as their properties. The PANI films are grown electrochemically followed by the subsequent spontaneous reduction of tetrabromoaurate into metallic gold within the polyaniline film. It was seen via SEM that with increasing immersion time, the gold cluster sizes increased and the work function (as measured by Kelvin Probe) of the composite increased. The correlation between increasing gold amount/cluster size is seen to improve with the use of thick PANI films which had been doped by a weak acid. This improvement in correlation is attributed to the buffering capacity of the acid doping concentration in the films of a weak vs. a strong acid.

3.7 References

1. G. Schmid, G.L. Hornyak, *Solid State and Material Sciences*, **1997**, *2*, 204.
2. J. Janata, M. Josowicz, *Nature Materials*, **2**, 19 (2003).
3. K. Domansky, Jing Li, J. Janata, *J. Electrochem. Soc.*, **1997**, *144*, L75.
4. Jeong-Hwan Kim, Joung-Hwan Cho, Geun Sig Cha, Chi-Woo Lee, Hyong-Bai Kim and Se-Hwan Paek, *Biosensors and Bioelectronics*, **2001**, *14*, 907.
5. D. C. Trivedi, in *Handbook of Organic Conductive Molecules and Polymers: Synthesis and electrical properties Vol. 2. Conductive Polymers: Synthesis and Electrical Properties*, H. S. Nalwa, Editor, p. 550, John Wiley & Sons, New York, NY, **1997**.

6. D. J. Strike, N. F. De Rooij, M. Koudelka-Hep, M. Ulmann, J. Augustinski, *J. of Applied Electrochemistry*, **1992**, *22*, 922.

7. F. Fiçicioğlu, F. Kadirgan, *J. Electroanal. Chem.*, **1997**, *430*, 179.

8. A. G. MacDiarmid, *Synth. Met.*, **2001**, *25*, 11.

9. M. Yamamura, K. Sato, T. Hagiwara, *Synth. Met.*, **1991**, *41*, 439.

10. Guofeng Li, M. Josowicz, J. Janata, *Electrochem. Solid-State Lett.*, **2002**, *5*, D5.

11. D.W. Hatchett, M. Josowicz, J. Janata, D.R. Baer, *Chemistry of Materials*, **1999**, *11*, 2989.

12. K. L. Tan, B.T.G. Tan, E.T. Kang, K.G. Neoh, *J. Phys. Chem.*, **1991**, *94*, 5382.

13. E.T. Kang, K.G. Neoh, K.L. Tan, *Polymer*, **1996**, *37*, 925.

14. Hong-Shi Li, M. Josowicz, D.R. Baer, M. Engelhard, J. Janata, *J. Electrochem. Soc.*, **1995**, *142*, 798.

15. M. Josowicz, Hong-Shi Li, K. Domansky, D. R. Baer, *Electroanalysis*, **1999**, *11*, 774.

16. E. T. Kang, K. G. Neoh, S. W. Huang, S.L. Lim, K. L. Tan, *J. Phys.Chem.B*, **1997**, *101*, 10744.

17. L. I. Daikhin, M. D. Levi, *Synth. Met.*, **1992**, *52*, 367.

18. D.W. Hatchett, M. Josowicz, J. Janata, *J. Phys. Chem B*, **1999**, *103*, 10992.

19. C. Menardo, M. Nechtschein, A. Rousseau, J. P. Travers, *Synth. Met.*, **1998**, *25*, 311.

20. S. Gorer, R. M. Penner, *J. Phys. Chem. B*, **103**, 5750, (1999).

21. H. Lee, Z He, C. L. Hussey, D.L. Mattern, *Chem. Mat.*,**1998**, *10*, 4148.

22. R. Holze, *Electrochim. Acta*, **1993**, *38*, 947.

CHAPTER IV

ELECTROCHEMICALLY CONTROLLED POLYANILINE/GOLD COMPOSITE SYNTHESIS

4.1 Introduction

This chapter outlines a novel technique for electrochemical growth of thin (<1 μm) PANI films with electrochemically controlled growth of gold nanoparticles. The typical particle size is between 1 and 10 nm which means that TEM is the most appropriate technique for imaging the particles. TEM analysis requires freestanding films. The films were characterized by TEM and electrochemical methods.

Creating smaller particles is interesting for a number of reasons. First, it should be possible to see a much larger work function (WF or Φ) effect with smaller particles because of two contributions, the smaller particles size/larger surface area and because of the quantization effects that occur in particles whose size is on the order of the particle-in-the-box electron wavelength. Using the solution phase reduction methods from Chapter 3, presented a number of problems. The concentrations that could be used for experiments were limited because they had to be

concentrated enough to see the minor peak in the $KAuBr_4$ solution, λ_{max} = 254 nm). Also, there was good evidence to suggest that smaller size particles formed than would be visible by SEM (~20 nm)[1]. However, no suitable methods were available to microtome or otherwise remove as grown electrochemically grown PANI films for TEM examination. An attempt was made coat either gold or copper TEM grids with platinum which would not interfere with gold characterization and could be used for electrochemical PANI growth. Purchase of these grids was prohibitively expensive. Satisfactory platinum films were difficult to achieve and growth of PANI on these grids proceeded primarily on the metal lines that formed the grid. The film would rarely span the grid gaps and even when this occurred film growth was too thick for electron penetration. The subject of this chapter is the development of the method for creating films with small cluster sizes appropriate for TEM analysis.

4.2 Experimental

4.2.1 Chemicals and Solutions

Tetrafluoroboric acid, HBF_4 (Aldrich, 44 wt %, 20,793-4), potassium chloride, KCl (J.T. Baker, 99.9%, 3040-01), Bright Electroless Gold (Transene Company), aniline, $C_6H_5NH_2$ (Aldrich, 99.9%, 13,293-4) were used as received. The gold solution was used for galvanostatic

deposition, not for electroless deposition. All solutions were prepared using 18.3 MΩ•cm water from a U.S. Filter Modulab Water Systems filter. Buehler polishing pads and various size alumina powders were used in water slurries for electrode polishing.

4.2.2 Electrochemical Apparatus and Conditions

All electrochemical measurements used a Solartron 1287 Electrochemical Interface potentiostat/galvanostat controlled via Scribner Associates Corrware® software v.2.7. The experiments were performed with a one-compartment, three-electrode cell. The potential of the working electrode was always referenced against a 1 M Ag/AgCl electrode with 1 M KCl filling solution and a 1 M KNO_3 junction unless otherwise stated. The counter electrode was 0.5 mm platinum wire approximately 0.5 m long with an area exceeding the immersed area of the working electrode by more than a factor of ten. The primary working electrode was a single Pine Instruments 5.0 mm diameter platinum disc electrode. Bioanalytical Systems (BAS) platinum disc electrodes (0.75 mm diameter) were used for some experiments.

4.2.3 Transmission Electron Microscopy

A portion of the freestanding composite was placed on a copper grid, dried in a vacuum pumped desiccator, and mounted in a TEM grid holder. Imaging mode micrographs of the composites were recorded on

large format film negatives (Kodak SO-163, 3x4 inch). Diffraction mode images were also made but were used only for verification of gold crystallinity, which was also visible in high resolution imaging mode. The instruments used were a Hitachi HF2000 with a field emission gun poised at 200 kV and a 400 kV JEOL 4000EX field emission gun TEM.

4.2.4 Image Analysis

The TEM negatives were scanned using a backlight scanner to produce digital images. The digital images were analyzed using NIH ImageJ v1.31 to obtain particle size information. Particle size histograms were graphed in Microsoft Excel.

4.3 Results and Discussion

4.3.1 Freestanding Polyaniline/Gold Film Preparation

Freestanding composite films of PANI matrix and gold nanoclusters were grown in a seven step process as shown in figure 4.1 (seventh step not shown). All but the fourth step (figure 4.1d), were standard steps. Each step is described briefly below and then the fourth step, stripping, in more detail.

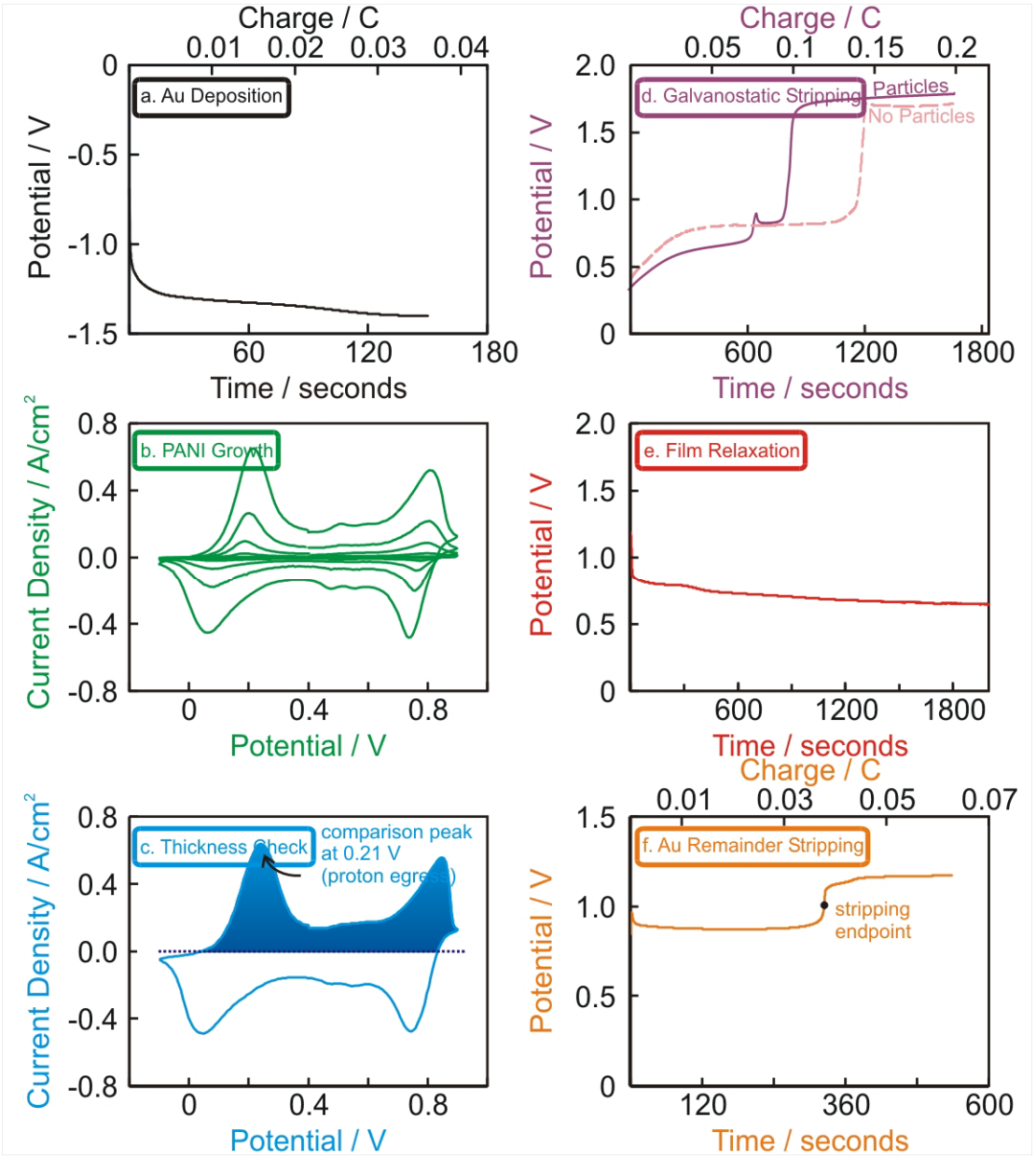

Figure 4.1. PANI/Au composite preparation steps. (a) Galvanostatic gold deposition (b) Cyclic voltammetric PANI growth, 50 mV/sec, 0.1 M aniline & 2 M HBF4, (c) Cyclic voltammetric thickness check, 50 mV/sec, 2 M HBF4, (d) Galvanostatic stripping in 2 M HBF4 at 600μA/cm².(e) Film relaxation (f) Residual gold stripping which is performed if necessary after the film blow off.

4.3.1.1 Gold Deposition

The initial step was galvanostatic gold deposition, figure 4.1a. The deposition process was $Au^{3+} + 3e^- \rightarrow Au(s)$, thus the amount of gold deposited was: $mol_{Au} = i \cdot t \cdot F^{-1} \cdot n^{-1}$,

where i is current, t is time, F is Faraday's constant and n is the number of electrons involved in the process. With 100% efficient gold reduction, a typical deposition time of 150 seconds yielded a 65 nm gold layer thickness (125 nanomoles) on the 5.0 mm diameter electrode.

4.3.1.2 Polyaniline Film Growth

Thin (< 500 nm), high density, visually flawless PANI films were grown on the Pt/Au surface by cyclic voltammetry (figure 4.1b, every 20th cycle shown) then gently rinsed with deionized water. Film thickness had to be controlled within the range from 250-500 nm. Most films fell at 300 nm but there was some interest in examining thinner and thicker films for determining the thickness effect on electrochemistry. This was important because films that were too thin lacked cohesion and could not be manipulated onto TEM grids while electrons from the TEM would not pass through films that were too thick. The potential of the oxidation peak at 0.21 V was monitored and growth terminated at a predetermined current density. The appropriate thickness was reached at about 120 scans from a fresh growth solution.

4.3.1.3 Thickness determination

The electrodes were placed in 2 M HBF_4 and the oxidation peak current density at 0.21 V compared to the standard (figure 4.1c). If necessary the electrodes were placed back into the growth solution and then retested. Integration of the area under the oxidation curve was then used to calculate the number of moles, or more accurately the activity, of PANI repeat units according to the equation:

$$mol_{PANI\_units} = Q \cdot F^{-1} \cdot n^{-1},$$

where Q is the charge from the integration area. There are 4 benzenoid/quinoid units per repeat unit of PANI and each unit of four can interact with two BF_4^- ions. This information was used to calculate the PANI/Au molar ratio assuming the univalent BF_4^- is responsible for the electric current.

4.3.1.4 Stripping, Relaxation and Blowoff

After charge measurement, each film was placed into an electrolyte solution and constant oxidation current was applied. The electrochemical responses were found to be reproducible but were also found to depend on concentration, composition, pH and stripping rate. Representative curves are presented in figure 4.1d. A number of electrolyte solutions including HCl, NaCl, KBr, KNO_3, HNO_3, HBF_4, and sodium citrate stripping solutions were investigated. The stripping

response in KCl neutral pH solutions was the primary focus. In this electrolyte, gold oxidation to tetrachloroaurate takes place followed by [$AuCl_4^-/PANI^+$] salt formation (K_{eq} ~ 10^{10}) and a subsequent redox reaction which yields metallic gold according to the equations:

$Au + 4Cl^- \rightarrow AuCl_4^- + 3e^-$ $E > 0.80$ V

$AuCl_4^- + PANI^+ \rightarrow [AuCl_4^-/PANI^+]$ $E > 0.65$ V

$[AuCl_4^-/PANI^{++}] + 3e^- \rightarrow Au(0) + PANI^+ + 4Cl^-$ $E_p > 0.55$ V

This led to dissolution of most of the gold interlayer through which the PANI was adhered to the platinum surface. If a sufficient quantity of gold was dissolved, the film could be detached in a single piece by hydrogen evolution from the application of a 1-2 sec, -15 V potential pulse in a process referred to as blowoff. Between stripping and blowoff the film relaxation was monitored until it reached the open cell potential (figure 4.1e).

4.3.1.5 Residual Gold Analysis

In some instances, there was residual gold left on the working electrode after the blowoff. The gold quantity was determined by comparing the stripping endpoint time (figure 4.1f) to the average value determined as follows. Gold layers were deposited from fresh deposition solutions, rinsed in deionized water then stripped directly in 1 M KCl without growing PANI on the electrode.. The comparison to the residual

relies on the assumption that there is no residual PANI on the gold after blowoff. This assumption sometimes gave erroneously high values as could be seen in some stripping responses. Namely, the potential rose as a small amount of residual PANI was oxidized then peaked and fell back to the gold oxidation potential. The error is difficult to estimate but is likely on the order of ~ 5-10%.

It has been shown that cycling the voltage of a PANI film from -0.1 V to 0.85V vs. SCE (saturated calomel electrode) in the presence of the Cl- ion on gold substrates induces gold complexation and dissolution[1]. Conversely, in other literature, PANI has been suggested as a corrosion inhibitor. This research will address this contradiction.

4.3.2 Electrochemical Analysis

Polyaniline films were grown repetitively as above with the stripping solution as the differentiating feature. There are many solutions for which stripping would lead to nothing more than film oxidation. The focus, then, was on cases where particle formation occurred or where it might reasonably have been projected to occur but did not. An ordinary neutral pH electrolyte, potassium chloride, serves as a good starting point to visualize the process.

4.3.2.1 Neutral pH, Chloride Solutions

The typical features of stripping in a neutral pH, high concentration potassium chloride solution are shown in figure 4.2. The inset shows the corresponding electrochemical processes in the more intuitive cyclic voltammogram features. The stripping processes can bethought of as beginning at the position of the green dot and tracing to the right along the light blue line. This line corresponds to the slope of the stripping experiment so that a peak on the CV will resemble and endpoint on the stripping curve. The CV switches potential at 0.8 V and so does not show the electrolysis, the stripping curve does not contain the reversal of current indicated by the beginning of the red curve. The stripping conditions were pH 7, 1 M KCl and 600μA/cm^2. The curve shows three apparent regions, suggesting different electrochemical processes:

Region 1 – The curve began at, or slightly above, the solution-dependent open cell potential of the PANI film then immediately began to rise as the galvanostatic stripping progressed and as electrons were removed the film began to oxidize. The film started in the half benzenoid, half quinoid emeraldine state (x~y) then progressed toward the primarily quinoid pernigraniline state (x<<y). In addition to oxidation, the negative charge removal was compensated by egress of protons incorporated during growth and chloride ingress from the

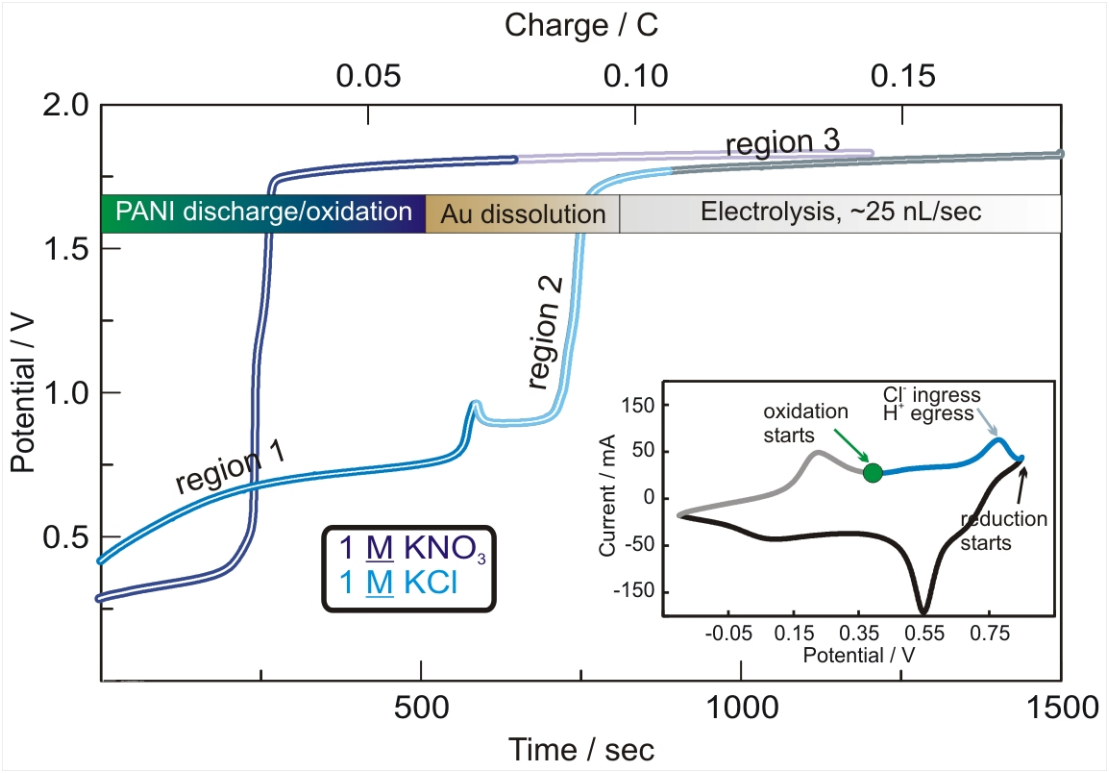

Figure 4.2 The stripping of a three layer, Pt/Au/PANI film in neutral pH, 1 M KCl. Three regions can be seen. Region 1: Stripping initiation, ion ingress/egress and PANI oxidation; Region 2: Gold oxidation and dissolution as $AuCl_4^-$ complex formation; Region 3: Electrolysis that lasts indefinitely. No $AuCl_4^-$ forms in this region. The KNO_3 curve is shown for comparison. Inset shows the point at which stripping begins when in a comparative cyclic voltammogram curve.

stripping solution. In response, the three electrode layers became nobler and the potential to withdraw additional charge continued to increase.

Region 2 – At approximately 0.75 V the slope of the curve increased sharply, analogous to a titration endpoint. As can be seen from the comparison with the 1 M KNO_3 stripping curve, an analogous electrolyte to the KCl, this trend might have been expected to continue in the absence of a complexation agent. That is, in the KNO_3 case, when there was no more film to oxidize, and no agent to complex with the gold, the potential rose quickly toward the electrolysis potential. Note that the solutions had different endpoint potentials but that the electrolysis potential was approximately the same. In the KCl case the gold corrosion began as the chloride ions which had been attracted to the gold surface began to complex with the oxidized gold species forming tetrachloroaurate and releasing three electrons. This process continued until the potential reached about 1.0 V and then peaked and fell to about 0.85 V and remained flat for a time. This was an unexpected result and suggested a few possibilities. Either at this point charge was temporarily easier to extract or some charge was being injected back into the film or film conductivity increased. The potential flattened as this process reached steady state and then rose rapidly as all the gold was fully oxidized and the underlying platinum, which had a higher oxidation potential was exposed.

Region 3 – The slope of the potential rate rose rapidly at this second endpoint to 1.8 V and the reaction with the next lowest potential was water electrolysis which occurs at the platinum surface. The potential *typically* remained constant indefinitely (at least up to 3 hours) but occasionally fluctuated on the order of 0.5 V after electrolysis began. This was most likely due to oxygen bubble formation at the platinum surface. A detailed schematic of the preparation process is represented by figure 4.3.

Stripping Time vs. Stripping Charge – The curves above use time as the independent axis, but may be plotted with charge instead. That is, $Q = i \cdot t$ because the stripping rate is constant. Figure 2 is also plotted with charge as the secondary axis. The colored band relates the charge abstracted from the film to the specific electrochemical process. The first portion represents the charge from the cyclic voltammogram integration, about 0.6 Coulombs. When the quantity of charge abstracted from the film reached this value, the film was fully oxidized to the pernigraniline state and the potential began to rise quickly. In this stripping experiment, the gold interlayer was completely removed and when the quantity of charge abstracted matched that used for gold deposition, the stripping was completed and the remaining reaction was electrolysis. Note that approximately

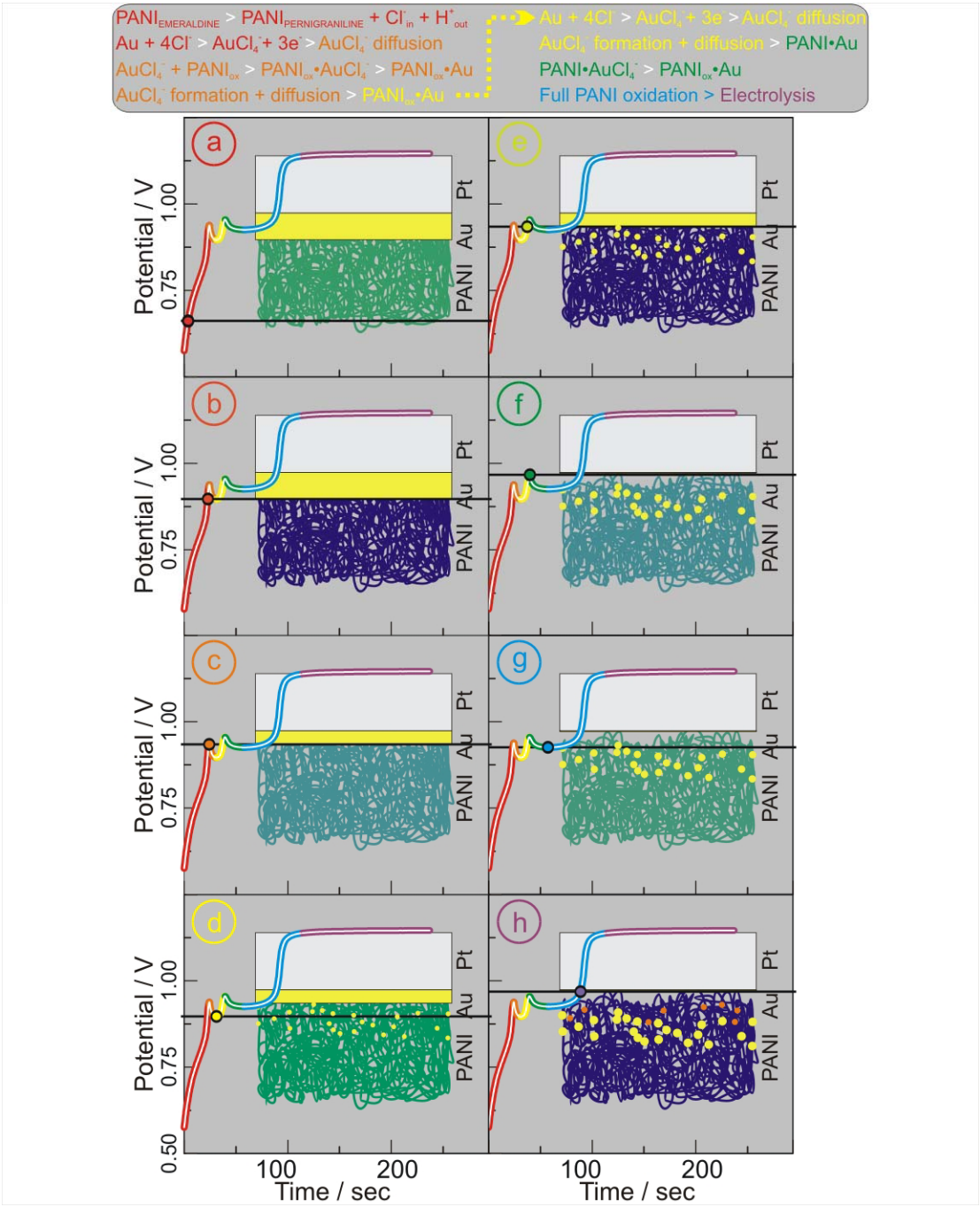

Figure 4.3 Gold dissolution and particle formation schematic.

25 nL/sec of O_2 gas was generated during electrolysis according to Faraday's law.

Figure 4.3 shows a detail schematic for the electrochemical stripping mechanism outlined above. This is overlaid by the stripping trace of a very thin film (<50 nm) stripped in 3 M KCl. Although this film appeared to have an additional peak, this peak, in fact occurs in all the chloride stripping experiments but is normally unresolved. A black line shows the position of electrochemical front relative to the solution/PANI and PANI/Au interfaces. The stripping curve changes color to indicate a region where a specific process prevails. The PANI, indicated by the spaghetti-like lines also changes color based on the conductivity at that stage. Green represents a more conducting state, blue a more insulating state. The drawing is not to scale and the colors are artificial. See section 4.3.3.6 for a more detailed explanation of the schematic.

4.3.2.2 Stripping Characteristics

The time (or alternately the charge) that would elapse before the appearance of the peak in the stripping plot was related to film thickness. The value could be calculated if the PANI thickness was known. These time values were dependent on the stripping current density but independent of the chloride concentrations in the range of 1-

3 M KCl. The responses of 15 films of varying thickness that were stripped at different rates and in solutions of either 1 or 3 M KCl are shown in figure 4.4a. For simplicity, the films thicknesses were normalized to the thinnest film. These films were produced for the purpose of elucidating the stripping electrochemistry rather than for TEM studies, thus a range of thicknesses were used.

The plot shows the normalized thickness versus peak onset time as discussed above. As can be seen from the overlaid line, the values follow a linear trend passing nearly through the origin. The triangles, squares and diamonds represent stripping at 400, 600, and 1200, $\mu A/cm^2$; respectively. The linearity of the data confirms that stripping rate is proportional to current. The 1 M KCl concentrations are denoted by the filled shapes while the unfilled shapes are from 3 M KCl. Gold particles were seen to form in these films and it was postulated that the Cl^- concentration would affect the peak appearance time and that two stripping calibration curves would result from the two concentrations. Although this may be true at lower concentrations, it did not appear to be the case for this concentration range. It was concluded that the peak appearance marked the completion of film oxidation, but that gold oxidation, a process dependent on the chloride concentration, was not involved. The BAS electrodes were used for these experiments. Figure 4.4b shows the same type of experiments but in this case all parameters

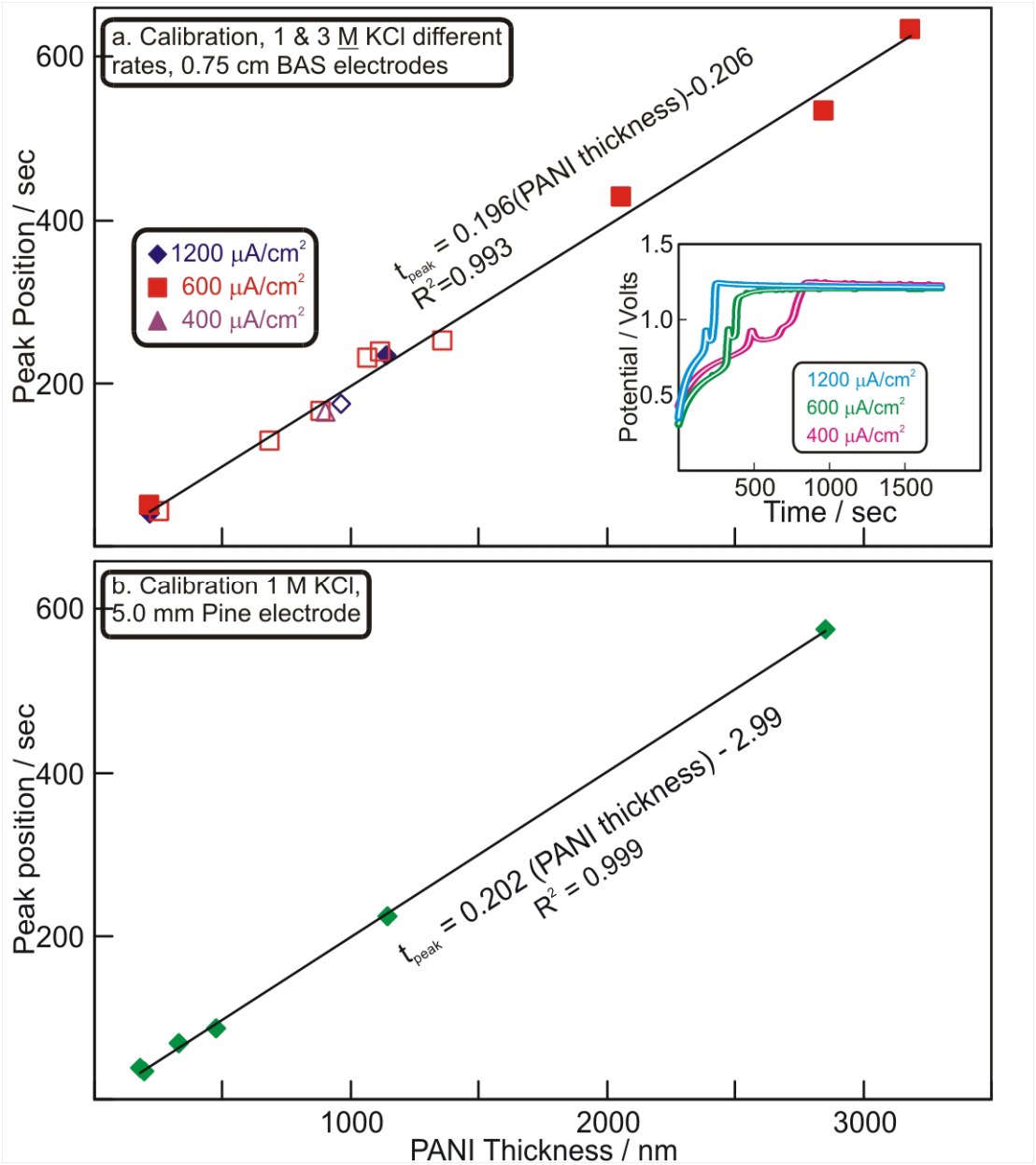

Figure 4.4. Peak appearance time versus film thickness for (a) a variety of films grown to different thicknesses, stripped in different solutions and at different stripping rates. Inset shows a related trend in films with constant thickness, the peak appearance time is linearly related to stripping rate. (b) The same curve is for the 0.50 cm disc electrodes but keeps variables besides film thickness constant.

besides film thickness were held constant and the peak appearance time measured. The 5.0 mm Pine electrode was used for these experiments.

The plot in figure 4.4a effectively assumes a constant stripping rate (via assumption). In contrast, the inset of figure 4.4a shows the stripping potential vs. time curves for three films of nearly constant thickness stripped at 400, 600, and 1200 $\mu A/cm^2$. The 1200 $\mu A/cm^2$ curve reached the oxidation endpoint peak in half the time of the 600 $\mu A/cm^2$ curve. The 400 $\mu A/cm^2$ curve took three times as long. The inset, then, shows that the stripping time was linear with stripping rate. These experiments were also performed using the BAS electrodes.

4.3.2.3 Composite Characteristics

While insight into the stripping electrochemistry is important, the stated purpose was to produce PANI nanofiber/gold nanoparticles composites. Some typical end results of the stripping process are shown in figure 4.5. Figure 4.5a shows a portion of a PANI/Au nanocomposite film mounted on the center of a copper TEM grid. The films must be retrieved from solution and carefully placed on the grids. Typically there was some solution residue and some small PANI/Au composite particulate left dried on the grid. This was the origin of the dark area around the film marked by the orange ellipse. Figure 4.5b shows a high resolution TEM micrograph of the film on the in figure 4.5a taken

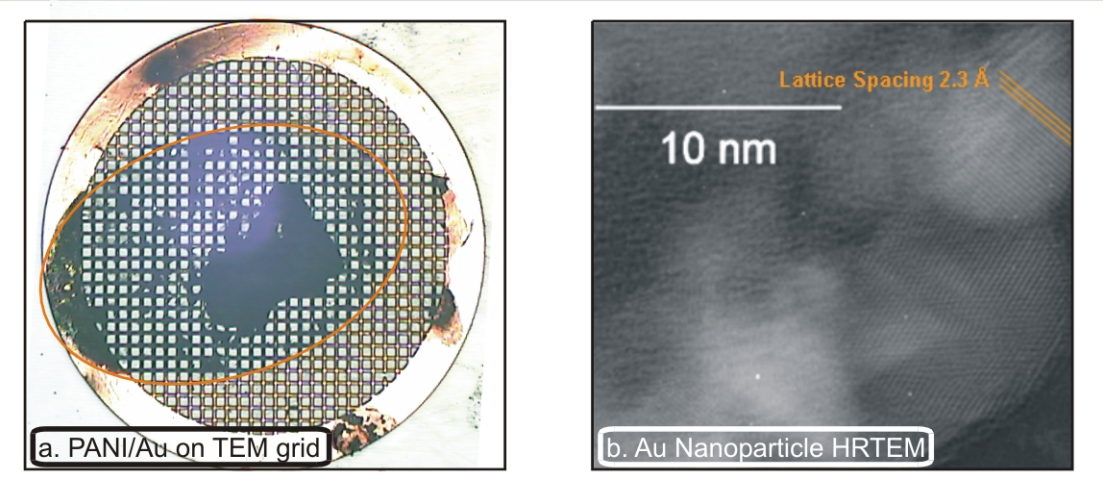

Figure 4.5 (a) Typical PANI/Au composite film mounted on a copper TEM grid. Each grid line is 100 microns center-to-center. (b) Typical cluster size and lattice characteristics.

originally at 1.0 million times magnification then digitally scanned. The crystallinity and lattice spacing of a 6 nm particle can be seen in the upper right hand corner. The 7.5 nm particle in the lower right hand corner shows particle misalignment with corresponding Moiré fringing. This misalignment appeared infrequently but understanding its cause was important to elucidating the formation mechanism. The details of how the small particle size and nanofibers interact will be the subject of chapter 5.

4.3.3 Particle Formation Dependencies

4.3.3.1 Stripping Rate

A series of stripping experiments and the composites produced are shown in figure 4.6. The stripping curves are shown here in order to highlight the relationship between the particle sizes and the different stripping conditions. The histograms show the particle size distribution in nm as a percentage. The micrographs show a wide area to maximize the number of displayed particles. The 400 $\mu A/cm^2$ stripping curve in figure 4.6a has particles ranging from 8-15 nm with ~ 70% of particles falling between 11-13 nm. Figure 4.6b shows the 600 $\mu A/cm^2$ stripping results. Here, the most common particle size is 4 nm with approximately 75% of particles falling between 3-5 nm. Figure 4.6c shows stripping at 1200 $\mu A/cm^2$ which yielded a broader distribution

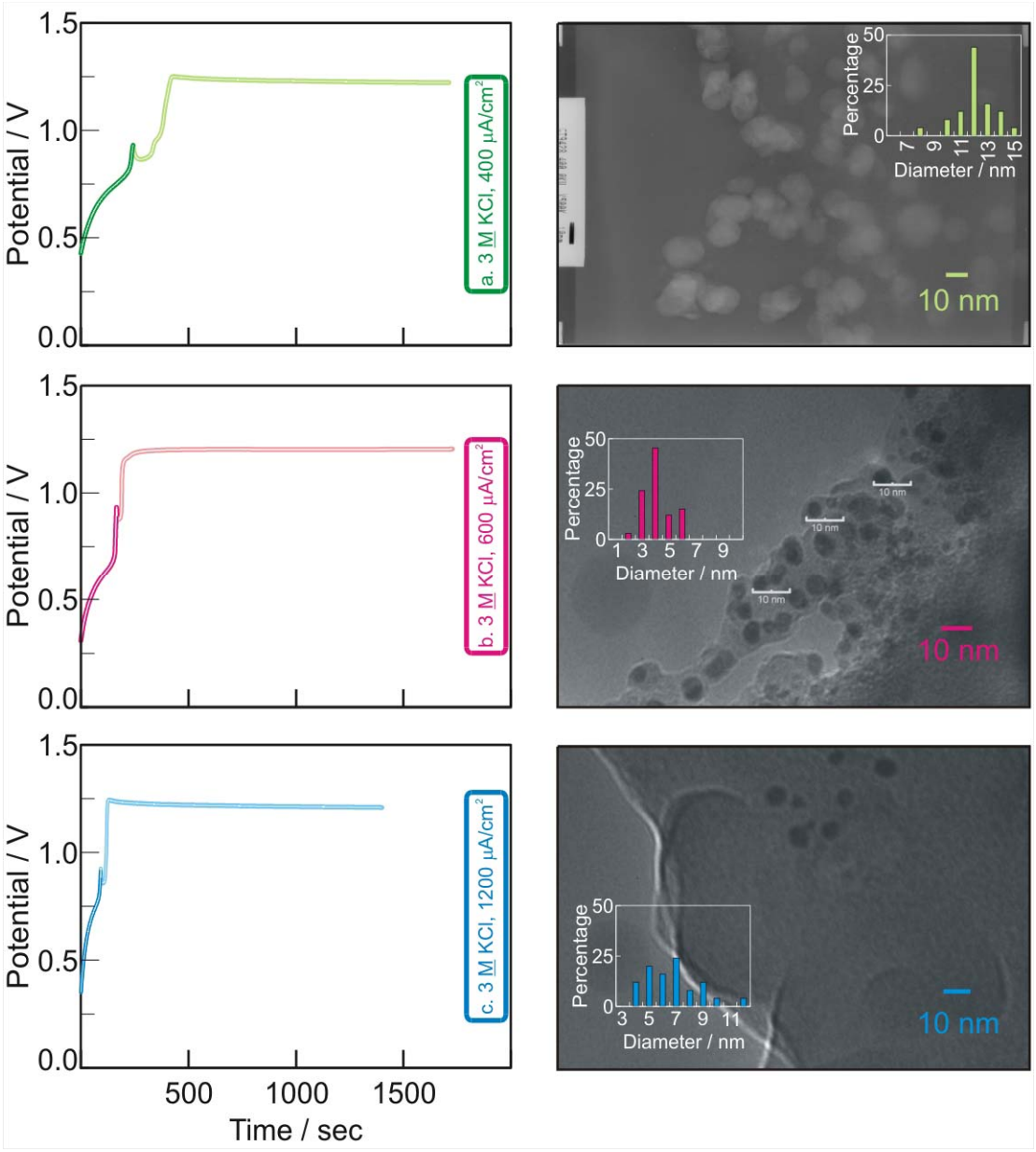

Figure 4.6. Stripping curves and TEM results for Pt/Au/PANI in (a) 3 M KCl stripped at 400 μA/cm², (b) 3 M KCl stripped at 600 μA/cm², and (c) 3 M KCl stripped at 1200 μA/cm².

with the most numerous particle size being 7 nm and 90% of particles falling between 4 and 9 nm. Based on these results, a stripping current density of 600 $\mu A/cm^2$ was used for all subsequent experiments.

While the particle density is difficult to quantify, a subjective statement should be made about it. The final composite characteristics are dependent on both the quantity and size of the particles. This is particularly true because the nanoscale influences from the gold are often a non-linear function of particle size, rather the smaller the particle size, the larger the effect. Each micrograph only captures a small fraction of the overall picture, so that particle density can only be estimated. In addition, usually, the smallest particles that can be captured on film are about 1-1.5 nm. This is due to low contrast and interference between the particle lattice and the PANI film. Additionally PANI is paramagnetic which necessitates constant microscope astigmatism adjustment on the order of the time necessary to expose the film. Thus, if a large portion of the particles are below 1 nm they will not be seen on the micrograph. It is possible, then, that some films will have a small number of relatively large particles say 25-100 nm but will also have a large number of small particles below the imaging limit.

4.3.3.2 Neutral pH Halides and Ammonium Citrate Capping

Figure 4.7 shows the dependence on the electrolyte solution of both the electrochemical stripping trace and on the resulting particles size. Note that the images shown are lower magnification on the left (LRTEM) and higher magnification on the right (HRTEM). Figure 4.7a shows the familiar stripping in 1 M KCl. This stripping environment regularly gave particles < 10 nm. In this case, the particles ranged from 2-8 nm with 5 nm as the most prevalent size and about 65% of the particles fell within 4-6 nm. The particles appeared to be evenly distributed throughout the film (figure 4.7a LRTEM) which was not always the case under other stripping conditions. The color change of the curve indicates the predicted time for complete oxidation. The reaction in 1 M KBr which is shown in figure 4.7b is:

$$Au + 4Br^- \rightarrow AuBr_4^- + 3e^- \quad \ldots\ldots\ldots\ldots\ldots\ldots\ldots\ldots\ldots\ldots\ldots\ldots\ldots\ldots\ldots\ldots E > 0.60\ V$$

This stripping produced a narrow distribution range from 4-9 nm with 6 nm as the most prevalent size and 88% of particles fell between 5-7 nm. There are significant differences in these stripping traces. First, the starting stripping potential was 0.37 V compared to 0.45 V for KCl. Second, and more notably, although there are two distinct regions where the slope plateaued, then increased, there was no “peak” as in the KCl stripping. The curve flattened at about 0.65 V and again at 0.75 V but progressed monotonically upward and stabilized at 0.88 V. While

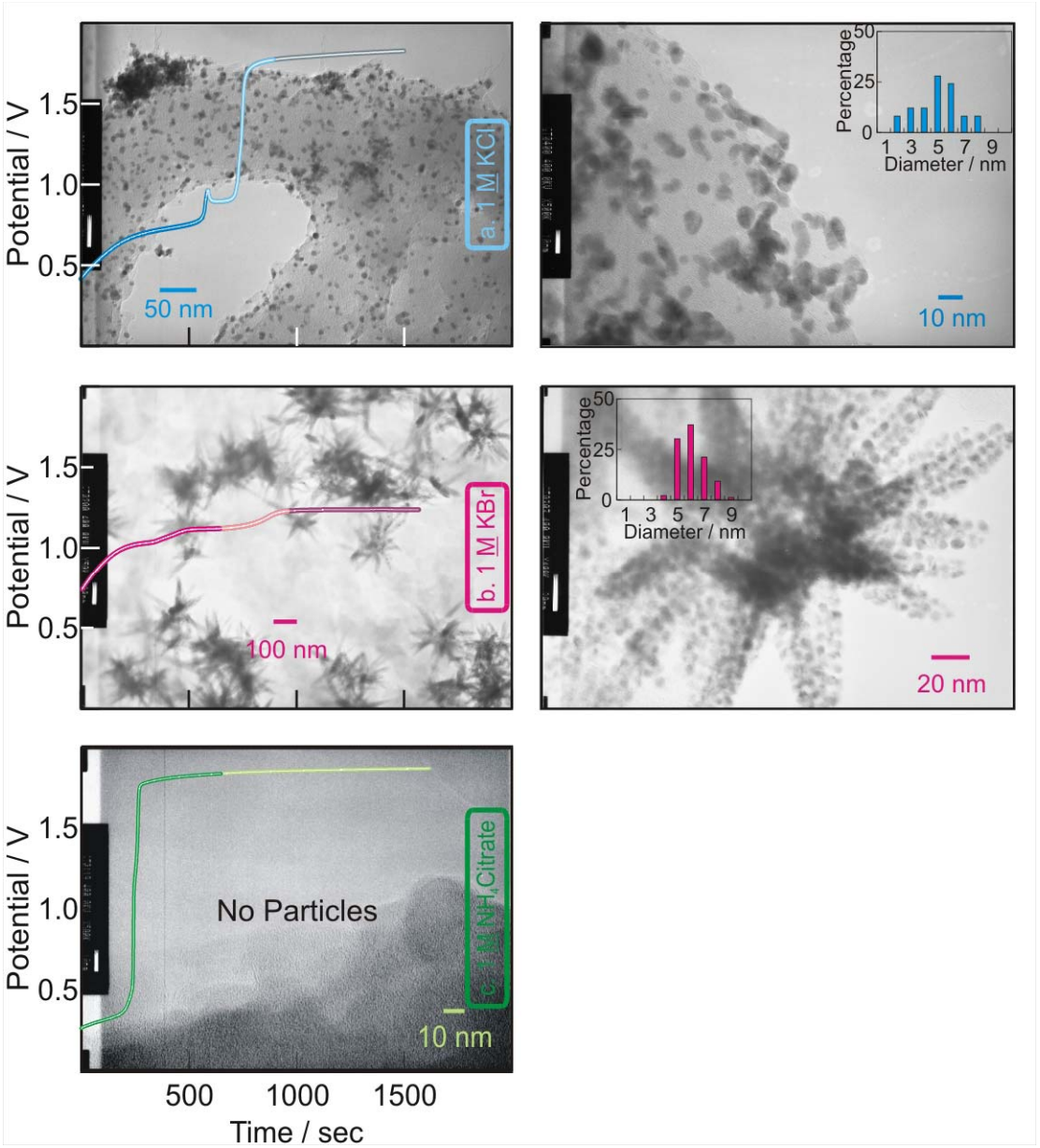

Figure 4.7. Stripping curves and TEM results for Pt/Au/PANI in (a) 1 M KCl, (b) 1 M KBr, and (c) 1 M KCl, 1 M or 40 mM NH_4Citrate.

the particle properties were advantageous, there were two negative aspects. KBr stripping led reproducibly to the leaf like morphology pictured in the background picture of the stripping trace. The particles did not appear in other areas. For later measurement dealing with the effect of the of the particles on the electronic properties of the composites, this inhomogeneity was undesirable. As such, KBr was not used as the preferred stripping medium. NaCl stripping was also tried but the films were not evaluated for particle size as the electrochemical behavior was similar to KCl.

Figure 4.7c shows stripping in 1 M ammonium citrate, a material that was known to be a gold capping agent.[2, 3] Stripping begins at a lower potential, 0.20 V and the potential remains relatively flat until the transition to electrolysis. This transition, again, occurs somewhat before might be expected from the film thickness. Somewhat surprisingly, no peak appeared and no particles formation or corrosion was evident.

4.3.3.3 Low pH Halides, KCl Additions

Figure 4.8a shows the curve for stripping in 1 M HCl. The curve is clearly different from that seen previously in the other halide solutions as there is only one transition. The stripping starts at about the same potential as the KCl, transitions to an endpoint and then stays at the

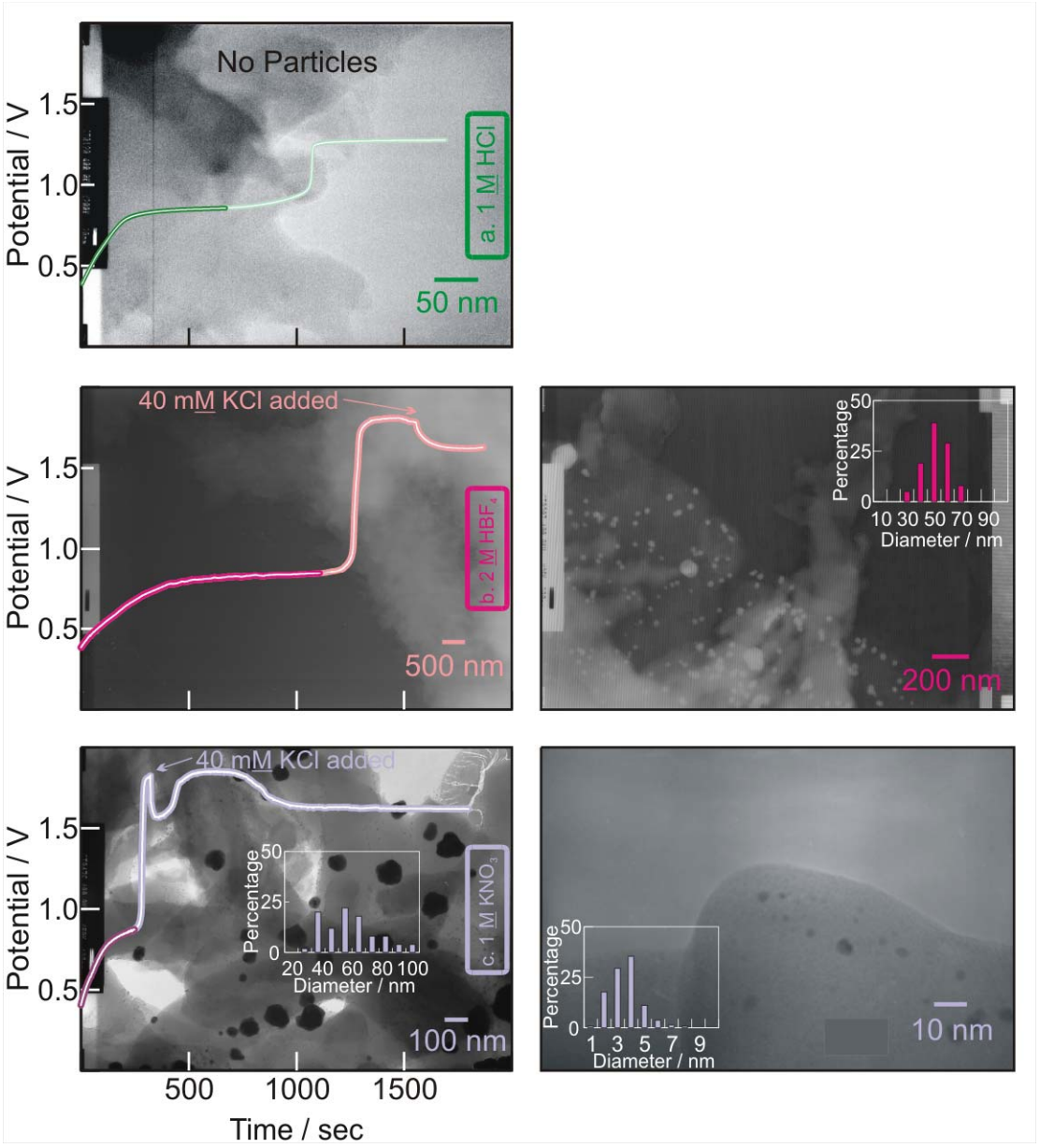

Figure 4.8. Stripping curves and TEM results for Pt/Au/PANI in (a) 2 M HCl, (b) 2 M HBF_4 with 40 mM KCl added at 1500 sec and (c) 1 M KNO_3 with 40 mM KCl added at 320 sec.

electrolysis potential indefinitely. The curve changes color from dark to light green at the value calculated from the thickness check and represents where the peak should appear if stripping in KCl. Note that this transition is well before what appears to be the oxidation endpoint. There did not appear to be particles in either the LRTEM or HRTEM micrographs. This was an unexpected but reproducible result. Stripping experiments run at much longer times (up to 3 hours) eventually led to the removal of some gold (~20%) and the formation of a few large particles (> 100 nm). In light of the fact that both the KBr and KCl stripping curves did not show the peak, it seemed possible that either potassium or hydrogen ions played a role. A somewhat analogous experiment was performed and shown in 4.8b in which stripping was begun in 2 M HBF_4. The stripping potential started out at 0.38 V then, passed through the PANI oxidation endpoint at 0.8 V indicated by the color change and then transitioned to the electrolysis potential at 1.8 V. Shortly after the electrode reached this potential at 1500 sec, an aliquot sufficient to make 40 mM KCl was added with vigorous stirring. As the KCl mixed the potential quickly dropped about 180 mV and stripping was terminated. Examination of four such films revealed particles in only one of the films. The few particles that formed were quite large with almost 40% of 50 nm and 85% falling between 40-60 nm. The particle formation results were similar to those for the 1 M HCl stripping. This

indicated that pH likely played a role in blocking the particle formation. A corollary experiment was used to further understand the role of pH. Figure 4.8c shows a stripping curve begun in a neutral pH, 1 M KNO_3 solution. The stripping potential passes through the oxidation endpoint at 0.8 V, where the color change indicates complete PANI oxidation and then rises sharply to 1.8 V. Shortly after plateauing, a KCl aliquot was added. As with the stripping in 2 M HBF_4 and 1 M KCl, the potential drops by about 0.25 V but unlike before it rises back to the electrolysis potential before falling again. This rise and fall of potential is most likely due to gas evolution blocking the working electrode. In the HRTEM regular, well separated, gold nanoclusters are seen with 4 nm particles being the most numerous 75% of particles falling between 3-5 nm. Additionally, the smallest particles yet, on the order of 1 nm are visible. If the formation of the smallest particles is the goal, this appeared to be the best preparation yet. However, as can be seen from the wide area view micrograph, a number of larger particles were also formed. These particles formed a second distribution that did not overlap the first. It is plotted above LRTEM. This preparation meets the objective to form small particles but for other means of studying the films such as XPS and fluorescence, it would be optimal to have a homogenous distribution of the small particles.

4.3.3.4 Stripping Anomalies

At this point it seemed cogent to focus on some additional electrochemical evidence, as shown in figure 4.9. This was both to understand particle formation and to explain some unexpected electrochemical results. Figure 4.9a shows stripping of a Pt/Au electrode in 2 M HCl, 1 M KCl, and 1 M KNO_3. KNO_3 stripping was evaluated to examine the stripping shape. It did not, of course, promote any dissolution. This is apparent from the curve which rises almost immediately to 1.6 V. In comparison, both the KCl and HCl stripping show a flat potential during the corrosion. Figure 4.9b shows stripping of Pt/Au/PANI electrodes in 1 M KNO_3 and 2 M HBF_4. An additional 2 M HCl curve is shown and the 1 M ammonium citrate is replotted for comparison. The purpose here was not to produce particles but to determine the electrochemical and particle formation mechanism. Stripping of Pt/Au/PANI in 1 M KNO_3 starts at a slightly lower potential, 0.35 V, passes through a flat region as the PANI is oxidized and then rises to the same final potential. The HBF_4 stripping of a thicker film shows the same gradual trend but the rise to the oxidation potential passes through a longer flat region as expected. These curves show the differences between films in different pH absent of the corrosion process.

The inset shows the same data with the curves overlaid in order to show more clearly the similarities in the shape. That is to say,

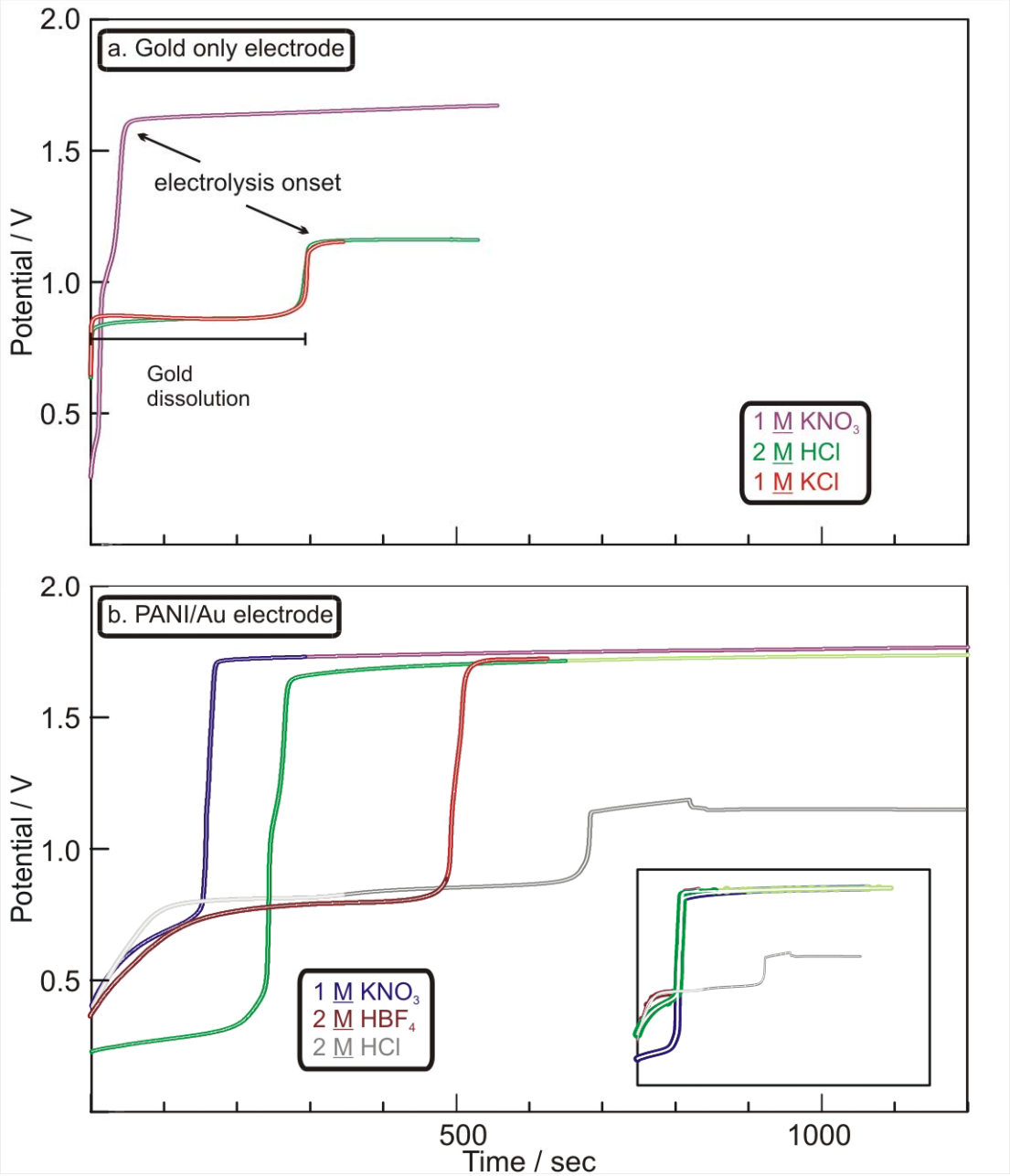

Figure 4.9 (a) Stripping of bare Pt/Au electrode in 1 M KCl, 2 M HCl, and 1 M KNO_3. (b) Stripping of PANI/Au electrode in 1 M NH_4Citrate, 1 M KNO_3, 2 M HBF_4, 2 M HCl.

ammonium citrate was at a higher pH, approximately 10, and had a different starting potential and took longer to reach the final potential but the overall shape was similar. The shapes of the neutral pH KNO_3 and the low pH HBF_4 were even more alike but the KNO_3 shared an important difference with the ammonium citrate stripping, namely the potential reached the final potential well before the time predicted for PANI oxidation. This is likely due to the interplay between the oxidation of the PANI and the proton egress from the film in the different solution. That is, the conductivity of the film decreases more rapidly due to proton egress and so reaches insulating state before the PANI is fully oxidized. The oxidation prediction is indicated by the curve color changes. Notice that it predicts too short a time for the low pH stripping experiments and too long a time for the neutral and high pH. It should be noted that the calibration curve for where oxidation should end is limited in scope due to differences in film porosity and morphology and the fact that the calibration was produced for KCl.

4.3.3.5 Citrate Capping

The preparation conditions under which the smallest particles have been formed thus far included neutral pH and a chloride complexation agent. The smallest particles seen so far were found in the 1 M KNO_3, with an aliquot of KCl but this preparation could also form a

number of larger particles (>25 nm). With this in mind, it was decided that stripping in ammonium citrate could be used to cap particle growth and reduce the size distribution. Ammonium citrate has been used a capping material for the formation of gold nanoparticles from tetrachloroauric acid solutions.[2, 3] Figure 4.10 shows three experiments in which 1 M KCl was used as the complexation agent and ammonium citrate was used for capping. In figure 4.10a, the red curve shows stripping in 1 M KCl with 40 mM ammonium citrate. Both electrolytes were present prior to the stripping onset. The stripping trace started at about 0.4 V and progressed as if it were a KCl stripping trial up to about 1.0 V. However, the peak appeared before the time predicted for complete oxidation from the PANI thickness check. This occurred at the curve color change, at 1.085 V and then the curve transitioned up to a high potential, 1.97 V before falling back to the normal electrolysis potential at 1.80 V. This did not appear to be due to electrode blocking from gas evolution. Note that the time axis is magnified compared to other experiments in order to better see the small peaks. As can be seen in the figure 4.10a micrographs, this actually led to much larger particles, with 30 nm as the most numerous particle size and 60% of particles falling between 20-40 nm. There were very few particles visible in the 2 x 2 mm film sample compared to what was an uncountable number when prepared with 1 M KCl. Additionally, there did not

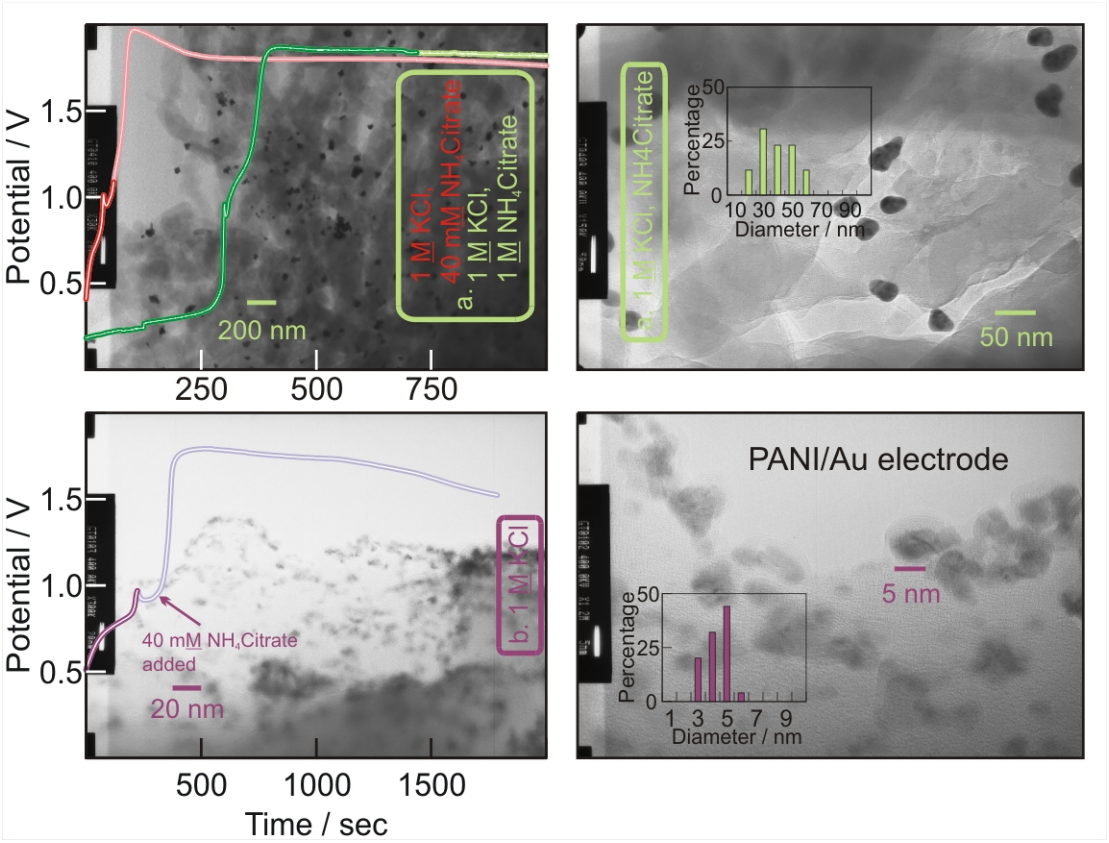

Figure 4.10 (a) Stripping of Pt/Au/PANI in (red) 1 M KCl and 40 mM NH_4Citrate and (blue) 1 M KCl with 1 M NH_4Citrate. (b) Stripping of Pt/Au/PANI electrode in 1 M KCl, with 40 mM NH_4Citrate added after dissolution began at 300 sec.

appear to be any smaller particles which normally form even if only in limited quantities.

Because of the unsatisfactory particle size, the experiment was repeated with 1 M ammonium citrate solution (the curve shown in green) as it seemed possible the higher citrate concentration would lead to "encapsulation" of smaller particles. Here, the trace starts at a somewhat lower potential of 0.18 V due to the higher pH and the interaction between the PANI and gold surface with the ammonium citrate. The curve proceeds up to about 1.0 V and a peak that is small relative to that formed in 1 M KCl. This peak appeared before the time predicted from the thickness. The potential then rose to the electrolysis potential at 1.8 V. In that case as well, the peak is reached at about 300 sec, well before the predicted oxidation endpoint. Primarily large particles were formed (not shown).

Figure 4.10b shows stripping in 1 M KCl but this time, 40 mM ammonium citrate was added after the corrosion onset, at the bottom of the tetrachloroaurate saddle at 300 sec as indicated. This yielded excellent results with some particles in the 5 nm range as the most prevalent and 96 % of particles falling in the range from 3-5 nm. Although both the particle size and distribution were the best thus far, the goal here was to produce particles from the simple two-part system.

This preparation uses citrate capping which could possibly interfere with later experiments.

4.3.3.6 Particle Formation and Electrochemical Front Movement

PANI is a porous, three dimensional material. This become important when discussing the location at which electrochemical processes occur in the direction normal to the electrode surface. Within this thickness an electrochemical boundary or "front" may develop beyond which electrochemical processes do not occur. During the course of an electrochemical experiment with PANI the position of this front can move depending on solution conditions and the local conductivity of the PANI. The Emeraldine salt (ES) is the only conducting PANI form and even if a film begins in this state, it may be converted to an insulating state by the solution conditions or changes in oxidation[4]. See figure 4.11 which relates various oxidation and doping states of polyaniline. An abbreviated version is shown below.

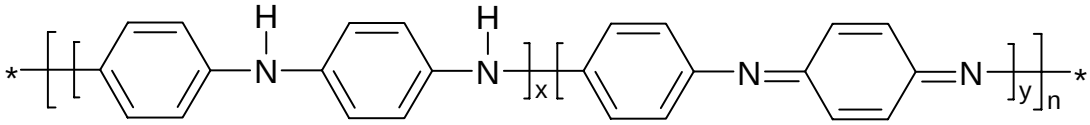

The gold cluster formation can be explained on the basis of conductivity of the PANI layer and its interaction with tetrachloroaurate. The semi-oxidized (x ~ y) acidic form of PANI, "emeraldine salt", is electrochemically conducting.[5] Its transition from conducting to

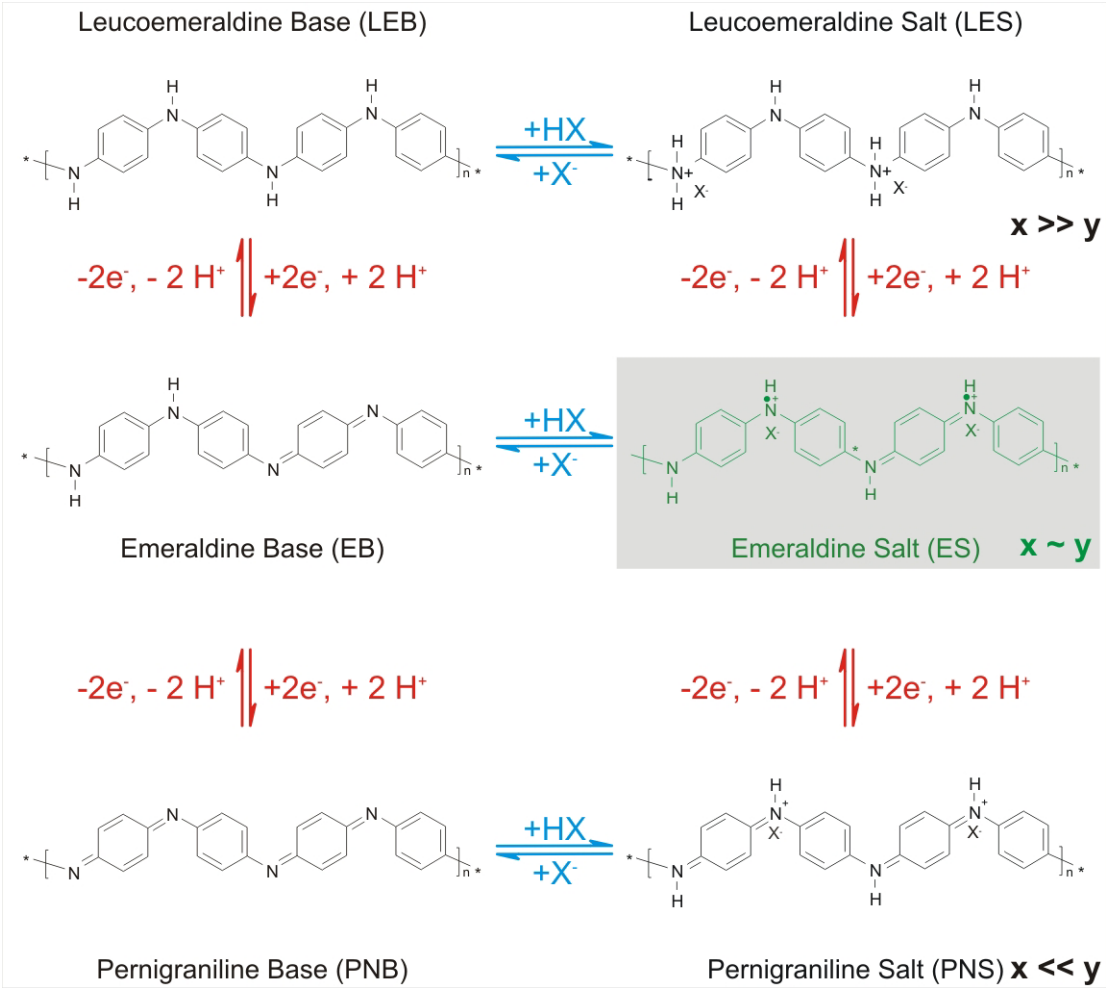

Figure 4.11. Polyaniline inter-conversion scheme.

non-conducting form causes the shift of the electroactive interface back and forth, the "moving redox front".[6] The role played by this inter conversion is highlighted in figure 4.12.

Starting with the simplest case, figure 4.12a shows a stripping trace performed in the presence of KCl or HCl on a bare gold electrode. The electrode surface is not impeded by PANI and dissolution occurs rapidly, showing the classic chronopotentiometric stripping curve.

In neutral pH halide solutions, (figure 4.12b) PANI is non-conducting during stripping. This allows the electrochemistry to happen at the PANI/Au interface. In KCl the PANI film began in the emeraldine salt form (ES) with an equal quinoid (y) to benzenoid (x) ratio (x ~ y). As stripping proceeded, the film oxidized to the pernigraniline salt form (PNS) where (x << y existed).[5] This conversion increased the potential to remove additional electrons and decreased the PANI conductivity. This was likely coupled with Cl^- ion ingress which occupied the imino sites and proton exchange for K^+. When the potential reached ~ 0.8 V vs. the Ag/AgCl reference, tetrachloroaurate formation was initiated. As the tetrachloroaurate ions formed they diffused away from the PANI/Au interface due to the high local concentration gradient and simultaneously the electrochemical front retreated. At this stage the PANI film was composed predominantly of quinoid groups, so many imino moieties which may have previously been occupied were available

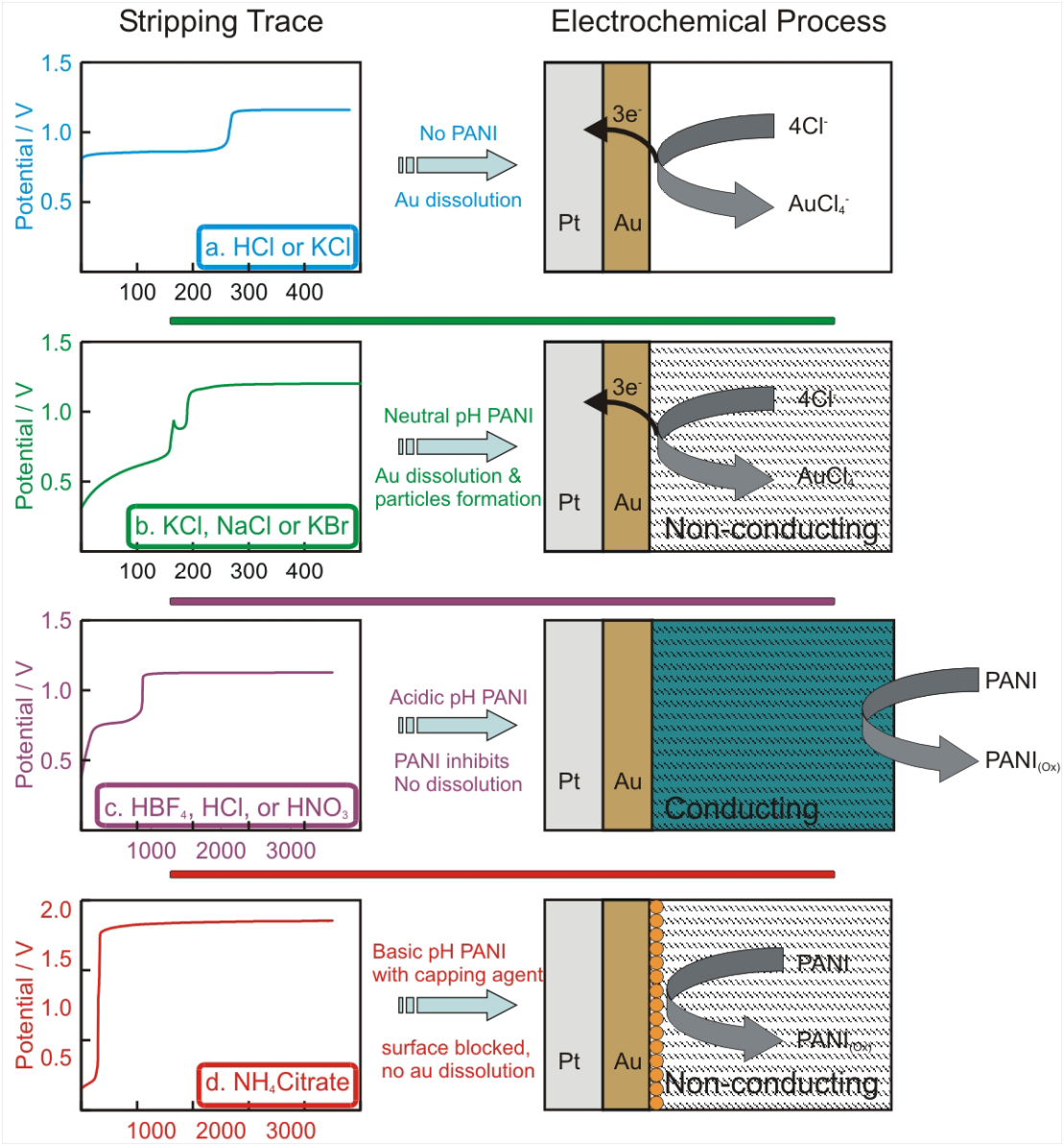

Figure 4.12 (a) Electrochemical stripping on bare Pt/Au in HCl or KCl. PANI in (b) neutral pH KCl, (c) strong acid, and (d) basic pH NH_4Citrate solutions.

for complex formation with the tetrachloroaurate ions. These could form a salt at the imino group ion together with the K^+ counter ion and temporarily dope the film and increase film conductivity. This led to the potential drop and thus peak formation. However, tetrachloroaurate is a very strong oxidant and it was able to overoxidize the PANI and reduce as single gold atoms. Conductivity decreased and the electrochemical front moved back toward the gold surface and the film was converted back to PNS. It is believed that not all the tetrachloroaurate ions reduced and that many do not reduce until oxidation stops. As the front moved back toward the PANI/Au interface, more tetrachloroaurate formed and the gold dissolution process continued. The newly formed tetrachloroaurate diffused into solution where many of the imino quinoid groups were occupied so the ions moved further before reaching new imino sites. As the stripping continued, corrosion completed and the film again converted to the fully oxidized PNS form.

When the stripping current is stopped, the film falls to the open cell potential and the tetrachloroaurate ions may reduce at either an unoccupied imino group or attach to a previously formed gold cluster. Some of the $AuCl_4^-$ will reduce by over oxidizing PANI and the reduction pulse used for blowoff will reduce the residual.

When PANI is stripped in a strong acid (figure 4.12c) the acid concentration is high enough that the emeraldine salt form is

maintained by the constant PANI doping is maintained in steady state and conductivity is maintained. This effectively forces the electrochemistry to occur at the PANI/solution interface, thus gold dissolution does not occur (figure 4.12c). In the presence of citrate, (figure 4.12d) the gold surface is blocked by citrate and PANI is no longer conducting. Thus, only a small amount of dissolution is observed.

The appearance of a peak in figure 4.12b during stripping in KCl is explained in terms of the change in conductivity of the film. As the PANI is oxidized, ions are expelled and potential reversal occurs when, during tetrachloroaurate formation, the tetrachloroaurate ion diffuses into the film, binds strongly to the imino nitrogen and increases film conductivity. Thus, temporarily halting the gold dissolution and shifting the electrochemical interface away from the PANI/Au interface. This process sometimes repeats (see figure 4.3) and a second peak is formed but this second peak is rarely resolved and is due to the same process.

4.4 Conclusions

Freestanding, composite films of gold nanoparticles and polyaniline fiber supporting matrix may be formed by electrochemical means. Film removal is facilitated by corrosion of the gold electrode surface prior to film blowoff. Particle formation does not require an explicit capping agent although adsorption of anions from the stripping

process or physical contact with polyaniline nanofibers may perform the same task by acting to decrease surface energy. Particles of different size may be formed but in all cases required a complexation agent to act as a corrosion promoter, in this case halide or bromide ions. The smallest particles formed in reactions where chloride was the limiting reagent with respect to gold which was the limiting reagent with respect to and imino units of polyaniline. The methods which formed the smallest films proceeded by stripping in 1 M KNO_3 then adding small amounts of KCl followed by citrate capping.

Corrosion proceeded in pH neutral solutions and was blocked when the polyaniline was in its conducting state or when the gold-polyaniline interface was blocked by adsorbed citrate. This was a result of the movement of the electrochemical front from the solution/PANI boundary through the PANI film to the PANI/Au boundary. The results of this study help to explain some of the seemingly contradictory literature regarding PANI acting as a corrosion inhibitor in one situation and as a corrosion promoter in another. This leads to the somewhat counterintuitive conclusion that at low pH, PANI assists in corrosion prevention.

4.5 Acknowledgements

Thanks go to Z.L. Wang and particularly to Yolande Berta for assisting in the TEM analysis and for maintaining the Georgia Tech Electron Microscopy Center.

4.6 Summary

This chapter describes the electrochemical synthesis of freestanding PANI/Au composite films and the resulting gold particle sizes. The composite synthesis is accomplished by growing PANI films on a sacrificial gold electrode followed by stripping of the electrode in the presence of different solutions. In the presence of neutral pH chloride solutions the gold dissolves in the form of tetrachloroaurate which then diffuses into the PANI film where it is bound to the imino and amino nitrogen groups of the polyaniline. The tetrachloroaurate is subsequently reduced to metallic gold and the film blown off by hydrogen evolution. This method is capable of producing 1-10 nm gold particles and perhaps smaller without the need for a separate capping agent. Polyaniline is seen to be a corrosion inhibitor in the presence of acids but a corrosion promoter in the presence of neutral pH halides.

4.7 References

1. Hatchett, D. W.; Josowicz, M.; Janata, J.; Baer, D. R. *Chemistry of Materials* **1999**, *11*, 2989-2994.

2. Link, S.; Wang, Z. L.; El-Sayed, M. A. *Journal of Physical Chemistry B* **1999**, *103*, 3529-3533.

3. Turkevich, J.; Stevenson, P. C.; HIllier, J. *Discuss. Faraday Soc.* **1951**, *11*, 55.

4. Genies, E. M.; Boyle, A.; Lapkowski, M.; Tsintavis, C. *Synthetic Metals* **1990**, *36*, 139-182.

5. Heeger, A. J. *The Journal of Physical Chemistry B* **2001**, *105*, 8475-8491.

6. Johansson, T.; Persson, N.-K.; Inganas, O. *Journal of the Electrochemical Society* **2004**, *151*, E119-E124.

CHAPTER V

POLYANILINE/GOLD NANOCOMPOSITE XPS AND TEM ANALYSIS

5.1 Introduction

This chapter focuses on the effects of incorporating different size gold particles into polyaniline thin films. The particles sizes rage from 1 to 100 nm but in most composites the particles were less than 10 nm. Composites were prepared as freestanding films which allowed them to be imaged by TEM (chapter 4). The work function of the electrochemically/chemically grown composites in chapter 3 was characterized by Kelvin probe but X-ray Photoelectron Spectroscopy (XPS) was a more appropriate technique for the freestanding films. TEM was used to investigate the unusual characteristics exhibited during particle formation. X-ray diffraction, surface enhanced Raman spectroscopy and visible range spectroscopy were also performed on the composites but yielded inconclusive results and will not be discussed here.

The impetus for the creation and examination of these composites was to study how gold particles of the truly nanoscale (1 nm and smaller) would interact with polyaniline. Chapter 3 related the change

in the PANI work function to the mass of incorporated gold but with particles of bulk dimensions (from ~0.25 – 1.00 μm). In those experiments the gold was dispersed into a constant mass of PANI to obtain $\left(\partial\Phi_{Composite}/\partial Mass_{Au}\right)_{Mass_{PAN}}$. Initially, the goal of this phase of research was to study the change in composite work function with respect to particle size while maintaining a constant mass of PANI and gold to obtain $\left(\partial\Phi_{Composite}/\partial Size_{Particle}\right)_{MassP_{ANI}}^{Mass_{Au}}$. However, although a constant mass of gold was deposited as the substrate (sacrificial layer) for the PANI film growth, under many conditions the stripping yielded incomplete gold dissolution (as described in chapter 4). Although future studies using neutral pH KCl solutions could be performed to study this relationship, the reported experiments do not maintain a constant gold mass.

Visual and SEM inspection (not shown) indicated a gradient of particle density normal to the electrode surface. It is likely that this led to larger gold particles than would be expected if the particle growth proceeded homogenously throughout the film. For this reason, incomplete dissolution was beneficial as it allowed the formation of gold particles that were smaller than would be expected if all the gold from the sacrificial electrode was dispersed into the PANI film.

Regardless of the actual particle size, the study of the dependence of the composite work function on particle size (under the conditions of constant gold mass) would be interesting due to the inverse proportional relationship between the size and the total surface area (and capacitance) of the gold particles. It can be theorized that in this situation, the decrease in particle size would lead to an increase in the charge transferred from the polyaniline to the gold and thus a change in the composite work function. This effect would be due to the change in contact potential. In this study, different masses of gold were dispersed in the polyaniline films and although the overall composite work function is not measured, the contact potential is thought to influence the XPS measurements of the gold particle properties.

5.2 Experimental

5.2.1 Composite Preparation

Polyaniline/gold samples were prepared as described previously. Samples were mounted in one of two ways for later XPS analysis. Freestanding PANI/Au samples were mounted on copper grids for TEM analysis. Initially, these were also used for XPS analysis but attaching the grids under metallic clips on the XPS sample holder proved difficult as the copper peaks from discontinuous films interfered with the signal coming from the composite. Subsequent, films were prepared separately

with the XPS samples mounted on 1 cm^2 silicon wafers to facilitate mounting.

5.2.2 X-ray Photoelectron Spectroscopy.

The XPS measurements were performed using a Physical Electronics Quantum 2000 Scanning ESCA Microprobe. This system uses a focused, monochromatic Al Kα X-rays (1486.7 eV) source for excitation and a spherical section analyzer. The instrument has a 16 element multi channel detection system. The X-ray beam used for this data was a 40W, 200 μm X-ray beam spot. The X-ray beam is incident normal to the sample and the X-ray photoelectron detector is at 45° off-normal. This data was collected using a pass energy of 117.4 eV. For the Ag 3d5/2 line, these conditions produced a full width, half maximum (FWHM) energy of 1.63 eV. The binding energy (BE) scale was calibrated using the Cu 2p3/2 feature at 932.62 ± 0.05 eV and Au 4f at 83.96 ± 0.05 eV for known standards. An electron flood gun was used at 1 eV and 20 μA electrons to test for the presence of charging. The maximum error for the calibrated instrument could be as high as 0.10 eV but repetitive measurements on the same samples months apart showed no more than 0.01 - 0.03 eV difference. For both studies the carbon 1s peaks were assigned a binding energy of 284.6 eV and used

as the energy reference. A chamber pressure of 4 x 10^{-9} Torr or lower was maintained for all sample measurements.

5.3 Results and Discussion

5.3.1 XPS Analysis

The work function of the electrochemically/chemically grown composites in chapter 3 was characterized by Kelvin probe. In these composites, visual and SEM inspection showed a particle gradient with a higher density of particles near the PANI/Au interface. Additionally, the creation of the gold particles necessitated the removal of the substrate on which the PANI was originally grown. The Kelvin probe measurement could not survey the PANI/Au interface directly as it is on the opposite side of the reference probe.[1] More significantly, the PANI/Au interface was often partially of completely dissolved as necessitated by particle growth. XPS provides another means for examining work function that is more appropriate for these films.[2, 3] Its interpretation also affords further understanding of the electrochemical growth mechanism.

The XPS spectra of a number of freestanding PANI films are shown in figures 5.1 - 5.4. XPS provides information regarding density of occupied electronic states at a material surface. The X-ray beam penetrates the material and ejects electrons from the valence or core levels giving elemental composition and electronic structure detail. The

profiling depth is limited because the ejected electrons must escape to the detector but can be readily captured from a depth of even a few monolayers. This limits the practical investigation depth to a few nanometers. Each spectrum is aligned to the right edge of the ^{1s}C peak of a reference spectrum, the spectra shown in figure 5.1a. Binding energies are reported relative to the reference. The reported particles sizes are for the mode in the particle distribution.

Most of the spectra reported below show very small peaks for the ^{4f}Au doublet. The electron cross section coefficient for gold (6.8) is much higher than for the other elements of note, carbon (0.31), oxygen (0.73) and nitrogren (0.50) at the 45 degree measurement angle, so it is apparent that the relative quantity of gold is very small, ranging from 0.03 to 0.92 %. These small amounts are a consequence of the electrochemical growth method used for creation of the particles. While the measurement pushes the limits of the instrument, repetitive measurements of the peak binding energies gave good confidence for the accuracy of the measurements.

Figure 5.1 shows the survey (0 to 450 eV) spectrum of composites mounted on copper grids for TEM analysis. The survey from of a PANI film stripped in 1 M KNO_3 and 40 mM KCl which contained ~8 nm particles is shown in figure 5.2a. The spectrum shows prominent peaks at 400.0 (^{1s}N) and 284.8 eV (^{1s}C). Smaller peaks at 200 (^{2p}Cl) and 270

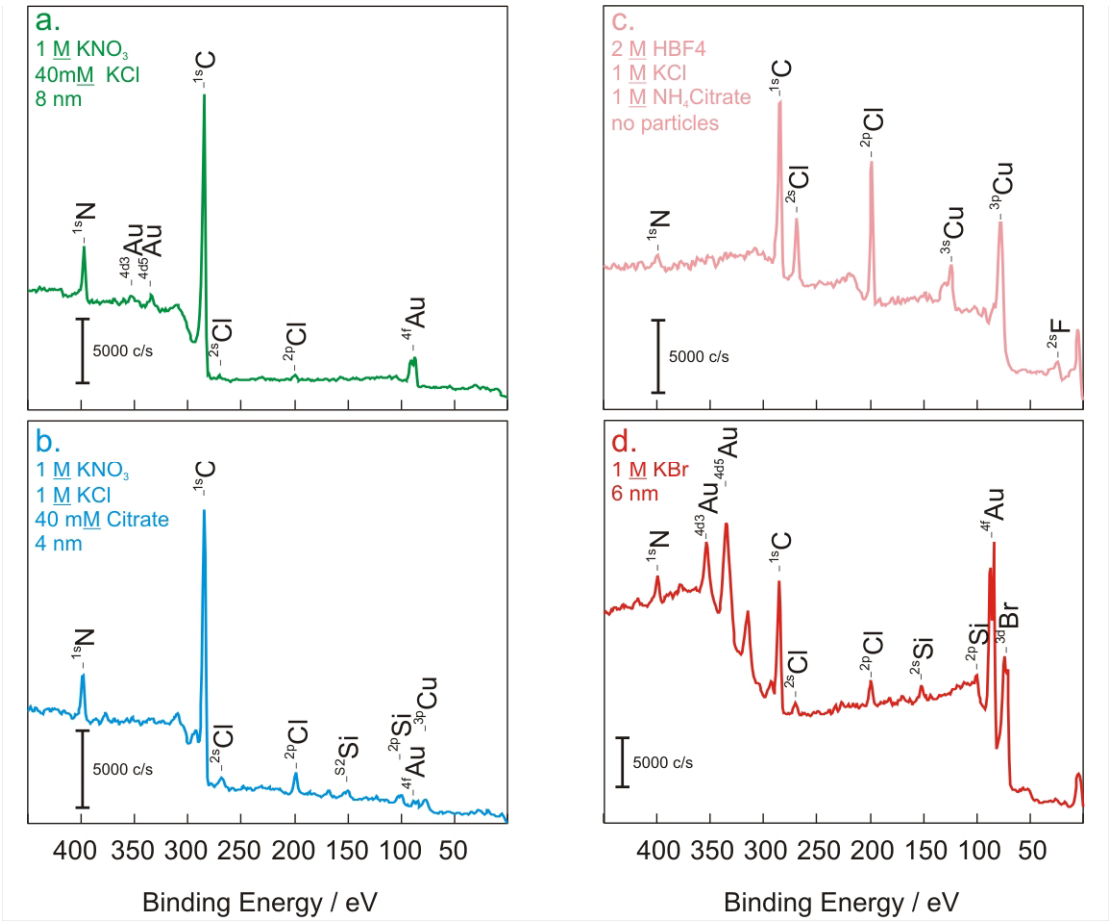

Figure 5.1 Low detail surveys of composites prepared in stripping solutions of (a) 1 M KNO_3, 40 mM KCl and 8 nm Au particles (b) 1 M KNO3, 1 M KCl with 4 nm Au particles, (c) 2 M HBF_4, 1 M KCl and 1 M NH_4Citrate with no particles and (d) 1 M KBr with 6 nm Au particles. Inserts are 10x horizontal scale blowups of the ^{4f}Au doublet.

eV (^{2s}Cl) indicate the presence of chloride some of which will adsorbed at the gold surface. The absence of the 25 (^{2s}F) or 687 eV (^{1s}F) fluorine peaks at, coupled with the lack of the 195 eV (^{1s}B) boron peak indicates that the chloride also replaces the BF_4^- ions with which the PANI was initially doped. The characteristic doublet at 84 (^{4f7}Au) and 88 eV (^{4f5}Au) together with the peaks at 355 (^{4d3}Au) and 340 (^{4d5}Au) eV, respectively indicate the presence of metallic gold.[4]. The presence of tetrachloroaurate would be marked by the Au(III) doublet at 87 (^{4f7}Au) and 92 eV (^{4f5}Au), respectively.

Figure 5.1b is the survey spectrum of a film stripped in 1 M KNO_3 and 1 M KCl with 4 nm particles. An aliquot sufficient to make the solution 40 mM in ammonium citrate was added at the chloride dissolution peak. The PANI films are comparable and ^{1s}N and ^{1s}C peaks exhibit essentially the same height and position. The ^{4f}Au gold doublet for this sample is somewhat smaller and the ^{4d3}Au and ^{4d5}Au peaks were not resolved. The reduced amount of gold was due to the citrate capping. Peaks at 150 (^{2s}Si) and 100 eV (^{2p}Si) indicate the presence of silicon from etching of the electrochemical cell (HBF_4 dissociates to form HF). Note that these peaks do not appear in all XPS spectra. For films grown from fresh solutions, the silicon peaks did appear. The ^{2s}Cl and ^{2p}Cl chlorine peaks are somewhat larger than for the ~8 nm composite in 5.1a while the ^{4f}Au peaks are somewhat smaller. This might seem

counterintuitive but probably reflects more chloride ion occupying the anionic PANI doping sites.

The spectrum for a PANI film stripped in 2 M HBF_4, 1 M KCl and 1 M ammonium citrate is shown in figure 5.1c. The expected peaks ^{1s}N, ^{1s}C appear but both are less well resolved. Prominent peaks for the ^{2s}Cl and ^{2p}Cl peaks are observed as well as the 25 eV (^{2s}F) and 687 eV (^{1s}F). Peaks at 80 (^{3p}Cu) and 120 eV (^{3p,3s}Cu) appear as a consequence of film discontinuity which allows the beam to strike the copper surface directly and causes the large charging background. It appears that the increased background was due to copper oxide formation from salt or acid induced corrosion. Under TEM analysis no gold particles were apparent in this film. However, the large background was problematic because even if there were small amounts of gold, the 84 eV (^{4f}Au) peak would probably be obscured by the large 78 eV (^{3p}Cu) peak. This background also explains why the ^{1s}N peak is obscured. Analysis of this sample indicated the need for separate XPS and TEM samples preparation.

The spectrum of a film stripped in the presence of 1 M KBr with 6 nm mean diameter particles is shown in figure 5.1d. This spectrum also exhibits a large background and the ^{1s}N, ^{1s}C are poorly resolved. The ^{2s}Cl and ^{2p}Cl peaks are present because blowoff for this film was performed in 1 M KCl for historical reasons. Charging occurred for the

reference ^{1s}C peak which necessitated the use of the flood gun. Prominent peaks for the ^{4f}Au and the 71 eV (^{3d}Br) peak at indicate the presence of both gold and bromine. This is expected from both the TEM and electrochemical preparation.

Figures 5.2a-d show the high energy resolution XPS spectra of the films described above. The dashed lines curves correspond to spectra taken during electron flood gun operation as described in 5.2.2. Figure 5.2a shows the ^{1s}O peaks centered at 532.4 eV. The oxygen peak is similar in magnitude for the 4 and 8 nm composite films that do not show copper interference. The films experience comparable electrochemical overoxidation during stripping and though further oxidation occurs during the post stripping tetrachloroaurate reduction, this amount was relatively small. For the discontinuous samples, the oxygen peaks had a 5x larger peak area. In all films the peaks do not shift off center more than 0.10 eV. This is the larger limit of the experimental apparatus error but practically speaking repeat measurements after 6 months of samples a and b varied by no more than ~ 0.03 eV. Regardless, this shift does not indicate a significant difference between the films.

Figures 5.2b and 5.2c show the ^{1s}N and ^{1s}C peaks. The ^{1s}C peaks were previously centered at 284.85 eV during referencing but are shown to indicate their shape similarity. The ^{1s}N peaks are centered at

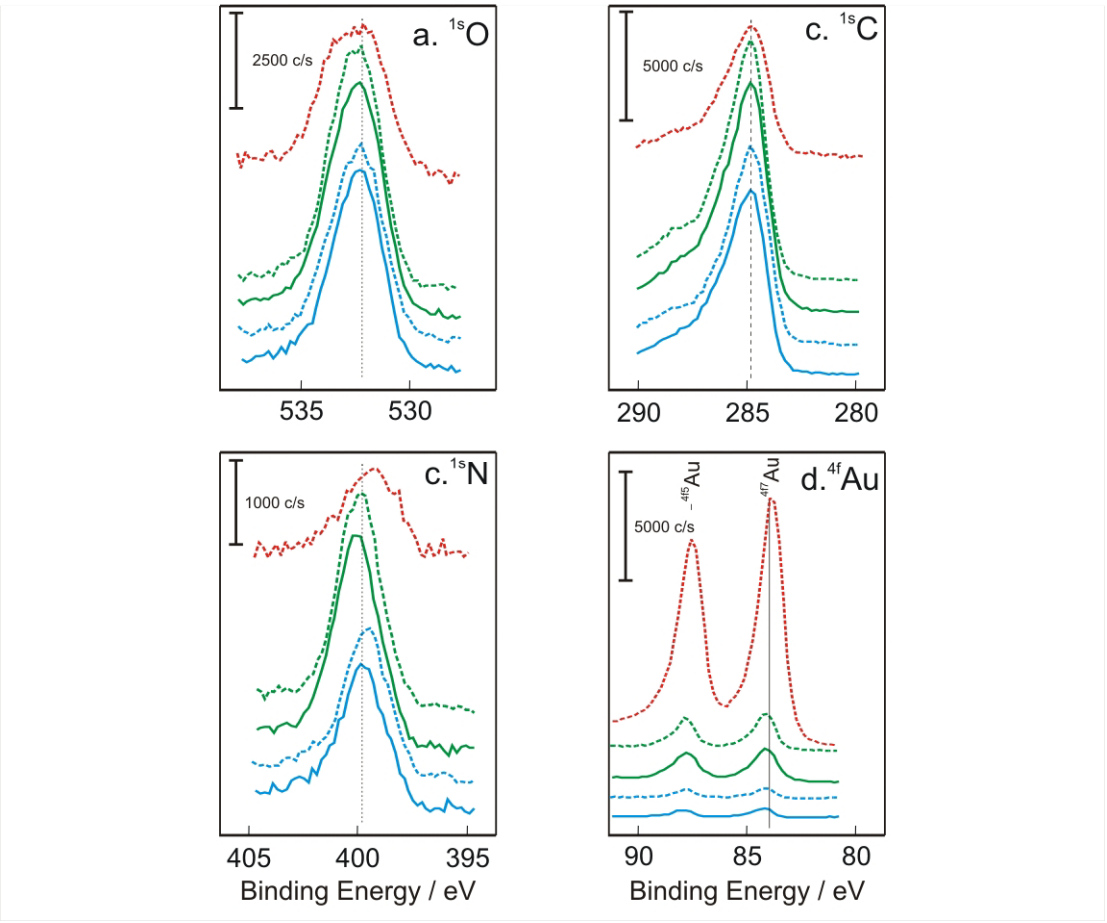

Figure 5.2 High Energy Resolution XPS of (a) ^{1s}O, (b) ^{1s}N, (c) ^{1s}C, and (d) ^{4f}Au peaks from samples prepared for figure 5.1.

approximately 400 eV. The difference between the full width half maximum with and without the flood gun is 0.24 eV for the 4 nm sample and 0.15 eV for the 8 nm samples. This is somewhat larger than for the corresponding differences in the gold peaks in figure 5.2d which were 0.06 eV for both samples. However, the ^{4f}Au unlike the nitrogen peaks shifted monotonically toward higher binding energy with decreasing particle size. Originally, it was thought that the shift in the two peaks should be related. That is, the change in electron density giving rise to the shift in the gold peaks was thought to come directly from the ^{1s}N and it was expected that the two would exhibit correlated shifts. This did not appear to be the case. The significance of both shifts will be discussed below.

Figure 5.3 shows survey spectra from (0 to 450 eV) of a second set of composites. Figure 5.3a was for a film stripped in 1 M KBr ~8 nm particles. The 71 eV (^{3d}Br) peak is clearly resolved as are the 257 (^{2s}Br) and 184 eV (^{2p}Br) peaks. The ^{4f}Au gold doublet is also well resolved and both the 355 (^{4d3}Au) 335eV (^{4d5}Au) are visible. This film was prepared in the same manner as 5.1d but did not exhibit charging. Both the 191 eV (^{1s}B) peak and the corresponding 21 eV (^{2s}F) peak indicative of the BF_4^- anion are residual from the growth solution.

Figure 5.3b is the spectrum of a composite formed from stripping in 1 M KCl which had ~ 10 nm particles, the size range arbitrarily

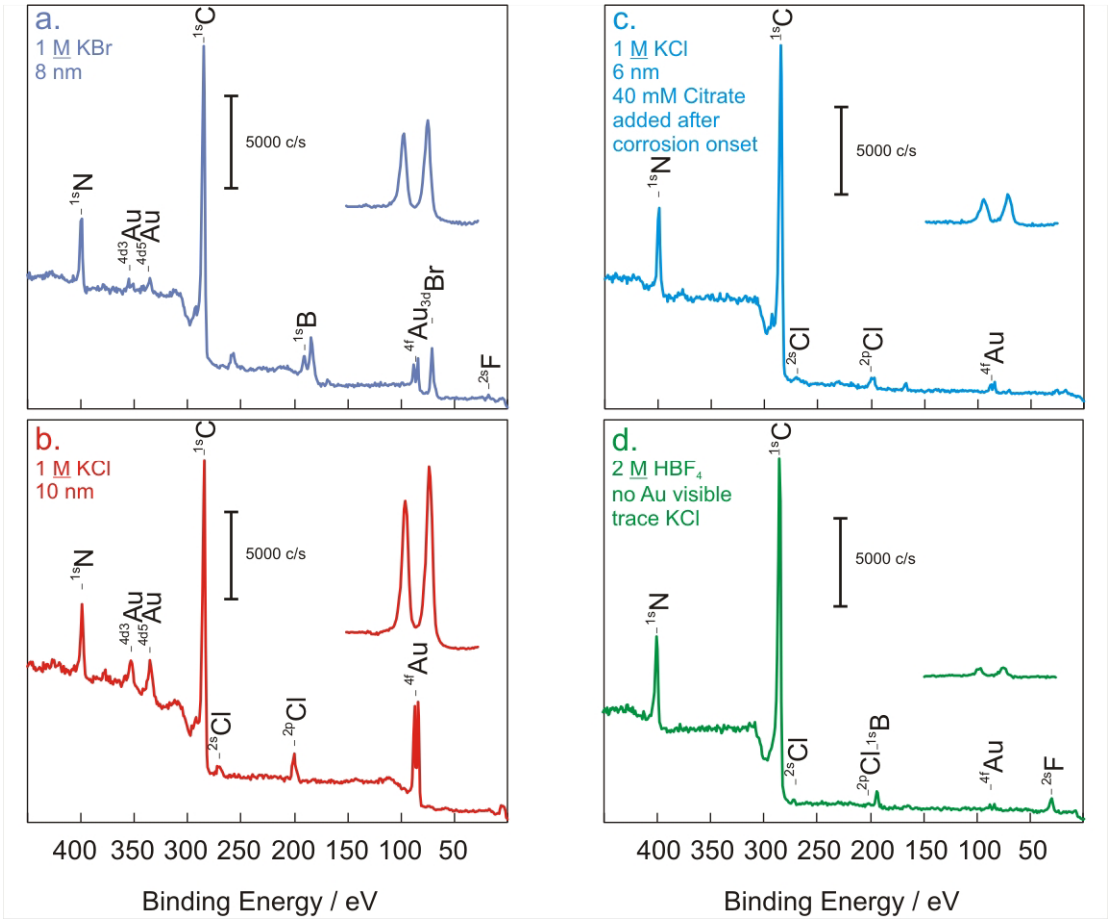

Figure 5.3 Low detail surveys of composites prepared in stripping solutions of (a) 1 M KBr, 6 nm Au particles (b) 1 M KCl, 10 nm Au particles, (c) 1 M KCl, 40 mM NH_4Citrate, 6 nm Au particles (d) 2 M HBF_4 no *visible* Au particles but some gold. Inserts are 10x horizontal scale blowups of the ^{4f}Au doublet.

defined nanoscale size limit. It shows the expected large ^{4f}Au peaks as well as the ^{1s}C, ^{1s}N, ^{2s}Cl and ^{2p}Cl peaks. The ^{2s}F peak is absent which is indicates full exchange of the initial dopant with Cl^- during cluster formation. This follows the general trend that as the relative gold peak area increased the area of the Cl^- related peaks increased while the BF_4^- related peak area decreased.

Figure 5.3c the spectrum of a film stripped in 1 M KCl with 40 mM citrate added just after the appearance of the gold dissolution peak. Stripping was terminated at this point. A few ~ 6 nm particles formed and the film was left with only a small amount of chlorine.

The spectrum in figure 5.3d was somewhat unexpected. The film was stripped in the presence of only 2 M HBF_4 and was to be used as a PANI only reference. The presence of a very small ^{4f}Au doublet is explained by the presence of a trace amount of chloride in the stripping solution which permeated into the film before stripping was initiated and dissolved a small amount of the gold before the electrochemical front was pushed beyond the PANI/Au interface. Examination under the TEM did not reveal any particles. The TEM can regularly resolve 1.5 to 2 nm and greater particle sizes at the lower limit, even with the complication discussed below in 5.3.3. For this reason the particle size is assumed to be < 1.5 nm.

The spectra in figures 5.4a-d are the high energy resolution spectra of the composite from 5.3a-d. The same trends are seen as for figures 5.2a-d. Both the oxygen ^{1s}O and nitrogen ^{1s}N peaks are located near the centroid marked by the dashed black line. The ^{1s}O centroid shift is a mostly due to the existence of overlapping oxidation states which causes peak broadening. This is also true of the ^{1s}N peaks but there will also be some effect from the interaction with the gold particles. Neither set of peaks exhibit a trend related to particle size. The ^{4f}Au doublets again show the trend to higher binding energy shifts with the smallest. For these films, no difference was seen between operation with or without the electron flood gun.

5.3.2 Contact Potential Effects and Particle Size Effects

Understanding the physical reasons for the shift in the ^{4f}Au binding energy requires the introduction of two concepts, contact potential and the "nanoscale effect".

5.3.2.1 Contact Potential

The development of the contact potential is a consequence of the thermodynamic equilibrium requirement that the electrochemical potential, $\bar{\mu}_e$, of phases in electrical contact be everywhere uniform (i.e. The phases must have the same Fermi level). Upon contact, charge will

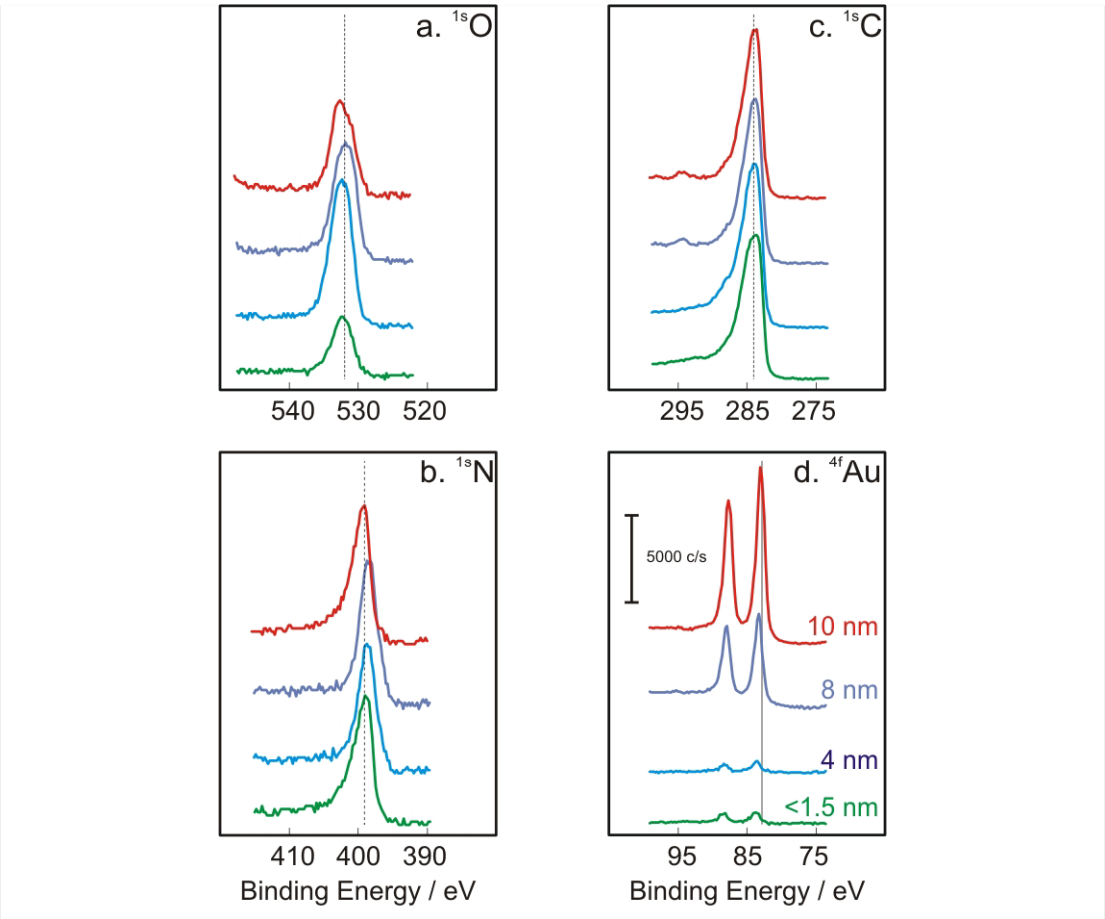

Figure 5.4. High Energy Resolution XPS of (a). ^{1s}O, (b) ^{1s}N, (c) ^{1s}C, and (d) ^{4f}Au peaks from samples prepared for figure 5.3

flow to the material with the lower $\bar{\mu}_e$ until the Galvani potentials are equalized.

When the two components of the composite have no net charge, as is the case prior to contact, $\bar{\mu}_e^{PANI} = \Phi_{PANI}$ and $\bar{\mu}_e^{AU} = \Phi_{Au}$. In bulk, $\Phi_{Au} = 5.1 > \Phi_{PANI} = 4.8$ so electrons will move toward the gold. As electrons are transferred, charge partitions at the PANI/Au interface until the potential across the interface, known as the contact potential, Ψ, is equal and opposite to the difference in work function. At equilibrium,

$$\bar{\mu}_e = \Phi_{PANI} - e\Psi = \Phi Au - e\Psi \tag{1}$$

and so the contact potential is equal to the difference in electron affinity.

$$\Delta\Phi = -e\Delta\Psi \,. \tag{2}$$

Consider the thought experiment regarding the contact potential between two dissimilar conductors (figure 5.5a). Two macroscopic conducting spheres, S_1 and S_2 in which $\Phi_1 < \Phi_2$ are brought into contact. Upon contact, a number of electrons flow toward S_2 leaving holes in S_1. The mass of S_2 is now divided into two identical spheres S_{2A} and S_{2B} so that there volume/mass equal that of S_2 and these are both placed in contact with S_1. If the volume, is maintained constant, the sphere diameter decrease is inversely proportional to the total surface area (figure 5.5b) so a 10x decrease in particle size would mean a 10x

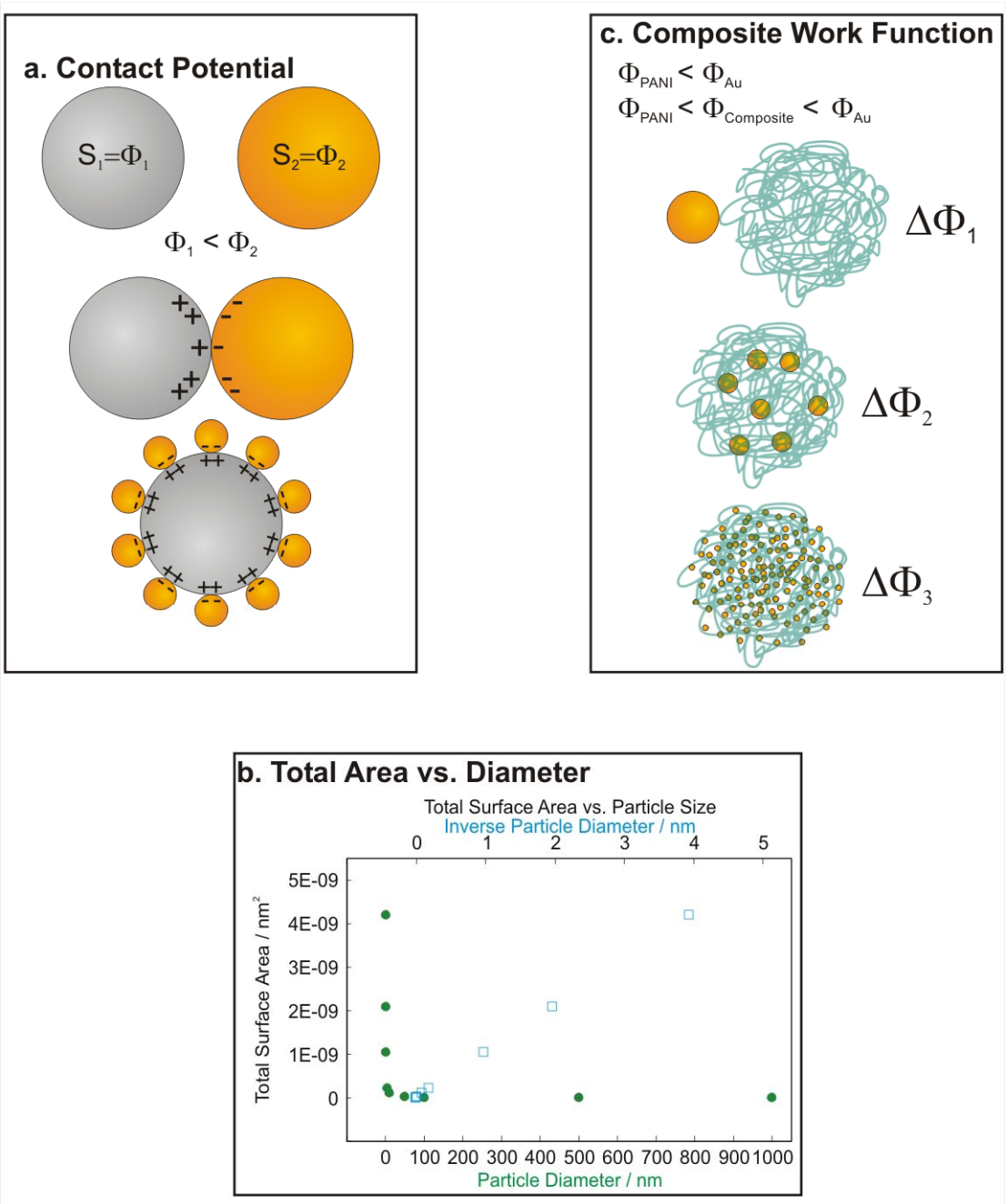

Figure 5.5. The origin of contact potential and electronic binding energy shifts in PANI composites arises from (a) contact potential which depends on (b) total surface area to particle size and (c) distribution of the particles throughout the film.

increase in total surface area. Each sphere should remove an equal number of electrons from S_1 and since the charges reside on the surface, the average distance between charges is increased. Because this reduces the electrostatic potential per charge transferred, it should take a few more charges to equalize the Fermi levels.

This concept may be extended to the composite system as in figure 5.5c. When placed in contact, the overall system will have an intermediate value of work function so that $\Phi_{PANI} < \Phi_{Composite} < \Phi_{Au}$. If that quantity of gold is divided into several smaller gold particles dispersed throughout the PANI, a different value should be measured because of the change in contact potential for each particle. This trend should continue and become more pronounced as the particle size approaches the nanoscale. These observations are used to help explain the effects seen in figure 5.6.

In the composite, changing the relative particle size would cause each particle to feel a different contact potential *on average* for each charge transferred from the PANI. Thus a different number of charges should be required to balance the difference in work function. This should lead to a dependence of the work function on the average particle size, even if the work function of the particles remains constant.

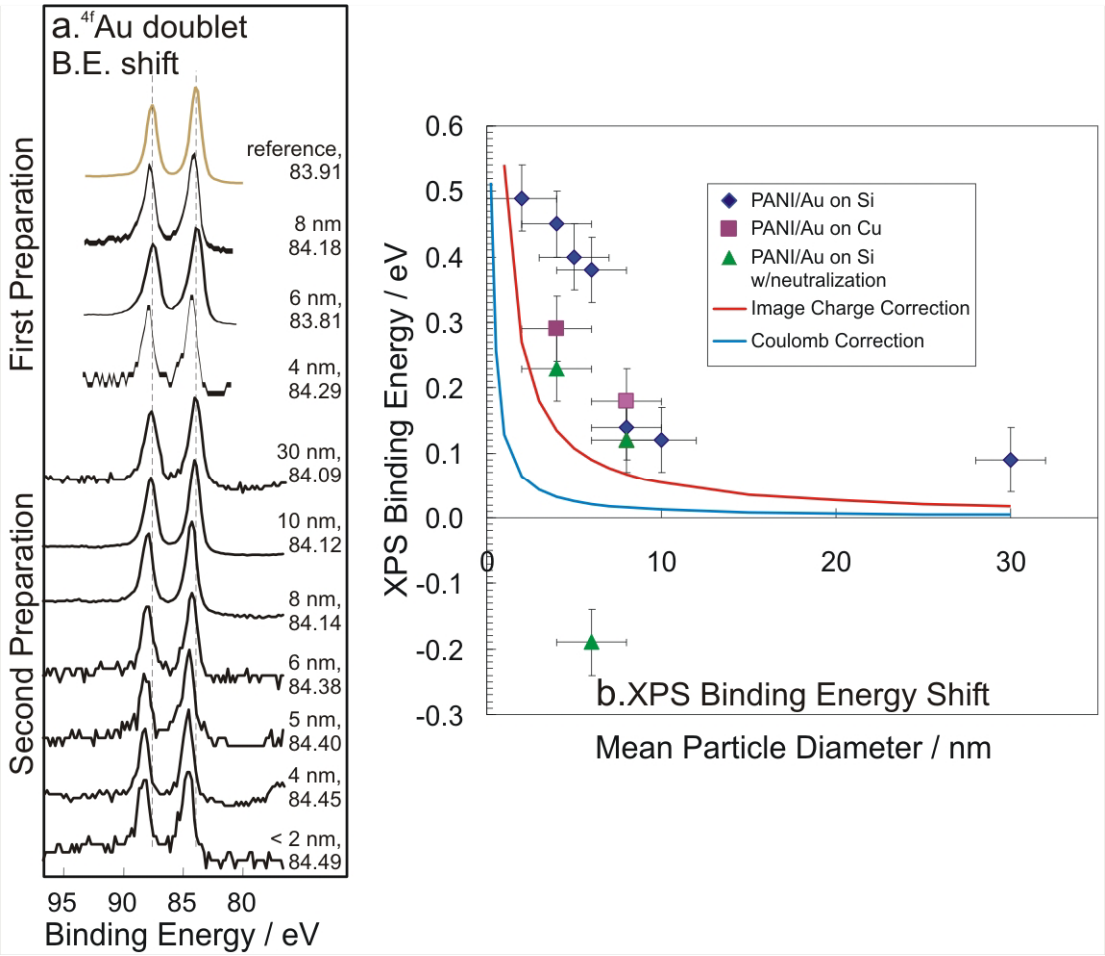

Figure 5.6. (a) Binding Energy shift in the $^{4f}_{7/2}$Au vs. particle size and (b) the peak shift difference of the 4fAu doublet relative to the bulk for the composites mounted on silicon wafers (red triangles), on copper TEM grids (blue diamonds and copper TEM grids with electron flood gun compensation for charging substrates. The coulomb interaction (solid line) and image charge (dashed line) models are also plotted.

5.3.2.2 Nanoscale Effect

The study of the nanoscale is concerned primarily with the change of material properties (e.g. the work function) as size decreases from the bulk to the atomic. For metallic particles, the size at which the properties begin to change is on the order of 10 nm.[5-8] At these sizes, the percentage of atoms on the surface begins to be appreciable relative to the bulk. These outer atoms experience a different electronic environment than the inner atoms and as their size decreases further, they begin to dominate the physical properties. As the particles approach the size of the de Broglie electron wavelength, the electrons delocalize over the entire surface and the particles begin to behave quantum mechanically as single, large atoms [5] whose properties are closely linked to their size and shape.

In small metallic clusters, measurement of the ionization potential shows an initial rapid drop from the atomic value followed by a slow continual decrease to the bulk work function value.[8] This was originally attributed to the image force[9] but later experiments fit this change to a dependence on the coulomb attraction between the ejected electron and the charged particle which yields the simple relationship,

$$IP = \Phi_{Bulk} + \frac{e^2}{R}. \qquad (3)$$

Here, IP is the ionization potential and R is the particle radius. Further refinements to this model take into account the size-related electronic energy changes, shell filling effects, spillover and edge effects based on the jellium sphere model. These refinements require a second order term the calculation of which is beyond the scope of this work.[7] The coulomb interaction, nevertheless, reproduces fairly accurately the experimental data and provides a good starting point from which to being the discussion.

The binding energy shift and coulomb in dependence of the ionization potential of nanoparticles in XPS measurements has been variously attributed to initial or final state effects of the measured particle.[7, 8, 10-17] Initial state effects are due to electronic configuration of the uncharged cluster while the final state effects arise from the charge rearrangement or relaxation which occurs in response to the core hole left when an electron is ejected from the particle. A rigorous treatment of the subject argues that both are important in different cases.[18] Much of the body of literature focuses on particles in free space, on non-conducting or semi-conducting supports, or for monolayer encapsulated particles. In some cases, the binding energy shift has been attributed to a time constant related to the slow transfer of an electron to the cluster from the support due primarily to the particle being electronically

decoupled from the experimental apparatus. This should not be the case for this system, as PANI is highly conductive.

While this work is certainly valid, it focuses primarily on the particle and does not address its interaction with the support substrate. As such, it does not explicitly address the electronic nature of the PANI/Au composite in which the PANI conductor is in intimate electrical contact with the gold nanoclusters. In consideration of the contact potential that develops between the materials, the measured value of binding energy in the XPS will likely depend on the electronic interaction of the PANI with the gold, particularly in consideration of the contact potential that develops between the two materials.

Verykios and others have modeled the work function based contact potential changes in gold nanoparticles embedded in a semi-conducting TiO_2 support substrates but their focus was primarily on the catalytic effects of the difference in work function between the two materials.[19, 20] They suggested simple-model theoretical calculations that as the particle diameter decreases, the number of charges transferred increases so that a 1.5 nm particle may abstract 0.5 electrons per metal atom, *e*/M whereas a 40 nm particle could be as low as 0.01 *e*/M.[19] This ration was found to be $\Delta\Phi$ dependent. It was also found to depend on the total electronic interaction volume[20] (the charged

volume over which the electronic potential interaction occurs) of the two conductors as well as the total surface area and contact area.

For bulk polyaniline prepared chemically the tabulated work function is approximately 4.8 eV while for gold it is 5.1 eV. In this situation electrons will flow toward the gold. However, the work function of polyaniline changes depending on the doping and oxidation state and, as such, the direction in which charges flow will reverse if the work function of the PANI shifts above that of gold.

The gold nanoparticle binding energy change for the 4fAu doublet as a function of particle size is seen in figure 5.6 which shows the doublets from all composites. A dashed vertical line marks the 83.91 eV ($^{4f}_{7/2}$Au) peak, the measured value of the gold foil reference whose surface had been freshly sputter cleaned with argon ions. The first set of XPS experiments are plotted above and the second are below with the gold standard at the top. All peak have been normalized to the same height. A clear shift in the binding energy is apparent relative to the particle size with the smallest particle size shifted about 0.58 eV relative to the reference and the largest being shifted by 0.17 eV. The two 8 nm samples show similar binding energies of 84.18 and 84.14 eV. The two 4 nm samples are not as close at 84.29 and 84.45 eV, respectively. The 6 nm sample prepared by stripping in 1 M KBr whose XPS spectrum is shown in figure 5.1d shows a binding energy lower than that of the gold

reference, 83.81 eV (also lower than any other samples). This is common for XPS peaks shifts on samples that exhibit significant charging. The difference in peak position for samples with the same size gold particles is attributed to different contact potential development as a consequence of the PANI support having slightly different values of work function.

Figure 5.6b shows a plot of all measured values of the binding energy shift as a function of particle size. The silicon mounted samples are indicated by blue diamonds while the copper mounted samples are shown by green triangles and purple squares for the binding energy with and without neutralization, respectively. The direction of this shift is agreement with the trend expected for particles as they approach the atomic ionization potential. All values are shifted above the nominal value of the gold reference and this difference is attributed to the development of a contact potential between the polyaniline and gold nanoparticles. The direction of the shift indicates a net loss of electron density on the gold particles which would mean that additional energy would be required to remove an electron from the particles. This is counterintuitive based on the measured bulk values of gold and polyaniline work function. Regardless, the offset frequently seen in the literature relative to the reference values is thought to have its origin in the contact potential between the substrate and the particles.

One significant question remains. If gold atoms are reduced one-by-one as suggested by the electrochemical evidence in chapter 4, how do they form such large particles? A simply calculation of bulk gold density (19.1 g/cm^3) divided by the molar mass (197 g/mol) and multiplied by Avogadro's number yields 6.0 x 10^{22} $atoms/cm^3$. Converting to $atoms/nm^3$ gives ~ 60 $atoms/nm^3$. Calculating the volume of the particle assuming that it is spherical yields $V=4/3*\pi*(5\ nm)^3$ x 60 $atoms/nm^3$. This is about 32,000 atoms. Even for the smallest captured gold particles ~ 1-2 nm, this yields about 30-250 atoms. The question of how so many atoms can collect in one spot is best answered from the TEM evidence in figure 5.7. Figure 5.7 a shows a particle of about 10 nm with a red circle highlighting the particle and a red line showing the alignment of the crystal lattice. A second, smaller particle is seen superimposed on the larger particle and is circled in orange with an orange line to indicate the lattice alignment. Notice that the two lattices exhibit about a 20^o difference in orientation. While particles typically agglomerate in solution in the absence of capping, in this system, the reduction occurs a the PANI surface at the imino nitrogen on the PANI chain. Some atoms are, of course, expected to reduce at already formed particle surfaces but this does not account for the particles agglomerating once formed. It is thought that this is a function of the high surface energy of the gold particle after formation

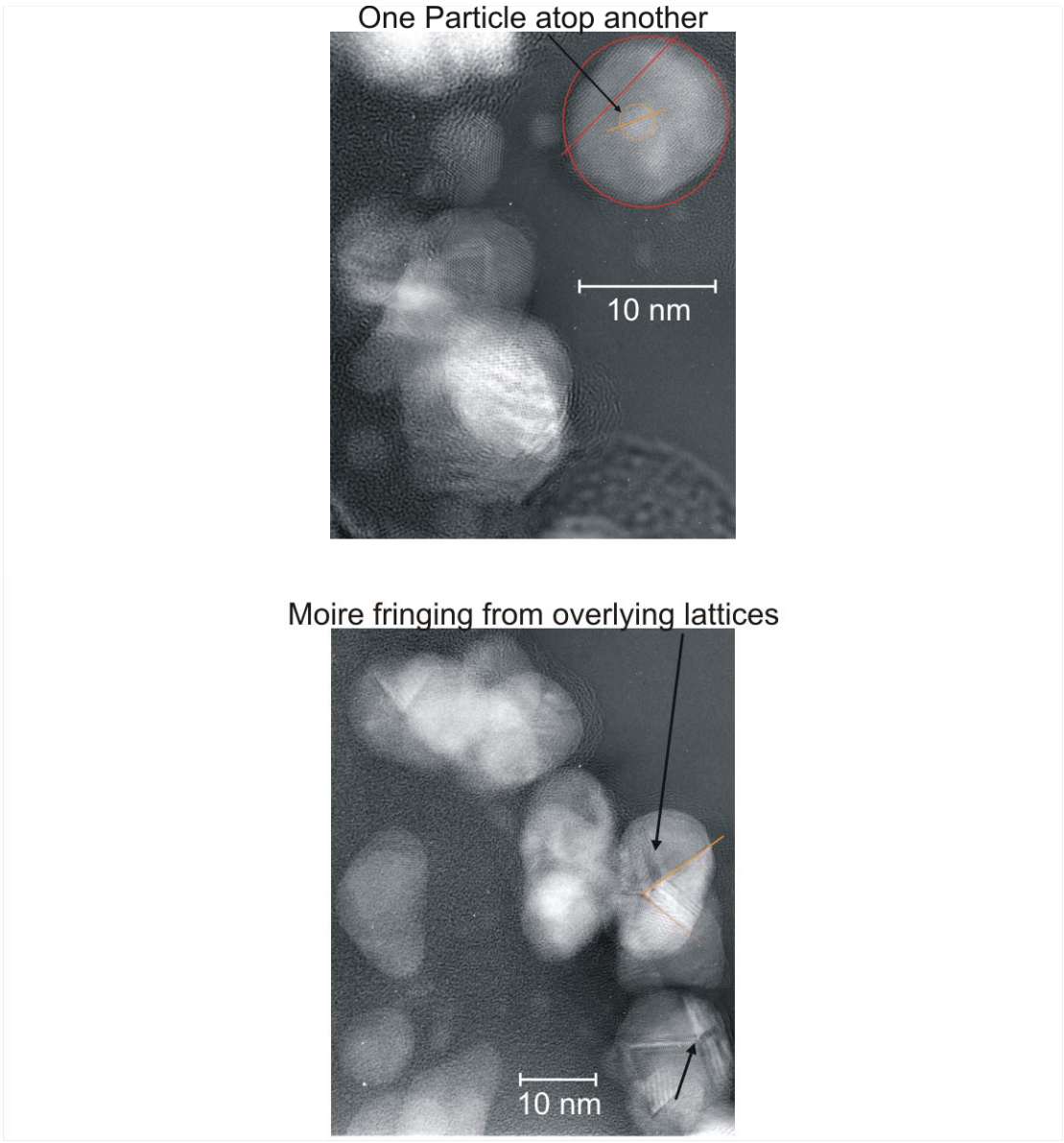

Figure 5.7 Movement and Aggregation of Particles.

which allows the particle to “float” on the delocalized electrons of the PANI chains until their surface energy is either decreased by agglomeration to another particle. The high degree of delocalization of the pi electrons making up the conducting electronic structure of the PANI is could contribute to this phenomenon. An additional image in figure 5.7b shows particles formed of what appear to be three different particles where each particles lattice interface can be clearly seen adjoining at 60^{o} angles marked by the orange lines.

5.4 Conclusions

XPS analysis of the electrochemically prepared freestanding films has shown a dependence of the XPS binding energy shift on the gold particle size. The shape of the binding energy curve is seen to follow that of the coulomb interaction correction to the radius dependent ionization potential. The concept of contact potential is developed to describe the origin of the change in Kelvin probe based work function measurements of the composite material and is extended to show its contribution to the offset of the measured binding energy differences of the gold particle $^{4f}{}_{7/2}$Au doublet.

TEM analysis shows the aggregation of particles thought to be due to the high energy of the gold particles upon formation and their need to minimize their surface energy which, along with the highly delocalized pi

electrons of the PANI allows them to "float" on the PANI surface to agglomerate to other particles and reduce their surface energy which terminate the process.

5.5 Acknowledgements

Thanks to both Don Baer and Mark Engelhard from PNNL for their help in obtaining and interpreting the XPS data.

5.6 Summary

This chapter discusses the incorporation of particles of size 10 and less nanometers into the freestanding composites whose synthesis was described in chapter 4. The XPS measurement of the composites is described along with an explanation of the size dependent shift in the ^{4f}Au binding energy. The offset of all particles above the baseline Au foil reference is attributed to the development of the contact potential between the gold particles and the PANI support. The direction of the electron transfer is found, unexpectedly, to be toward the PANI which is thought to be due to PANI doping shifting the work function of the PANI above that of gold. TEM micrographs are used to show the agglomeration of gold particles leading to relatively large particle sizes.

5.7 References

1. Janata, J.; Josowicz, M. *Analytical Chemistry* **1997**, *69*, 293A-296A.

2. Hatchett, D. W.; Josowicz, M.; Janata, J.; Baer, D. R. *Chemistry of Materials* **1999**, *11*, 2989-2994.

3. Woodruff, D. P.; Delchar, T. A. *Modern techniques of surface science*, 2nd ed.; Cambridge University Press, 1994.

4. Ting, Y. P.; Neoh, K. G.; Kang, E. T.; Tan, K. L. *J. Chem. Technol. Biotechnol.* **1994**, *59*, 31-36.

5. de Heer, W. A. *Reviews of Modern Physics* **1993**, *65*, 611-676.

6. Sanchez, A.; Abbet, S.; Heiz, U.; Schneider, W. D.; Haekkinen, H.; Barnett, R. N.; Landman, U. *Journal of Physical Chemistry A* **1999**, *103*, 9573-9578.

7. Seidl, M.; Meiwes-Broer, K. H.; Brack, M. *Journal of Chemical Physics* **1991**, *95*, 1295-1303.

8. Wertheim, G. K. In *Zeitschrift fuer Physik D: Atoms, Molecules and Clusters*, **1989**; Vol. 12, pp 319-326.

9. Wood, D. M. *Physical Review Letters* **1981**, *46*, 749.

10. Hovel, H.; Grimm, B.; Pollmann, M.; Reihl, B. *Physical Review Letters* **1998**, *81*, 4608-4611.

11. Hovel, H.; Grimm, B.; Pollmann, M.; Reihl, B. *European Physical Journal D: Atomic, Molecular and Optical Physics* **1999**, *9*, 595-599.

12. Mason, M. G. *Physical Review B: Condensed Matter and Materials Physics* **1983**, *27*, 748.

13. Nagasawa, T.; Tanaka, A.; Sasaki, H.; Kuriyama, Y.; Suzuki, S.; Sato, S.; Sekine, T. *Materials Research Society Symposium Proceedings* **2002**, *704*, 319-324.

14. Radnik, J.; Mohr, C.; Claus, P. *Physical Chemistry Chemical Physics* **2003**, *5*, 172-177.

15. Tanaka, A.; Takeda, Y.; Nagasawa, T.; Sasaki, H.; Kuriyama, Y.; Suzuki, S.; Sato, S. *Surface Science* **2003**, *532-535*, 281-286.

16. van der Putten, D.; Zanoni, R. *Journal of Electron Spectroscopy and Related Phenomena* **1995**, *76*, 741-745.

17. Yang, Z.; Wu, R. *Physical Review B: Condensed Matter and Materials Physics* **2003**, *67*, 081403-081401 - 081403-081404.

18. Bagus, P. S.; Illas, F.; Pacchioni, G.; Parmigiani, F. *Journal of Electron Spectroscopy and Related Phenomena* **1999**, *100*, 215-236.

19. Ioannides, T.; Verykios, X. *Journal of Catalysis* **1996**, *161*, 560-569.

20. Verykios, X. *Catalysis and Electrocatalysis at Nanoparticle Surfaces*; Marcel Dekker, Inc.: New York, **2003**.

CHAPTER VI

FUTURE WORK

6.1 Further Experiments on Composites with Sub 1 nm Particles

There are a number of experiments that could help to elucidate this system. This system pushes the boundaries for TEM size characterization. It may be possible to use mass spectrometry or even single particle fluorescence experiments for further size characterization in the sub 1 nm region. Also, since this work formulates new arguments regarding the drop in conductivity and the XPS binding energy shift of the ^{4f}Au doublet, additional XPS and conductivity experiments would prove beneficial. These would require having films whose difference is minimized as much as possible to the particle sizes. This is possible with the current preparation methods. These could be supported by theoretical calculations on how the interplay of the contact potential between the gold nanoparticles and polyaniline film affects the charge delocalization and how this affects the macroscopic PANI conductivity.

6.1.1 Size Characterization

Mass spectrometry experiments could be performed to investigate the sub 1 nm regime. Matrix assisted laser desorbtion ionization

(MALDI) is a likely candidate for ionizing the embedded particles.[1] The expectation is that even smaller particles than are discernable in TEM form during the electrochemical experiment. In fact, for the smallest particles it is expected that the TEM would not be able to resolve the particles due to the PANI interference in the imaging mode. This is supported by the XPS experiment where the ^{4f}Au doublet was seen to have the highest peak shift for a film in which no particles were visible in the TEM.

Preliminary experiments were performed in which PANI powder prepared electrochemically according to Hatchett, et al[2] was mixed with fluorescent gold dendrimer solutions as prepared by Zheng and Dickson.[3] The PANI and dendrimer solutions were mixed with 1 M KOH. In this solution PANI is non-conductive and fluorescence was observed. In acidic solutions, the PANI is conducting and here the solutions were found to have ~10x lower fluorescence. This is thought to be due to quenching from electron transfer by the polyaniline which is in its conducting state as suggested by Heeger.[4]

An additional preliminary experiment was performed on a composite prepared by limiting the chloride concentration during electrochemical stripping. This yielded particles as small as ~0.7 nm which were only visible on the phosphorescent TEM screen. As described earlier, in ideal conditions it is possible to view such particles,

but due to paramagnetism in polyaniline requires constantly adjusting the microscope astigmatism. Capturing the images on film which requires exposure time of ≥ 2 seconds is therefore improbable. This film exhibited fluorescence upon laser excitation with 1064 nm frequency doubled to 532 nm, laser radiation. The fluorescence wavelength was not measured. This fluorescence is shorter wavelength than the later plasmon that develops and the source is thought to be the sub nm gold particles.

The fluorescence background of PANI-only films prepared as similarly as possible need to be performed to discriminate this fluorescence from the possible PANI fluorescence contribution, reported for basic forms of PANI.[5, 6] Fluorescence lifetime quenching experiments should be performed for both the film and the dendrimer/powder systems to help determine the source and mechanism of fluorescence. Provided that it can be proved that the fluorescence originates from the gold particles, it should be possible to see the fluorescence wavelength change dependent on the particle size. If the particles size is known well enough from other methods, (e.g. mass spectrometry) a calibration of fluorescence wavelength to size could then be used to determine particle sizes within a film. Also it may be possible to determine a method for switching the particle fluorescence depending on the PANI conducting state

6.1.2 Contact Potential

Further XPS experiments could be performed with films prepared by chloride concentration limited reactions. These films should be larger for use in multiple characterization methods. The films could be cut in half with one side up, one side down relative to gold side during the growth process. This should show the particle gradient in the composites. It is believed that these films will have smaller particles of more regular size and as they will be prepared with only PANI, gold and KCl and HBF_4 they should not suffer from interactions with other ions introduced during growth. The films could be grown a bit thicker in order to avoid artifacts due to the voids in the ultra-thin films. It is hoped that these experiments will provide more information on the binding energy shift vs. particle size and thus help correlate the contact potential details. With larger area films, a larger XPS spot size may be used and the ^{4f}Au signal to noise ratio will be improved.

The films prepared for the above experiments should be large enough to make macroscopic conductivity measurements. Section 2.4 described experiments showing that introduction of gold nanoparticles in the PANI reduces film conductivity, even when maintaining the same acid dopant concentration. Transmission infrared spectrometry could be performed on these larger films to confirm the conducting state from the near IR region.

The drop in composite film conductivity with small particles is believed to be due to the contact potential localizing the electrons from what would otherwise be the highly delocalized PANI electronic structure. This localization drops their mobility and effectively reduces the correlation length of the polaron along a single polyaniline chain. Conduction down a single chain is thought to be the fast step in conduction but when the charge is localized it may, in fact become slower than the inter-chain hoping. When the particles grow large enough this effect will reduce as the particles begin to join individual chains and effectively reduce the inter-chain hoping distance which is thought to be the slow step in the conduction process. Additionally as the particles grow larger the charges may not be as localized at the gold particle.

Finally, the affinity of the gold for sulfur containing compounds could be used to introduce specificity to layers used in solid state chemical sensors.

6.2 References

1. Folch, I.; Borros, S.; Amabilino, D.; Veciana, J. *Journal of Mass Spectrometry* **2000**, *35*, 550-555.
2. Hatchett, D. W.; Josowicz, M.; Janata, J.; Baer, D. R. *Chemistry of Materials* **1999**, *11*, 2989-2994.
3. Zheng, J.; Dickson, R. M. *Journal of the American Chemical Society* **2003**, *124*, 13983.

4. Fan, C.; Wang, S.; Hong, J. W.; Bazan, G. C.; Plaxco, K. W.; Heeger, A. J. *Proceedings of the National Academy of Science* **2003**, *100*, 6297-6301.

5. Li, N. B.; Zhang, S. T.; Ding, P. D. *Chinese Chemical Letters* **2000**, *11*, 681-684.

6. Thorne, J. R. G.; Masters, J. G.; Williams, S. A.; MacDiarmid, A. G.; Hochstrasser, R. M. *Synthetic Metals* **1992**, *49*, 159-165.